Institute of Molecular Virology, Ulm University Medical Center

Directors: Prof. Dr. Frank Kirchhoff & Prof. Dr. Jan Münch

Regulation of Autophagy by SARS-CoV-2 and Host Proteins

Dissertation

submitted in partial fulfilment of the requirements for the degree of
„*Doctor rerum naturalium*" (Dr. rer. nat.)
of the International Graduate School in Molecular Medicine Ulm

Lennart Koepke

Born in Nürtingen (Germany)

2022

Data page

Current dean of the Medical Faculty:

Prof. Dr. Thomas Wirth

Current chairman of the Graduate School:

Prof. Dr. Bernd Knöll

Thesis Advisory Committee:

1st supervisor: Prof. Dr. Frank Kirchhoff

2nd supervisor: Prof. Dr. Thomas Stamminger

3rd supervisor: Prof. Dr. Karl-Klaus Conzelmann

External reviewer:

Dr. Matthew Blango

Dr. Renke Lühken

Day doctorate awarded:

16.03.2023

Publication Index

Results gained in my thesis have previously been published in the following publication:

Koepke L*, Winter B*, Grenzner A, Regensburger K, Engelhart S, van der Merwe J A, Krebs S, Blum H, Kirchhoff F, Sparrer K M J: An Improved Method for High-Throughput Quantification of Autophagy in Mammalian Cells. **Sci Rep** 10 12241 doi.org/10.1038/s41598-020-68607-w (2020)
* These authors contributed equally to this work.
License: CC BY 4.0 (https://creativecommons.org/licenses/by/4.0/)

Hayn M*, Hirschenberger M*, Koepke L*, Nchioua R, Straub J H, Klute S, Hunszinger V, Zech F, Prelli Bozzo C, Aftab W, Christensen M H, Conzelmann C, Müller J A, Srinivasachar Badarinarayan S, Stürzel C M, Forne I, Stenger S, Conzelmann K-K, Münch J, Schmidt F I, Sauter D, Imhof A, Kirchhoff F, Sparrer K M J: Systematic Functional Analysis of SARS-CoV-2 Proteins Uncovers Viral Innate Immune Antagonists and Remaining Vulnerabilities. **Cell Reports** 35 109126 doi.org/10.1016/j.celrep.2021.109126 (2021)
* These authors contributed equally to this work.
License: CC BY-NC-ND 4.0 (https://creativecommons.org/licenses/by-nc-nd/4.0/)

Koepke L, Hirschenberger M, Hayn M, Kirchhoff F, Sparrer K M J: Manipulation of Autophagy by SARS-CoV-2 Proteins. **Autophagy** 17 2659–2661 doi.org/10.1080/15548627.2021.1953847 (2021)
License: CC BY-NC-ND 4.0 (https://creativecommons.org/licenses/by-nc-nd/4.0/)

Table of Contents

Data page I

Publication Index II

Table of Contents III

List of abbreviations V

1. Introduction 1

1.1. Autophagy 1

1.2. Cellular regulation of autophagy 4

1.3. Autophagy in (infectious) diseases 7

1.4. SARS-CoV-2 9

1.5. Measuring autophagy 11

2. Scientific aims 13

3. Material 14

4. Methods 29

5. Results 46

5.1. Establishing a reporter system for rapid quantification of changes in autophagy 46

5.2. Manipulation of autophagy by SARS-CoV-2 52

5.3. TRIM proteins inhibit autophagy induction 61

6. Discussion 70

6.1. High throughput quantification of autophagy 70

6.2. Limitations of LC3B processing-based autophagy screening systems 72

6.3. The interplay between SARS-CoV-2 and autophagy 73

6.4. Filamin-NHL TRIMs and CK2 inhibit autophagy 77

6.5. Outlook 80

7. Summary 82

8. References 83

9. Appendix I

10. Acknowledgements II

11. Statutory declaration IV

List of abbreviations

Table 1: List of abbreviations.

Abbreviation	Explanation
ACE2	Angiotensin converting enzyme 2
ALS	Amyotrophic lateral sclerosis
ATG	Autophagy-related protein
ATG14L	ATG14-like
BafA1	Bafilomycin A1
CCD	Coiled-coil domain
CK2	Casein kinase II
COVID-19	Coronavirus disease 2019
CQ	Chloroquine
DAPI	4’,6-Diamidino-2-Phenylindole, Dihydrochloride
DENV	Dengue virus
DMEM	Dulbecco’s Modified Eagle Medium
DMVs	Double membrane vesicles
DTT	Diethiothreitol
E	SARS-CoV-2 envelope protein
e.g.	exempli gratia “for example”
EDTA	Ethylenediaminetetraacetic acid
ER	Endoplasmic reticulum
ESCRT	Endosomal sorting complexes required for transport
FACS	Fluorescence activated cell sorting
FBS	Fetal bovine serum
FIP200	FAK family kinase-interacting protein of 200 kDa
FSC	Forward scatter
GL	eGFP-LC3B
HCMV	Human cytomegalovirus
HIV-1	human immunodeficiency virus type 1
HPIV3	Human parainfluenza virus type 3
Hsp70	Heat shock protein 70
HSV-1	Herpes simplex virus type 1

Abbreviation	Explanation
IAV	Influenza A virus
Ig	Immunoglobulin
IRF3	Interferon regulatory factor 3
kb	Kilo base
LAMP1	Lysosome-associated membrane glycoprotein 1
LC3B-I	C-terminally cleaved LC3B
LC3B-II	Lipidated LC3B
LFQ	Label free quantification
M	SARS-CoV-2 membrane protein
MAVS	Mitochondrial antiviral-signaling protein
MERS-CoV	Middle east respiratory syndrome–related coronavirus
MFI	Mean/median fluorescence intensity
MHC	Major histocompatibility complex
MHV	Mouse hepatitis virus
MOI	Multiplicity of infection
MS	Mass spectrometry
mTORC1	Mammalian target of Rapamycin complex 1
N	SARS-CoV-2 nucleocapsid protein
NBR1	Next to BRCA1 gene 1 protein
Nsp	Non-structural protein
NT	Non-treated
ORF	Open reading frame
p62	Sequestosome-1
PAMPs	Pathogen associated molecular patterns
PBS	Phosphate-buffered saline
PE	Phosphatidylinositol 3-phosphate
PFA	Paraformaldehyde
PI3K-3	PI3K type 3
PI3K-IV	PI3K regulatory subunit 4
PRRs	Pattern recognition receptors
PTM	Post translational modification
Rab5	Ras-related protein Rab5

Abbreviation	Explanation
Rapa	Rapamycin
RIG-I	Retinoic acid-inducible gene I
RING	Really Interesting New Gene
S	SARS-CoV-2 spike protein
SARS-CoV-1	Severe acute respiratory syndrome coronavirus type 1
SARS-CoV-2	Severe acute respiratory syndrome coronavirus type 2
SD	standard deviation
SDS	Sodium dodecyl sulfate
SDS-PAGE	Sodium dodecyl sulfate polyacrylamide gel electrophoresis
SEM	Standard error of the mean
si.NT	Non-targeting siRNA
SNAP29	Synaptosomal-associated protein 29
SSC	Sideward scatter
STAT1	Signal transducer and activator of transcription 1
STX17	Syntaxin-17
TBK1	TANK-binding kinase 1
TLRs	Toll-like receptors
TRIM	Tripartite motif
ULK1	Serine/threonine-protein kinase ULK1
UVRAG	UV radiation resistance-associated gene protein
VAMP8	Vesicle-associated membrane protein 8
V-ATPase	Vacuolar type H+-ATPase
VPS	Vacuolar protein sorting-associated protein homolog
WCL	Whole cell lysates
WT	Wildtype
ZIKV	Zika virus
ΔRING	Lacking the RING domain

1. Introduction

1.1. Autophagy

Autophagy is a catabolic process that degrades cytoplasmic cargo via lysosomes. In mammalian cells, there are three major types of autophagy: macroautophagy, microautophagy, and chaperon-mediated autophagy[141]. During macroautophagy, double membraned vesicles, called autophagosomes, deliver their cargo to the lysosome via fusion. In microautophagy, cargo is taken up through invaginations in the lysosomal membrane and in chaperon-mediated autophagy the cargo is translocated across the lysosomal membrane by chaperons. My work focuses on macroautophagy and its machinery, which is referred to as 'autophagy' from here on.

Autophagy is one of the central processes required to maintain cellular homeostasis. While it can degrade virtually any cytoplasmic cargo, it is well known to target misfolded or aggregated proteins and damaged or surplus organelles for lysosomal degradation[103]. Nutrients generated by degradation are released back to the cell, providing a source of energy. Accordingly, autophagy is activated under conditions of starvation to aid cell survival[193]. The autophagy machinery can either degrade parts of the cytoplasm indiscriminately in bulk or recognize selected targets earmarked for degradation. Selective autophagy is one of the key protein turnover processes, and thus autophagy plays a role in the regulation of many signaling pathways and is crucially involved in development[103]. Finally, emerging evidence demonstrated that autophagy is an integral part of the innate immune defense system, combating invading pathogens by targeting pathogens or their components for degradation and facilitating exposure of pathogen associated molecular patterns (PAMPs) to trigger further defense mechanisms[137].

1.1.1. The autophagic machinery

In brief, during autophagy, cytoplasmic cargo is engulfed by autophagosomes which subsequently fuse with lysosomes to form an autolysosome and mediate degradation of the cargo as well as the inner membrane. The process can be roughly separated into four steps: (I, red) Initiation, (II, yellow) Elongation, (III, orange) Maturation, and (IV, purple) Degradation (Fig. 1).

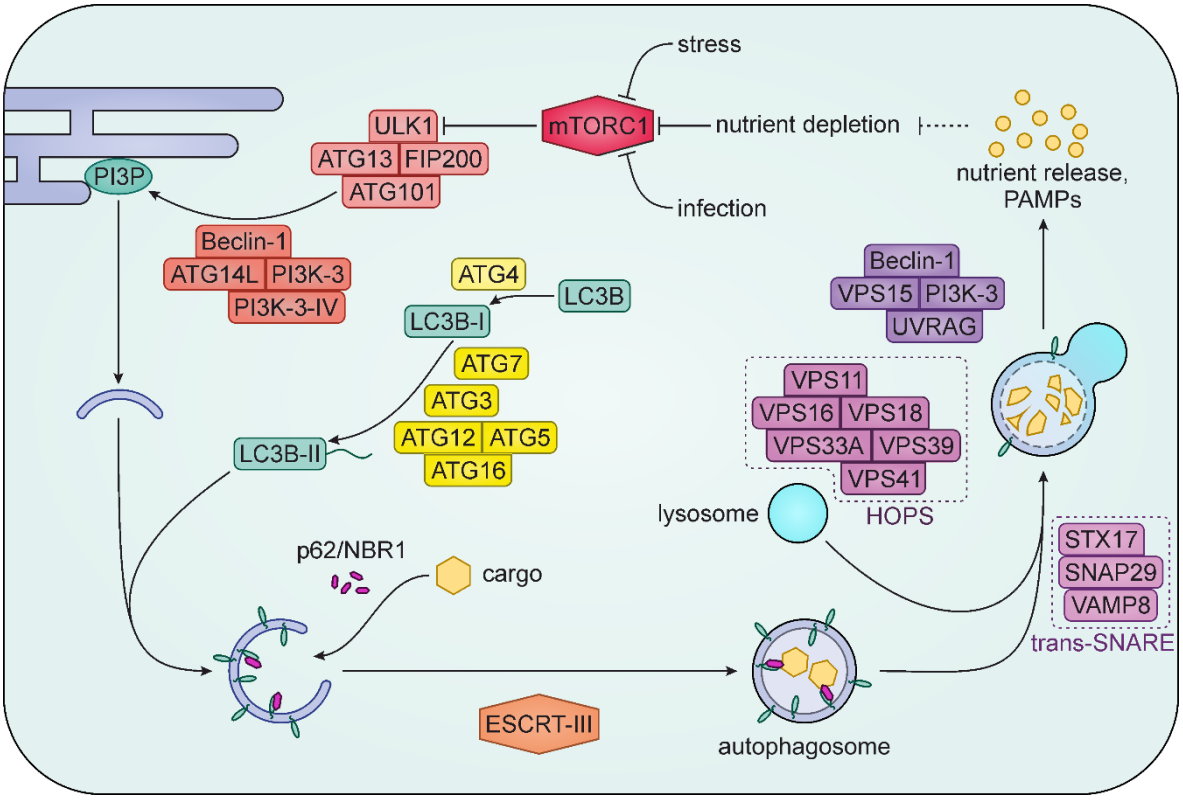


Figure 1: Schematic depiction of the autophagy machinery. mTORC1 is the master regulator/inhibitor of autophagy. To induce autophagy, the ULK1 complex (ULK1, ATG13, FIP200, ATG101) associates with autophagy initiation sites on the ER and recruits the PI3K type 3 (PI3K-3) complex (Beclin-1, ATG14L, PI3K-3, PI3K-3-IV). The PI3K-3 complex produces PI3P to induce phagophore formation. LC3B is proteolytically cleaved by ATG4 (LC3B-I: cleaved form of LC3B), PE is attached to its C-terminus via an E1-E2-E3 (ATG7 – ATG3 – ATG12-ATG5-ATG16) cascade (LC3B-II: PE-bound form of LC3B) and it is incorporated into the phagophore membrane. Autophagy receptors such as p62 and NBR1 target cargo to the phagophore where they bind to LC3B-II. The ESCRT-III subcomplex mediates scission of the membrane and the phagophore closes to form an autophagosome. The HOPS complex (VPS11, VPS16, VPS18, VPS33A, VPS39, VPS41) bridges the autophagosomal and lysosomal membranes and facilitates formation of the trans-SNARE complex (STX17, SNAP29, VAMP8) which in turn mediates fusion. The second PI3K-3 complex (Beclin-1, VPS15, PI3K-3, UVRAG) enhances fusion. The cargo is degraded in the autolysosome and released back to the cell to serve e.g. as nutrients or PAMPs.

(I) Initiation of autophagy is governed by two complexes. The ULK1 complex[195] consists of Serine/threonine-protein kinase ULK1 (ULK1), FAK family kinase-interacting protein of 200 kDa (FIP200), autophagy-related protein (ATG)13, and ATG101. It is the target of the mammalian target of Rapamycin complex 1 (mTORC1), which inhibits autophagy induction by phosphorylation and inactivation of ULK1 in nutrient-rich conditions. Upon induction of autophagy by e.g. cellular stress, nutrient depletion or pathogen infection, the dephosphorylated ULK1 complex assembles at autophagy initiation sites on the endoplasmic reticulum (ER) where it recruits the PI3K type 3 complex[73] comprised of

Phosphatidylinositol 3-kinase catalytic subunit type 3 (PI3K type 3), Beclin-1, Phosphoinositide 3-kinase regulatory subunit 4 (PI3K regulatory subunit 4) and ATG14-like (ATG14L).

(II) Elongation is initiated by the PI3K type 3 complex, which produces phosphatidylinositol 3-phosphate (PI3P) at the autophagy initiation site to recruit the factors necessary for the formation and expansion of an autophagy initiation membrane, called the phagophore. The ATG8 family of proteins, most prominently including microtubule-associated proteins 1A/1B light chain 3B (LC3B), decorate autophagosomes where they are required for membrane elongation, cargo recognition, closure, and eventually fusion with lysosomes[100]. The C-terminus of LC3B is proteolytically cleaved (the cleaved form is called LC3B-I) before a ubiquitin-like conjugation cascade mediates the attachment of phosphatidylethanolamine (PE) to LC3B-I to anchor it to the autophagosomal membrane. To this end, LC3B-I is recruited onto ATG7 (E1) and moved to ATG3 (E2), which mediates the attachment of the LC3B-I C-terminus to the PE headgroup. This process is enhanced by the E3-like ATG12-ATG5-ATG16 complex[120,135]. The lipidated form of LC3B is referred to as LC3B-II. Selective autophagy receptors like Sequestosome-1 (p62) and Next to BRCA1 gene 1 protein (NBR1) recognize poly-ubiquitinated cargo and target them to elongating phagophores by interaction with LC3B-II[138]. The autophagy receptors are later degraded alongside the cargo.

(III) To mature into an autophagosome, the opening of the phagophore membrane needs to be closed. The required scission of the membrane is mediated by components of the endosomal sorting complexes required for transport (ESCRT) machinery[6]. Studies have shown that the ESCRT-III subcomplex alone can mediate scission. Still, additional proteins, such as Ras-related protein Rab5 (Rab5) and ATG8 family members, are known to play crucial roles in this process, for example, in the recruitment and assembly of the complex. After membrane closure, ATG4 can recycle LC3B-II that is present on the outer autophagosomal surface by cleavaging its C-terminus.

(IV) To facilitate cargo degradation, the autophagosome fuses with a lysosome. The HOPS complex[76], comprised of vacuolar protein sorting-associated protein homolog (VPS) 11, VPS16, VPS18, VPS33A, VPS39, and VPS41, is recruited to autophagosomes and bridges the autophagosomal and lysosomal membranes. It further interacts with Syntaxin-17 (STX17) and facilitates the formation of the trans-SNARE complex[76], made up of STX17,

Synaptosomal-associated protein 29 (SNAP29), and Vesicle-associated membrane protein 8 (VAMP8), which in turn mediates fusion of the membranes. The fusion of autophagosomes and lysosomes is further enhanced by a complex of PI3K type 3, Beclin-1, VPS15, and UV radiation resistance-associated gene protein (UVRAG)[73,106], giving most parts of the PI3K type 3 complex a dual role in both autophagy initiation and degradation of autophagic cargo.

Once delivered to the acidic environment of the lysosome, lysosome-resident hydrolases degrade the autophagic cargo. The generated nutrients are released back to the cell to help maintain nutritional balance, and fragments generated from pathogens and their components can trigger further immune defense mechanisms[103].

1.2. Cellular regulation of autophagy

Both hyperactivation and lack of autophagy have detrimental effects on a cell. Thus, a plethora of cellular proteins are required to regulate autophagy levels and keep it balanced. Among these proteins are several kinases, like Casein kinase II (CK2) and members of the tripartite motif-containing (TRIM) protein family[116,163,165].

1.2.1. TRIM proteins

Members of the family of TRIM proteins are known to play important roles in autophagy modulation[64,116,117,163,164]. TRIMs are highly versatile E3 ligases comprised of a conserved N-terminal Really Interesting New Gene - BBox - coiled-coil domain (RING-BBox-CCD) motif and a variable C-terminal region containing domains with a wide range of functions (Fig. 2). The RING domain confers E3 ligase activity and mediates post-translational modification (PTM) of targets, usually conjugation of ubiquitin-like proteins. These PTMs can influence the stability and activity of the target and, thus, the associated pathways[64]. The function mediated by the BBox is unknown, and the CCD is thought to be involved in the oligomerization of the TRIMs, which is often required for full activity[153]. The variable domains at the C-terminus usually define substrate specificity through protein-protein interactions but domains that confer different functions such as binding of nucleic acids or enzymatic activity are also represented[89].

In addition to their multitude of functions, TRIM proteins are increasingly recognized for their role in the modulation of autophagy. Most autophagy-modulating TRIMs display autophagy-inducing properties[64,116,163]. For example, TRIM16 acts as an interaction platform for the p62-NRF2 axis, which is a crucial part of the response to protein aggregates[75]. TRIM16 further targets the negative regulator of NRF2, KEAP1, for degradation in

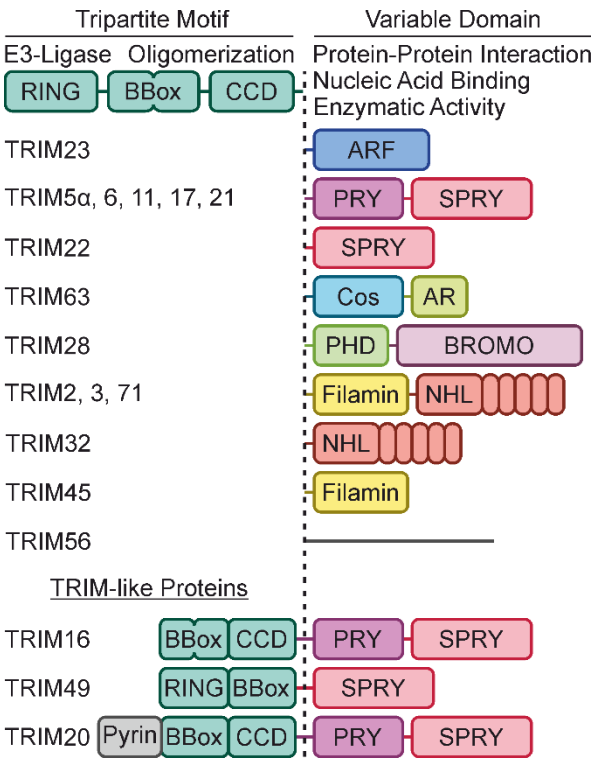


Figure 2: Domain organization of autophagy modulating TRIMs. TRIMs are comprised of a conserved tripartite motif at their N-terminus and variable C-terminal domains. The tripartite motif contains a RING domain with E3 ligase activity, one or two BBox domains and a CCD domain. TRIM-like proteins lack one of the characteristic domains or have it replaced. The C-terminal domains are highly variable and confer a range of functions, including protein-protein interaction, nucleic acid binding and enzymatic activity. The C-terminal domain organization of exemplary autophagy altering TRIMs are shown, sorted by their appearance in the main text.

autophagy. TRIM23 positively regulates the activity of the TANK-binding kinase 1 (TBK1) by facilitating its dimerization and enabling TBK1-mediated activation of the autophagy receptor p62. TRIM5α, TRIM6, TRIM22, and TRIM49, all containing C-terminal SPRY domains, were shown to act as an interaction platform for ULK1 and Beclin-1, enhancing the activation of Beclin-1 by ULK1[116]. TRIM5α was further shown to interact with Atg8 family members and p62 and, through this interaction, target the human immunodeficiency virus 1 (HIV-1) capsid protein p24 for degradation in autolysosomes[116,117]. TRIM17 interacts with parts of the autophagy initiation machinery and focuses its activity to a specific region where it co-localizes with them[116]. TRIM63 is implicated in the degradation of the nicotinic acetylcholine receptor in selective autophagy[82]. TRIM28 interacts with acetylated Heat shock protein 70 (Hsp70) and the PI3K type 3 complex, enhancing autophagy induction[191]. TRIM20 targets parts of the inflammasome for degradation in autophagy, acting as a selective receptor, and TRIM21 mediates the degradation of activated IRF3[86]. Finally, TRIM11 directly interacts with p62 and leads to the degradation of AIM2 in the autophagosome[110].

In contrast to the autophagy-activating role of TRIMs, little is known about TRIMs that negatively modulate autophagy. A previously performed screen[163] indicates that one group of TRIMs could be involved in reducing autophagy levels are the highly conserved filamin-NHL TRIMs[154,163]. TRIM2, TRIM3, and TRIM71 contain a filamin domain followed by

multiple NHL repeats at their C-terminus. These three TRIMs were previously implicated in other non-autophagy functions as well. TRIM71 has been shown to interact with mRNAs and suppress their expression. It plays a role in development by promoting cell cycle progression in stem cells through repressing Cdkn1a expression[19], and TRIM71 is further described to target mutant p53 for proteasomal degradation via ubiquitination, hence suppressing ovarian tumorigenesis[25]. TRIM2 is described to confer anti-viral functions[156] and to play a role in neurodegeneration and neuropathies[5,115,194]. TRIM3 was reported to mediate tumor suppressing functions[23,70,112,145] and seems to inhibit apoptosis in the context of Parkinson's disease[38]. The closest relatives of the filamin-NHL TRIMs are TRIM32 (containing only the NHL repeats), TRIM45 (containing only the filamin domain), and TRIM56 (containing neither of the two domains). Both TRIM56 and TRIM32 are described to impact autophagy. TRIM32 is known to induce autophagy and act as a selective autophagy receptor[34,35,166], and TRIM56 is involved in the sensing of double-stranded DNA by the cGAS-STING axis and subsequent activation of autophagy[175].

In summary, TRIMs are a highly diverse protein family influencing a wide range of cellular mechanisms. Many TRIMs are well-known to positively regulate autophagy by providing a platform for complex assembly and acting as specific autophagy receptors. At the same time, little is known about TRIMs that reduce autophagic flux.

1.2.2. Casein kinase 2

CK2 has prominent but conflicting roles in autophagy. It is a highly conserved[39], constitutively active Ser/Thr protein kinase that influences most cellular pathways and mechanisms via its hundreds of substrates[124]. CK2 is usually present in a tetrameric complex made up from two catalytically active subunits, either CK2α and/or CK2α', and two regulatory subunits, twice CK2β. While the CK2α and CK2α' subunits alone are sufficient to confer kinase activity, CK2β increases stability and activity of the complex and changes substrate specificity[45]. The CK2 complex is found in the nucleus and the cytoplasm and is described to associate with the plasma membrane, mitochondria, and the cytoskeleton[45]. Broad cellular distribution is further implied by the varying localisations of the vast range of proteins targeted by CK2[1,3,187]. Dysregulation of CK2 is associated with many malignancies, including neurodegenerative diseases such as Parkinson's disease[98] and Alzheimer's disease[102], and CK2 activity is increased in coronavirus disease 2019 (COVID-19) patients[11,93]. Severe acute respiratory syndrome coronavirus type 2 (SARS-CoV-2) uses CK2-mediated phosphorylation of its proteins to facilitate viral replication, raising interest

in inhibition of CK2 as a treatment approach for COVID-19[11]. In addition, CK2 is well studied for its elevated activity in many cancers. In cancer cells, high CK2 activity promotes cell survival and growth, increasing viability. Accordingly, inhibition of CK2 via the small molecule inhibitor CX-4945 is being investigated as a co-treatment in anti-cancer therapy and has acquired the orphan drug designation by the FDA[27,37,46,63,197,202]. Cellular pathways influenced by CK2 include gene expression and signaling pathways but also auto-degradative pathways like the proteasome system and autophagy[176].

CK2 was reported to have conflicting roles in autophagy regulation. It was described to be required for the specific degradation of mitochondria via autophagy[92] and to target specific proteins for autophagic degradation[74]. CK2 has further been published to induce autophagy in response to calorie restriction[140] and to be implicated in the delivery of excess protein aggregates to autophagosomes when the proteasome is impaired or overloaded[182]. Conversely, inhibition of CK2 has been shown to induce autophagic flux, with the proposed underlying mechanism stating that CK2 activates the Akt-mTOR axis, which in turn inhibits autophagy[83].

In summary, the protein kinase CK2 plays a major role in a number of different malignancies and influences many cellular pathways, including autophagy. However, the precise role played by CK2 in autophagy and the underlying molecular mechanisms are currently incompletely understood and require further study.

1.3. Autophagy in (infectious) diseases

In addition to its role in maintaining cellular homeostasis, autophagy is increasingly recognized as an essential part of innate immune defenses.

As autophagy interconnects many other pathways in the cell, it is no surprise that dysregulation of autophagy characterizes a large number of diseases. For example, during metastasis, tumors benefit from elevated levels of autophagy as this counteracts detachment-induced apoptosis and increases the motility of the metastatic tumor cell[21]. Increased autophagy levels can further help meet the high energy demand of cancer cells and assist in evading recognition by the immune system[189] e.g. by degrading granzyme B and thus avoiding NK cell-mediated cell death[4]. Low levels of autophagic turnover, e.g. caused by aging, can contribute to malignancies as well. When autophagy fails to degrade misfolded proteins, including, for example, amyloid beta, they accumulate intracellularly, contributing to neurodegeneration[133,139]. Mutation of the autophagy receptor p62 has further been linked

to familial amyotrophic lateral sclerosis (ALS) and is suspected of playing a role in removing pathogenic misfolded proteins[171].

Recently, autophagy has been appreciated for its integral role in the defense against microbial pathogens. The degradation of viruses or viral components is the direct anti-viral impact of autophagy. In addition, PAMPs are revealed from viral capsids through autophagic degradation and exposed to pattern recognition receptors (PRRs) such as toll-like receptors (TLRs)[13] to trigger further immunity cascades. Peptide fragments of pathogen proteins generated by autophagic degradation can also be presented on major histocompatibility complex (MHC)-class molecules to assist the adaptive immune response[137]. However, many successful pathogens, such as viruses, have developed mechanisms to suppress autophagy or evade it and, in some cases, even subvert parts of the autophagy machinery to benefit their own replication. For example, human parainfluenza virus type 3 (HPIV3) inhibits the fusion of autophagosomes and lysosomes by interfering with the formation of the trans-SNARE complex using its phosphoprotein P[36]. Both herpes simplex virus type 1 (HSV-1) and human cytomegalovirus (HCMV) encode proteins that block Beclin-1, thereby simultaneously inhibiting induction of autophagy and decreasing autophagic degradation[20,130,136]. Coronaviruses like the mouse hepatitis virus (MHV) have evolved to use autophagosome-like double-membrane vesicles (DMVs) to facilitate genome replication and evade detection by the innate immune system[58,146]. Poliovirus is known to increase DMV formation and, in parallel LC3 lipidation[8]. Flaviviruses, such as dengue virus (DENV) and zika virus (ZIKV), are described to use ER-derived membranes for their replication[16,29,61,143], and ZIKV is known to activate autophagy initiation with its non-structural protein 4A[107]. Finally, influenza A virus (IAV) uses its M2 ion channel to redirect LC3 to the plasma membrane[7,200], and a highly pathogenic strain of IAV has been shown to induce autophagy to promote its replication[114].

In summary, autophagy is an integral part of innate immune defenses against viruses, but its dysregulation is also involved in the pathogenesis of many diseases, including infectious diseases. However, successful viruses have evolved strategies to evade restriction by autophagy and often even hijack parts of the autophagy machinery to facilitate their replication.

1.4. SARS-CoV-2

The severe acute respiratory syndrome coronavirus 2 (SARS-CoV-2) is the causative agent of the COVID-19 pandemic and has caused tremendous social and economic damage around the world. As of now, more than 615 million COVID-19 cases have been reported worldwide, and over 6.5 million deaths have been associated with SARS-CoV-2 infection. As a member of the coronavirus family, SARS-CoV-2 is an enveloped virus with a ~30 kilobase (kb) positive single-strand RNA genome. The *in vivo* tropism of SARS-CoV-2 is defined by the surface glycoprotein spike (S) that mediates binding to its receptor angiotensin converting enzyme 2 (ACE2). ACE2 is present on cells in many tissues, including the lungs, colon, and heart[104]. SARS-CoV-2 is mainly recognized as a respiratory virus initially infecting cells of the upper and lower respiratory tract, which is also the main infection route, with the potential for causing lung damage. However, viremia spreads to the gut and heart, eventually leading to cytokine storms and/or multiple organ failure in severe cases of COVID-19[190,196]. Public health measurements and the rapid development of vaccines have dampened the impact of the COVID-19 pandemic. However, emerging variants of SARS-CoV-2 are increasingly able to escape antibody-mediated neutralization[49]. The severity of the associated diseases, is nonetheless still drastically reduced by vaccination[79].

SARS-CoV-2 expresses 30 proteins from its 15 open reading frames (ORFs)[56] (Fig. 3). The polyproteins encoded by ORF1ab are auto-proteolytically processed into 16 non-structural proteins (Nsp) with functions including the formation of the replicase-transcriptase complex and the defense against anti-viral host pathways. Four separate ORFs encode the structural proteins S, envelope (E), membrane (M), and nucleocapsid (N) that are part of the virion. Finally, the remaining ten ORFs code for accessory proteins that improve viral fitness and shape the host environment.

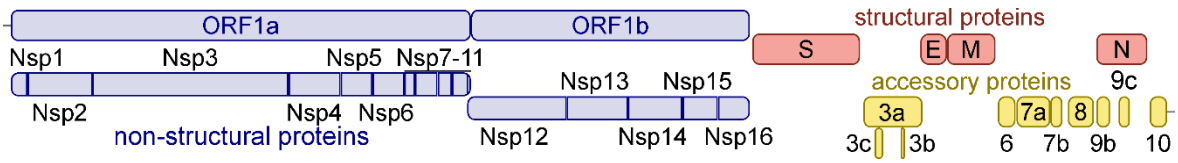


Figure 3: Schematic depiction of the genome organization of SARS-CoV-2. SARS-CoV-2 expresses 30 proteins from 15 ORFs. The polyproteins encoded by ORF1ab are auto-proteolytically processed into 16 Nsps (Nsp1-16). Four ORFs encode the structural proteins of SARS-CoV-2 (S, E, M and N) and the remaining 10 ORFs encode accessory proteins (ORF3a-10).

1.4.1. Interplay between SARS-CoV-2 and the innate immune system

To escape restriction by the human innate immune system, many proteins of SARS-CoV-2 antagonize the activity of the anti-viral defenses. Innate immune pathways are counteracted by non-structural, structural, and accessory proteins of SARS-CoV-2[65,99]. For example, Nsp1 has been shown to inhibit host translation by binding to and plugging the ribosome, effectively counteracting any defense pathways that rely on translation[172], such as the interferon (IFN) system. Nsp5 has been shown to reduce the efficiency of interferon induction by inhibiting the innate immune sensors retinoic acid-inducible gene I (RIG-I) and targeting the essential adaptor mitochondrial antiviral-signaling protein (MAVS) for degradation[111,185], and Nsp15 achieves the same by interfering with the activation of the transcription factor interferon regulatory factor 3 (IRF3)[56]. N is described to inhibit both immune sensor activation and interferon signaling[134], dampening both interferon induction and signaling. Likewise, M and ORF3a decrease the activation of signal transducer and activator of transcription 1 (STAT1)[101,181], a crucial transcription factor that mediates the upregulation of hundreds of anti-viral genes, and ORF7a prevents efficient activation of STAT2[186]. ORF3a has further been shown to reduce autophagic flux[126]. Taken together, SARS-CoV-2 has a repertoire of multifunctional proteins at its disposal that shape the host environment to favor virus replication and prevent restriction by the immune system.

The interplay between SARS-CoV-2 and autophagy has been in the spotlight since the beginning of the COVID-19 pandemic. Early on, hydroxychloroquine (an inhibitor of autophagic turnover) was making headlines as a potential treatment for COVID-19[109]. Of note, the observed inhibition of SARS-CoV-2 replication *in vitro* might not be related to hydroxychloroquine's effects on autophagy but rather caused by inhibiting virus entry through raising endosomal pH levels[160]. Hydroxychloroquine has since been dropped as a treatment for COVID-19 due to a lack of efficacy in patients[28]. The interest in autophagy modulators to treat SARS-CoV-2 infection, on the other hand, has remained. Generally, SARS-CoV-2 is considered mostly autophagy resistant, but it is moderately affected by treatment with autophagy-inducing drugs, especially in the early stages of replication[65]. Coronaviruses are further known to use parts of the autophagy machinery and autophagosomes to facilitate their replication machinery, cellular egress and likely avoid detection by PRRs[22,54,58,146]. As SARS-CoV-2 is described to use the lysosomal route for egress[22,54], interfering with lysosome trafficking and autophagy could further reduce virus release from infected cells. Thus, both autophagy induction and autophagy inhibition have

the potential to aid in combating SARS-CoV-2. Accordingly, autophagy modulating drugs[40,199], such as niclosamide[15,51] and Rapamycin[71,142], have all been suggested as potential treatments for COVID-19.

As stated before, coronaviruses are known to hijack parts of the autophagy machinery to facilitate their replication. In line with this, SARS-CoV-2 has been shown to reduce autophagy initiation and block autophagic turnover[51,65,90]. Part of this is mediated by its ORF3a protein, which sequesters VPS39, a core component of the HOPS complex[126]. The HOPS complex is required to bridge the autophagosomal and lysosomal membrane and is critically involved in the assembly of the trans-SNARE complex. Thus, the sequestration mediated by ORF3a impairs autophagosome-lysosome fusion and subsequent degradation of the cargo. However, which other viral proteins are employed by SARS-CoV-2 to control autophagy and the underlying molecular mechanisms remain unknown.

1.5. Measuring autophagy

Autophagy induction is mediated by modifications on the protein level rather than a transcriptional response[193], making typical promotor-based reporter assays and RT-qPCR incompatible with autophagy quantification. Despite that, an extensive repertoire of methods to measure autophagy is available[87]. While autophagosomes can be directly identified as double-membrane vesicles in electron microscopy[44], most other methods rely on a set of established hallmarks of autophagy. One of these hallmarks is the degradation of autophagy markers, such as the autophagy receptor p62 or the autophagosome-associated LC3B-II. This hallmark can be used to observe autophagic flux directly. Changes in the degradation rate of p62 can, for example, be detected in Western blot by using specific antibodies[128]. An alternative is to express reporter proteins that fuse a fluorescent protein to the autophagy marker and thus allow the use of flow cytometry as a readout[97,161]. The approaches using antibodies can be adapted easily to a wide range of cells, while the use of reporter proteins allows rapid quantification via flow cytometry, albeit with high background and thus low sensitivity. Another hallmark of autophagy is the processing of LC3B and the association of LC3B-II with autophagosomes[100]. In these systems, LC3B-II abundance can be used to estimate the number of autophagosomes and thus indicate changes in autophagic flux. In Western blot, the relative amount of the hydrophobic LC3B-II (lipidated form) can be quantified as it has a shorter retention time than LC3B/-I (non-lipidated forms) and thus is detected at a lower “weight”[170]. Autophagosomes decorated with eGFP-LC3B-II can further be visualized as eGFP-puncta in fluorescence microscopy[78], allowing their quantification.

Finally, eGFP-LC3B-II bound to autophagosomal membranes can be isolated from soluble LC3B/-I in a permeabilization and washing step, allowing its quantification in flow cytometry[43,81]. These approaches allow quantification of changes in autophagic flux with high sensitivity. However, they cannot easily distinguish between an increase in autophagy induction and a block of autophagosome degradation, as both result in increased autophagosome numbers. The final hallmark commonly used to measure autophagy is the acidification of autophagosomes after fusion with a lysosome. These late steps of autophagy directly precede degradation of the cargo, and analysis of this hallmark gives valuable mechanistic insights into defects in fusion or acidification. An elegant way to visualize the acidification in autolysosomes makes use of a reporter fusion protein that links LC3B to a pH sensitive eGFP and a pH resistant mCherry[85,138]. This way, eGFP signal is lost in autolysosomes after acidification, while the mCherry signal is retained. Alternatively, dyes specific for acidic organelles, such as CytoID or Lysotrackers, can be used to measure the abundance of acidic autolysosomes[57], albeit with varying specificity for autolysosomes depending on the employed dye. The fusion rate of autophagosomes and lysosomes can further be measured by analyzing the colocalization of autophagosome markers, such as LC3B, and lysosome markers, such as lysosome-associated membrane glycoprotein 1 (LAMP1)[17,159]. These approaches are most valuable to characterize defects in acidification of autolysosomes or the fusion steps and provide clues to the mechanism.

Due to the associated labor, most methods mentioned above, such as Western blot or manual fluorescence microscopy, are not feasible for rapid quantification. Automated fluorescence microscopy, on the other hand, can be combined with automated analysis of the acquired images to achieve high throughput at reasonable costs. However, the specialized equipment and proprietary software required for such an approach often make it unfeasible. A lack of specificity or high per sample cost renders dyes specific for acidic organelles unsuitable for high throughput approaches. The low sensitivity of approaches measuring the degradation of autophagy markers in flow cytometry makes them unfavorable. Thus, we currently lack the means to specifically, rapidly, and cost-effectively quantify autophagy for large-scale analyses of drugs and autophagy-modulating cellular and viral proteins.

2. Scientific aims

Autophagy is a crucial part of cellular homeostasis through mediating lysosomal degradation of aggregated proteins and obsolete organelles, as well as acting as a source of nutrients in starvation conditions. Dysregulation of autophagy is associated with many malignancies, including cancer and neurodegenerative diseases. Thus, its activity needs to be tightly controlled. In addition, autophagy is emerging as an important part of the innate immune defenses. For example, autophagy can mediate the degradation of viral components and expose PAMPs to trigger downstream anti-viral signaling. Accordingly, successful viral pathogens have evolved mechanisms to evade restriction by autophagy and, in some cases, use parts of the autophagy machinery to their benefit.

In order to identify and characterize novel host and viral proteins that regulate autophagy, the first aim of this thesis was to establish an accessible and easy-to-set-up method for quantifying autophagy that allows rapid but exact analysis of large sample sizes and mutational analysis by protein overexpression. The next aim was to use this method to determine which SARS-CoV-2 proteins manipulate autophagy to evade restriction. This thesis's third aim was to identify and characterize novel host factors among the TRIM family of proteins that keep autophagy in check. Altogether, the overall goal of my PhD thesis was to improve our understanding of cellular autophagy regulation and yield novel insights into immune evasion by SARS-CoV-2.

3. Material

3.1. Key resource table

Table 2: Key resource table.

Reagent or Resource	Source	Identifier
Antibodies		
anti-GFP: Anti-GFP antibody	abcam	ab290; RRID:AB_303395
anti-CK2α: Casein Kinase 2 alpha antibody	GeneTex	GTX107897; RRID:AB_1950048
anti-CK2α': Anti-CSNK2A2 antibody	abcam	ab10474; RRID:AB_297214
anti-LC3: Monoclonal mouse anti-LC3α/β antibody, G-4	Santa Cruz Biotechnology	sc-398822; RRID:AB_2877091
anti-β-actin: Monoclonal mouse anti-β-actin antibody, AC-15	Sigma-Aldrich	A5441; RRID:AB_476744
anti-p62: Anti-SQSTM1 / p62 antibody [2C11]	abcam	ab56416; RRID:AB_945626
anti-FLAG: Monoclonal mouse anti-FLAG-tag antibody, M2	Sigma-Aldrich	F1804; RRID:AB_262044
anti-Beclin-1: Polyclonal rabbit anti-Beclin-1 antibody	Cell Signaling Technology	3738S; RRID:AB_490837
anti-ULK1: Monoclonal rabbit anti-ULK1 antibody, D8H5	Cell Signaling Technology	8054S; RRID:AB_11178668
anti-HA: HA-Tag (C29F4) Rabbit mAb	Cell Signaling Technology	3724S; RRID:AB_1549585
anti-V5: Monoclonal rabbit anti-V5-tag antibody, D3H8Q	Cell Signaling Technology	13202S; RRID:AB_2687461
anti-Strep II: Monoclonal mouse anti-strep II-tag antibody, 517	Novus Biologicals	NBP2-43735; RRID:AB_2916323
anti-LAMP1: Monoclonal rabbit anti-LAMP1 antibody, D2D11	Cell Signaling Technology	90919; RRID:AB_2687579
IRDye 800CW Donkey anti-Mouse IgG Secondary Antibody	LI-COR	926-32212; RRID:AB_621847

Reagent or Resource	**Source**	**Identifier**
IRDye 800CW Donkey anti-Rabbit IgG Secondary Antibody	LI-COR	926-32213; RRID:AB_621848
IRDye 680RD Donkey anti-Mouse IgG Secondary Antibody	LI-COR	926-68072; RRID:AB_10953628
IRDye 680RD Donkey anti-Rabbit IgG Secondary Antibody	LI-COR	926-68073; RRID:AB_10954442
anti-mouse-AF568: Goat anti-Mouse IgG (H+L) Cross-Adsorbed Secondary Antibody, Alexa Fluor 568	Invitrogen	A-11004; RRID:AB_2534072
anti-rabbit-AF568: Goat anti-Rabbit IgG (H+L) Cross-Adsorbed Secondary Antibody, Alexa Fluor 568	Invitrogen	A-11011; RRID:AB_143157
anti-mouse-AF488: Goat anti-Mouse IgG (H+L) Cross-Adsorbed Secondary Antibody, Alexa Fluor 488	Invitrogen	A-11001; RRID:AB_2534069
anti-rabbit-AF647: Goat anti-Rabbit IgG (H+L) Cross-Adsorbed Secondary Antibody, Alexa Fluor 647	Invitrogen	A-21244; RRID:AB_2535812
anti-mouse-AF647: Goat anti-Mouse IgG (H+L) Cross-Adsorbed Secondary Antibody, Alexa Fluor 647	Invitrogen	A-21235; RRID:AB_2535804
Recombinant DNA		
pBABE-puro mCherry-EGFP-LC3B	Addgene, Jayanta Debnath[132]	22418; RRID:Addgene_22418
pBOB-eGFP-LC3B	Konstantin Sparrer and Lennart Koepke[91]	N/A

Reagent or Resource	Source	Identifier
pCSC-SP-PW-GFP	Addgene, Inder Verma[119]	12337; RRID:Addgene_12337
pEGFP-N1_hTRIM32	Addgene, Martin Dorf[47]	69541; RRID:Addgene_69541
pIRES_CK2α'-HA	This thesis	N/A
pIRES_FLAG	This thesis	N/A
pIRES_FLAG-TRIM2	This thesis	N/A
pIRES_TRIM2ΔRING-FLAG	This thesis	N/A
pIRES_TRIM32-FLAG	Konstantin Sparrer and Lennart Koepke[91]	N/A
pIRES_TRIM3-FLAG	This thesis	N/A
pIRES_TRIM3ΔRING-FLAG	This thesis	N/A
pIRES_TRIM45-FLAG	This thesis	N/A
pIRES_TRIM56-FLAG	This thesis	N/A
pIRES_TRIM71-FLAG	This thesis	N/A
pIRES_V5-CK2β	This thesis	N/A
pLVX-EF1alpha-2xStrep-IRES-Puro	David Gordon and Nevan Krogan[56]	N/A
pLVX-EF1alpha-nCoV2019-E-2xStrep-IRES-Puro	David Gordon and Nevan Krogan[56]	N/A
pLVX-EF1alpha-nCoV2019-M-2xStrep-IRES-Puro	David Gordon and Nevan Krogan[56]	N/A
pLVX-EF1alpha-nCoV2019-N-2xStrep-IRES-Puro	David Gordon and Nevan Krogan[56]	N/A
pLVX-EF1alpha-nCoV2019-Nsp10-2xStrep-IRES-Puro	David Gordon and Nevan Krogan[56]	N/A
pLVX-EF1alpha-nCoV2019-Nsp11-2xStrep-IRES-Puro	David Gordon and Nevan Krogan[56]	N/A
pLVX-EF1alpha-nCoV2019-Nsp12-2xStrep-IRES-Puro	David Gordon and Nevan Krogan[56]	N/A

Reagent or Resource	**Source**	**Identifier**
pLVX-EF1alpha-nCoV2019-Nsp1-2xStrep-IRES-Puro	David Gordon and Nevan Krogan[56]	N/A
pLVX-EF1alpha-nCoV2019-Nsp13-2xStrep-IRES-Puro	David Gordon and Nevan Krogan[56]	N/A
pLVX-EF1alpha-nCoV2019-Nsp14-2xStrep-IRES-Puro	David Gordon and Nevan Krogan[56]	N/A
pLVX-EF1alpha-nCoV2019-Nsp15-2xStrep-IRES-Puro	David Gordon and Nevan Krogan[56]	N/A
pLVX-EF1alpha-nCoV2019-Nsp16-2xStrep-IRES-Puro	David Gordon and Nevan Krogan[56]	N/A
pLVX-EF1alpha-nCoV2019-Nsp2-2xStrep-IRES-Puro	David Gordon and Nevan Krogan[56]	N/A
pLVX-EF1alpha-nCoV2019-Nsp4-2xStrep-IRES-Puro	David Gordon and Nevan Krogan[56]	N/A
pLVX-EF1alpha-nCoV2019-Nsp5-2xStrep-IRES-Puro	David Gordon and Nevan Krogan[56]	N/A
pLVX-EF1alpha-nCoV2019-Nsp6-2xStrep-IRES-Puro	David Gordon and Nevan Krogan[56]	N/A
pLVX-EF1alpha-nCoV2019-Nsp7-2xStrep-IRES-Puro	David Gordon and Nevan Krogan[56]	N/A
pLVX-EF1alpha-nCoV2019-Nsp8-2xStrep-IRES-Puro	David Gordon and Nevan Krogan[56]	N/A
pLVX-EF1alpha-nCoV2019-Nsp9-2xStrep-IRES-Puro	David Gordon and Nevan Krogan[56]	N/A
pLVX-EF1alpha-nCoV2019-Orf10-2xStrep-IRES-Puro	David Gordon and Nevan Krogan[56]	N/A
pLVX-EF1alpha-nCoV2019-Orf3a-2xStrep-IRES-Puro	David Gordon and Nevan Krogan[56]	N/A
pLVX-EF1alpha-nCoV2019-Orf3c-2xStrep-IRES-Puro	David Gordon and Nevan Krogan[56]	N/A
pLVX-EF1alpha-nCoV2019-Orf6-2xStrep-IRES-Puro	David Gordon and Nevan Krogan[56]	N/A

Reagent or Resource	Source	Identifier
pLVX-EF1alpha-nCoV2019-Orf7a-2xStrep-IRES-Puro	David Gordon and Nevan Krogan[56]	N/A
pLVX-EF1alpha-nCoV2019-Orf7b-2xStrep-IRES-Puro	David Gordon and Nevan Krogan[56]	N/A
pLVX-EF1alpha-nCoV2019-Orf8-2xStrep-IRES-Puro	David Gordon and Nevan Krogan[56]	N/A
pLVX-EF1alpha-nCoV2019-Orf9b-2xStrep-IRES-Puro	David Gordon and Nevan Krogan[56]	N/A
pLVX-EF1alpha-nCoV2019-Orf9c-2xStrep-IRES-Puro	David Gordon and Nevan Krogan[56]	N/A
pLVX-EF1alpha-nCoV2019-S-2xStrep-IRES-Puro	David Gordon and Nevan Krogan[56]	N/A
pMD2.G	Addgene, Didier Trono	12259; RRID:Addgene_12259
pMDLg	Addgene, Didier Trono[41]	12251: RRID:Addgene_12251
pMXS-hs-3xHA-LIN-41	Addgene, Shinya Yamanaka[184]	52717; RRID:Addgene_52717
pRS2	Addgene, David Litchfield[177]	27093; RRID:Addgene_27093
pRSV-Rev	Addgene, Didier Trono[41]	12253; RRID:Addgene_12253
pTwist_ 3xFLAG_optTRIM2	Twist Biosciences	N/A
pTwist_ 3xFLAG_optTRIM3	Twist Biosciences	N/A
pTwist_ 3xFLAG_optTRIM3-S661A	This thesis	N/A
pTwist_ 3xFLAG_optTRIM3-SS83-84AA	This thesis	N/A
pTwist_ 3xFLAG_optTRIM3-T40A	This thesis	N/A
pTwist_ 3xFLAG_optTRIM71	Twist Biosciences	N/A
pZW16	Addgene, David Litchfield[177]	27087; RRID:Addgene_27087

Reagent or Resource	**Source**	**Identifier**
pZW6	Addgene, David Litchfield[177]	27086; RRID:Addgene_27086
TRIM3 cDNA clone	SourceBioscience	IRALp962D0162Q
Cell lines and viruses		
HEK293T	ATCC	CRL3216; RRID:CVCL_0063
HEK293T GL (eGFP-LC3B)	Konstantin Sparrer and Lennart Koepke[91], this thesis	N/A
HEK293T mGL (mCherry-eGFP-LC3B)	Konstantin Sparrer	N/A
HeLa	ATCC	CCL-2; RRID:CVCL_0030
HeLa GL (eGFP-LC3B)	Konstantin Sparrer and Lennart Koepke[91], this thesis	N/A
Calu-3	Manfred Frick	RRID:CVCL_0609
Caco-2	Holger Barth	RRID:CVCL_0025
BetaCoV/France/IDF0372/2020	European Virus Archive, Virus stocks were provided and handled by Rayhane Nchioua	014V-03890
Oligonucleotides and siRNAs		
CK2a'f: 5'-AGC TAG CGC CCT CGA GGC CAC CAT GCC CGG CCC GGC-3'	Biomers	N/A

Reagent or Resource	**Source**	**Identifier**
CK2a'r: 5'-GGC GGA ATT GGG CTA GAG CGG CCG CTT AAG CGT AAT CTG GAA CGT CAT ATG GAT AGG ATC CTG CAT AGT CCG GGA CGT CAT AGG GAT AGC CCG CAT AGT CAG GAA CAT CGT ATG GGT ATC GTG CTG CCG TGA GAC CA-3'	Biomers	N/A
CK2bf: 5'-GGC AGC TAG CGC CCT CGA GGC CAC CAT GGG TAA GCC TAT CCC TAA CCC TCT CCT CGG TCT CGA TTC TAC GGG CGG CGG CGG GAG CGG AGG AGG TGG AAG CAG CAG CTC AGA GGA GGT GT-3'	Biomers	N/A
CK2br: 5'-GGG CGG AAT TGG GCT AGA GCG GCC GCT CAG CGA ATC GTC TTG ACT-3'	Biomers	N/A
GLf: 5'-GTG GGA TCC GCC ACC ATG GTG AGC AAG GGC GAG GAG CTT CAC C-3'	Biomers	N/A
GLr: 5'-CGC GTT TAA AC TTA CAC TGA CAA TTT CAT-3'	Biomers	N/A
N-Forward primer: 5'-TAA TCA GAC AAG GAA CTG ATT A-3'	Biomers	N/A
N-Probe: 5'-FAM-GCA AAT TGT GCA ATT TGC GG-TAMRA-3'	Biomers	N/A
N-Reverse primer: 5'-CGA AGG TGT GAC TTC CAT G-3'	Biomers	N/A
siGENOME Human ATG12 siRNA	Horizon Discovery	M-010212-02-0005
siGENOME Human ATG3 siRNA	Horizon Discovery	M-015375-01-0005
siGENOME Human ATG4A siRNA	Horizon Discovery	M-005789-01-0005

Reagent or Resource	**Source**	**Identifier**
siGENOME Human ATG5 siRNA	Horizon Discovery	M-004374-04-0005
siGENOME Human ATG7 siRNA	Horizon Discovery	M-020112-01-0005
siGENOME Human ATG9A siRNA	Horizon Discovery	M-014294-02-0005
siGENOME Human TRIM2 siRNA	Horizon Discovery	M-006955-00-0005
siGENOME Human TRIM3 siRNA	Horizon Discovery	M-006931-00-0005
siGENOME Human TRIM71 siRNA	Horizon Discovery	M-023459-01-0005
siGENOME Human ULK1 siRNA	Horizon Discovery	M-005049-00-0005
siGENOME Non-Targeting siRNA Control Pool #2	Horizon Discovery	D-001206-14-20
T2dRf: 5'-GAG CTC GAG GCC ACC ATG TGT CTG CAC ACT TTC TGC GAG AGG-3'	Biomers	N/A
T2dRr: 5'-CTC ACG CGT TTA CTG TAA GTA TCG ATA G-3'	Biomers	N/A
T2f: 5'-GCT CTT AAG GCA GCT AGC GCC CTC GAG GCC ACC ATG GAC TAC AAG GAC GAC GAT GAC AAG ACG CGT GCA TCT AGA CAC AGG AGT GGC CGT TAT G-3'	Biomers	N/A
T2r: 5'-GGG GCG GAA TTG GGC TAG AGC GGC CGC TCA CTG TAA GTA TCG ATA GAC TTT GAA ACA G-3'	Biomers	N/A
T32f: 5'-GCT CTT AAG GCA GCT AGC GCC CTC GAG GCC ACC ATG GCT GCA GCA GC-3'	Biomers	N/A
T32r: 5'-CTT GTA GTC TCT AGA TGC ACG CGT TGG GGT GGA ATA TCT TC-3'	Biomers	N/A
T3-40f: 5'-GTG CCT GCA CGC CTT CTG CGA-3'	Biomers	N/A

Reagent or Resource	**Source**	**Identifier**
T3-40r: 5’-GGC AGC ACC TTA GGA CAC TG-3’	Biomers	N/A
T3-661f: 5’-CAA GTT CGG CGC CCA TGG CGA AG-3’	Biomers	N/A
T3-661r: 5’-AAC AGG AAC TCG CCA TCA-3’	Biomers	N/A
T3-83f: 5’-TTT CTT CAT CGC CGC CCT GAT GGA AGC CAT GCA GC-3’	Biomers	N/A
T3-83r: 5’-TTG TTT TGC AGG GCG CTT-3’	Biomers	N/A
T3dRf: 5’-GCT CTT AAG GCA GCT AGC GCC CTC GAG GCC ACC ATG GAG AGA TGT CTC C-3’	Biomers	N/A
T3dRr: 5’-CCT TGT AGT CTC TAG ATG CAC GCG TCT GGA GGT AGC GAT AGG C-3’	Biomers	N/A
T3f: 5’-GCT CTT AAG GCA GCT AGC GCC CTC GAG GCC ACC ATG GCA AAG AGG GAG G-3’	Biomers	N/A
T3r: 5’-CCT TGT AGT CTC TAG ATG CAC GCG TCT GGA GGT AGC GAT AGG C-3’	Biomers	N/A
T45f: 5’-AGC TCT TAA GGC AGC TAG CGC CCT CGA GGC CAC CAT GTC AGA AAA C-3’	Biomers	N/A
T45r: 5’-GTA GTC TCT AGA TGC ACG CGT GAG AGC CAC AGT CCT AAG-3’	Biomers	N/A

Reagent or Resource	Source	Identifier
T56f: 5'-TCT TAA GGC AGC TAG CGC CCT CGA GGC CAC CAT GGT TTC CCA CGG GT-3'	Biomers	N/A
T56r: 5'-TCC TTG TAG TCT CTA GAT GCA CGC GTA CTG TCC GGA GAA CGG A-3'	Biomers	N/A
T71f: 5'-GCT CTT AAG GCA GCT AGC GCC CTC GAG GCC ACC ATG GCT TCG TTC CCC G-3'	Biomers	N/A
T71r: 5'-CCT TGT AGT CTC TAG ATG CAC GCG TGA AGA CGA GGA TTC-3'	Biomers	N/A
Reagents and kits		
Anti-FLAG M2 Magnetic Beads	Merck	M8823
Bafilomycin A1	Santa Cruz Biotechnology	sc-201550
BamHI-HF	New England BioLabs	R3136S
Blocker Casein in PBS	Thermo Scientific	37528
CellTiter-Glo Luminescent Cell Viability Assay	Promega	G7570
Chloroquine	Santa Cruz Biotechnology	sc-205629
CycLex CK2(Casein kinase II) Kinase Assay/Inhibitor Screening Kit	Biozol	MBL-CY-1170
DABCO	Carl Roth	0718
DAPI (4',6-Diamidino-2-Phenylindole, Dihydrochloride)	Invitrogen	D1306
Diethiothreitol (DTT)	Thermo Scientific	R0862
DNA Ligation Kit Ver.2.1	Takara Bio	
Dulbecco's Modified Eagle Medium	Gibco	41965039

Reagent or Resource	Source	Identifier
ethylenediaminetetraacetic acid (EDTA)	Sigma-Aldrich	E9884
Fetal Bovine Serum, qualified	Gibco	10270106
Glycerol	Sigma-Aldrich	G5516
HCl	VWR	20252
HEPES	Sigma-Aldrich	H3375
Immobilon-FL PVDF membrane	Millipore	05317-10EA
InSolution Rapamycin	Sigma-Aldrich	553211
L-Glutamine 200 mM	PAN Biotech	P04-80050
Lipofectamine LTX with Plus Reagent	Invitrogen	15338100
Lipofectamine RNAiMAX Transfection Reagent	Invitrogen	13778075
Lysotracker Deep Red	Invitrogen	L12492
MEM Non-Essential Amino Acids Solution (100X)	Gibco	11140050
MES-SDS running buffer (20X)	Alfa Aesar	J62138.K2
Minimum Essential Medium Eagle	Sigma-Aldrich	M4655
MluI-HF	New England BioLabs	R3198S
Mowiol 4-88	Carl Roth	0713
NaCl	Merck	106404
NEBuilder HiFi DNA Assembly	New England BioLabs	E5520S
NotI-HF	New England BioLabs	R3189S
NuPAGE 4 to 12 % Bis-Tris gel	Invitrogen	NP0321BOX
Opti-MEM	Gibco	31985070
Orange G	Sigma-Aldrich	O3756
Paraformaldehyde solution 4% in PBS	Santa Cruz Biotechnology	sc-281692
Passive Lysis 5X Buffer	Promega	E1941

Reagent or Resource	**Source**	**Identifier**
Penicillin-Streptomycin, 10,000 U/ml Penicillin, 10 mg/ml Streptomycin	PAN Biotech	P06-07100
Phosphate-Buffered Saline (PBS)	Gibco	14190144
Phusion High-Fidelity PCR Kit	Thermo Scientific	F553L
Pierce Rapid Gold BCA Protein Assay Kit	Thermo Scientific	A53225
PmeI	New England BioLabs	R0560S
Polyethylenimine, branched	Sigma-Aldrich	408727
Poly-L-lysine solution 0.1 % (w/v) in H_2O	Sigma-Aldrich	P8920
Protease Inhibitor Cocktail powder	Sigma-Aldrich	P2714
Q5 Site-Directed Mutagenesis Kit	New England BioLabs	E0554S
Revert 700 Total Protein Stain Kit	LI-COR	926-11016
Saponin	Sigma-Aldrich	47036
Semi dry blot transfer buffer (10X)	Alfa Aesar	J63664.K3
Silmitasertib (CX-4945)	Selleckchem	S2248
Sodium Dodecyl Sulfate (SDS)	Sigma-Aldrich	822050
Sodium Pyruvate 100 mM	Gibco	11360070
Synthetic SARS-CoV-2-RNA	Twist Bioscience	102024
TaqMan Fast Virus 1-Step Master Mix	Thermo Fisher	4444436
TransIT-LT1 Transfection Reagent	Mirus	MIR 2300
Tris	AppliChem GmbH	A2264
Triton X-100	Sigma-Aldrich	T8787
Trypsin 0.05 %/EDTA 0.02 % in PBS, w/o: Ca and Mg	PAN Biotech	P10-023100
Tween 20	Sigma-Aldrich	P9416
UltraPure DNase/RNase-Free Distilled Water	Invitrogen	10977015
Viral RNA Mini Kit	Qiagen	52906

Reagent or Resource	**Source**	**Identifier**
Whatman filter paper (0.34 mm thick)	VWR	588-3148
XhoI	New England BioLabs	R0146S
Devices		
Cytoflex LX	Beckman Coulter	N/A
FACSAria III	BD Biosciences	N/A
FACSCanto II	BD Biosciences	N/A
Zeiss Axiovert 40 CFL	Zeiss	N/A
LI-COR Odyssey	LI-COR	N/A
Orion II microplate Luminometer	Berthold	N/A
PerfectBlue SemiDry Blotter	VWR	700-1220
StepOnePlus Real-Time PCR System	Applied Biosystems	N/A
Zeiss LSM 710	Zeiss	N/A
Software		
Prism 9	GraphPad Software	https://www.graphpad.com
ImageJ (Fiji)	N/A	https://imagej.net/Fiji
Eukaryotic Linear Motif resource for Functional Sites in Proteins[94]	N/A	http://elm.eu.org
Corel Draw 2021	Corel Corporation	https://www.coreldraw.com
Microsoft Office Professional Plus 2019	Microsoft	https://www.microsoft.com
LI-COR Image Studio Version 5.2	LI-COR	https://www.licor.com
LI-COR Image Studio Lite Version 5.0.21	LI-COR	https://www.licor.com
Huygens Professional 19.10	Scientific Volume Imaging	https://www.svi.nl

3.2. Buffers and media

Table 3: Buffers

Buffer	Components	Comments
TM-lysis buffer	150 mM NaCl, 5 mM HEPES, 1 % (v/v) Triton X-100, 5 mM EDTA, and 0.2 % (v/v) Protease Inhibitor Cocktail dissolved in water	Adjust pH to 7.4 and store at 4 °C. Add Protease Inhibitor Cocktail immediately before use.
6x loading dye for western blot	187.5 mM Tris-HCL (pre-adjusted to pH 6.8), 75 % (v/v) Glycerol, 6 % (w/v) SDS and 0.3 % (w/v) Orange G dissolved in water	Dissolve everything except Glycerol at 37 °C, then add Glycerol and mix at 37 °C. Aliquots are stored at -20 °C.
DTT stock solution (10x)	1 M DTT dissolved in water	Filter the solution using a 0.45 µm sterile filter and store aliquots at -20 °C.
PBS-T	0.2 % (v/v) Tween 20 dissolved in PBS	Use for 1 week.
Mowiol mounting medium[201]	10 % (w/v) Mowiol 4-88, 25 % (w/v) Glycerol, 50 % (v/v) Tris-HCl (at 0.2 mM, pre-adjusted to pH 8.5) and 2.5 % (w/v) DABCO dissolved in water	Mix Mowiol 4-88 and Glycerol, then add water and leave at RT for several hours. Add Tris-HCL and stir at 50 °C. After the Mowiol 4-88 is dissolved, centrifuge at 5,000 g for 15 min and add DABCO. Aliquots are stored at -20 °C.

Table 4: Cell culture media

Medium name	**Components**
DMEMxxx	Dulbecco's Modified Eagle Medium (DMEM) supplemented with 10 % (v/v) fetal bovine serum (FBS), 100 U/ml penicillin, 100 µg/ml streptomycin and 2 mM L-glutamine
Calu-3 medium	Minimum Essential Medium Eagle supplemented with 10 % (v/v) FBS (during viral infection) or 20 % (v/v) FBS (during all other times), 100 U/ml penicillin, 100 µg/ml streptomycin, 1 mM sodium pyruvate, and 1x non-essential amino acids
Caco-2 medium	DMEM containing 10 % (v/v) FBS, 100 U/ml penicillin, 100 µg/ml streptomycin, 2 mM L-glutamine, 1 mM sodium pyruvate, and 1x non-essential amino acids

4. Methods

4.1. Cloning

pBABE-puro mCherry-EGFP-LC3B was a gift from Jayanta Debnath (Addgene, #22418[132]). pCSC-SP-PW-GFP (aka: pBOB-GFP) was a gift from Inder Verma (Addgene, #12337[119]). The ORF of eGFP-LC3B was subcloned into the pBOB-GFP vector replacing the GFP ORF. The insert was amplified by PCR using the Phusion High-Fidelity PCR Kit according to the manufacturer's instructions with the primers GLf and GLr purchased from Biomers. The insert was digested with BamHI and PmeI restriction enzymes. The pBOB-GFP vector was linearized with BamHI and PmeI restriction enzymes. The insert and linearized vector were ligated using the DNA Ligation Kit Ver.2.1 according to the manufacturer's instructions.

A plasmid containing TRIM2 was a kind Gift from Adolfo García-Sastre. The ORF of TRIM2 was subcloned into the pIRES_FLAG vector using NEBuilder HiFi DNA Assembly according to the manufacturer's instructions. The insert was amplified by PCR using the Phusion High-Fidelity PCR Kit according to the manufacturer's instructions with the primers T2f and T2r purchased from Biomers. The pIRES_FLAG vector was linearized with NotI and MluI restriction enzymes.

A cDNA clone of TRIM3 was purchased from SourceBioscience. The ORF of TRIM3 was subcloned into the pIRES_FLAG vector using NEBuilder HiFi DNA Assembly according to the manufacturer's instructions. The insert was amplified by PCR using the Phusion High-Fidelity PCR Kit according to the manufacturer's instructions with the primers T3f and T3r purchased from Biomers. The pIRES_FLAG vector was linearized with NotI and MluI restriction enzymes.

pMXS-hs-3xHA-LIN-41 was a gift from Shinya Yamanaka (Addgene, #52717[184]). The ORF of TRIM71 was subcloned into the pIRES_FLAG vector using NEBuilder HiFi DNA Assembly according to the manufacturer's instructions. The insert was amplified by PCR using the Phusion High-Fidelity PCR Kit according to the manufacturer's instructions with the primers T71f and T71r purchased from Biomers. The pIRES_FLAG vector was linearized with NotI and MluI restriction enzymes.

pEGFP-N1_hTRIM32 was a gift from Martin Dorf (Addgene, #69541[47]). The ORF of TRIM32 was subcloned into the pIRES_FLAG vector using NEBuilder HiFi DNA Assembly according to the manufacturer's instructions. The insert was amplified by PCR using the Phusion High-Fidelity PCR Kit according to the manufacturer's instructions with the primers T32f and T32r purchased from Biomers. The pIRES_FLAG vector was linearized with NotI and MluI restriction enzymes.

A plasmid containing the transcript variant 2 of TRIM45 was a kind Gift from Walther Mothes. The ORF of TRIM45 was subcloned into the pIRES_FLAG vector using NEBuilder HiFi DNA Assembly according to the manufacturer's instructions. The insert was amplified by PCR using the Phusion High-Fidelity PCR Kit according to the manufacturer's instructions with the primers T45f and T45r purchased from Biomers. The pIRES_FLAG vector was linearized with NotI and MluI restriction enzymes.

A plasmid containing TRIM56 was a kind Gift from Walther Mothes. The ORF of TRIM56 was subcloned into the pIRES_FLAG vector using NEBuilder HiFi DNA Assembly according to the manufacturer's instructions. The insert was amplified by PCR using the Phusion High-Fidelity PCR Kit according to the manufacturer's instructions with the primers T56f and T56r purchased from Biomers. The pIRES_FLAG vector was linearized with NotI and MluI restriction enzymes.

pIRES_FLAG-TRIM2ΔRING was generated using pIRES_FLAG_TRIM2 as a template. The truncated insert was amplified by PCR using the Phusion High-Fidelity PCR Kit according to the manufacturer's instructions with the primers T2dRf and T2dRr purchased from Biomers. The insert was digested with XhoI and MluI restriction enzymes. The pIRES_FLAG vector was linearized with XhoI and MluI restriction enzymes. The insert and linearized vector were ligated using the DNA Ligation Kit Ver.2.1 according to the manufacturer's instructions.

pIRES_TRIM3ΔRING-FLAG was generated using pIRES_TRIM3_FLAG as a template and NEBuilder HiFi DNA Assembly according to the manufacturer's instructions. The truncated insert was amplified by PCR using the Phusion High-Fidelity PCR Kit according to the manufacturer's instructions with the primers T3dRf and T3dRr purchased from Biomers. The pIRES_FLAG vector was linearized with NotI and MluI restriction enzymes.

pZW16 (CK2alpha') was a gift from David Litchfield (Addgene, #27087[177]). The ORF of CK2α' was subcloned into the pIRES_HA vector using NEBuilder HiFi DNA Assembly according to the manufacturer's instructions. The insert was amplified by PCR using the Phusion High-Fidelity PCR Kit according to the manufacturer's instructions with the primers CK2a'f and CK2a'r purchased from Biomers. The pIRES_HA vector was linearized with NotI and MluI restriction enzymes.

pRS2 (CK2alpha', CK2beta) was a gift from David Litchfield (Addgene, #27093[177]). The ORF of CK2β was subcloned into the pIRES_V5 vector using NEBuilder HiFi DNA Assembly according to the manufacturer's instructions. The insert was amplified by PCR using the Phusion High-Fidelity PCR Kit according to the manufacturer's instructions with the primers CK2bf and CK2br purchased from Biomers. The pIRES_V5 vector was linearized with NotI and MluI restriction enzymes.

pTwist_ 3xFLAG_optTRIM3 was purchased from Twist Biosciences. The T40A mutation was introduced using the Q5 Site-Directed Mutagenesis Kit according to the manufacturer's instructions. The PCR was performed with the primers T3-40f and T3-40r purchased from Biomers.

pTwist_ 3xFLAG_optTRIM3 was purchased from Twist Biosciences. The SS83-84AA mutation was introduced using the Q5 Site-Directed Mutagenesis Kit according to the manufacturer's instructions. The PCR was performed with the primers T3-83f and T3-83r purchased from Biomers.

pTwist_ 3xFLAG_optTRIM3 was purchased from Twist Biosciences. The S661A mutation was introduced using the Q5 Site-Directed Mutagenesis Kit according to the manufacturer's instructions. The PCR was performed with the primers T3-661f and T3-661r purchased from Biomers.

4.2. Cell culture and media

All cells were kept in ventilated cell culture flasks at 37 °C, 90 % relative humidity and 5 % CO_2. All cell lines were kept in their respective medium (see Table 5).

Table 5: Cell line-specific media.

Cell line	**Medium**
HEK293T	DMEMxxx
HEK293T GL	DMEMxxx
HEK293T mCherry-eGFP-LC3B	DMEMxxx
HeLa	DMEMxxx
HeLa GL	DMEMxxx
Calu-3	Calu-3 medium
Caco-2	Caco-2 medium

4.3. Transient transfection of cell lines

The Cells were seeded to reach a confluency of 60-80 % for transfection (e.g. 150,000 HEK293T GL cells per well in a 24-well plate in 400 µl DMEMxxx seeded the day before transfection). The scaling of the DNA amount and volume used for transfection in different plate sizes is shown in Table 6.

Table 6: Transfection in different plate sizes.

Plate size	**DNA amount per well**	**Total volume transfection-mix per well**
96-well	Up to 0.14 µg	17 µl
48-well	Up to 0.48 µg	60 µl
24-well	Up to 0.83 µg	100 µl
12-well	Up to 1.53 µg	200 µl
6-well	Up to 4.19 µg	500 µl

4.3.1. Transfection using polyethylenimine (PEI)

Plasmid DNA was suspended in ½ volume of Opti-MEM per well, and in parallel, PEI (2 µg PEI per 1 µg plasmid DNA, stock solution 1 µg/µl) was suspended in ½ volume of Opti-MEM for each well. Both suspensions were mixed 1:1. After incubation at RT for 20 min, 1 volume transfection mix was added to each well carefully without disturbing the monolayer. The medium can be replaced with fresh medium after 4-6 h. However, this is not mandatory.

4.3.2. Transfection using TransIT-LT1

Plasmid DNA was suspended in ½ volume of Opti-MEM per well, and in parallel, TransIT-LT1 transfection reagent (3 µl transfection reagent per 1 µg plasmid DNA) was suspended in ½ volume of Opti-MEM for each well. Both suspensions were mixed 1:1. After incubation at RT for 30 min, 1 volume transfection mix was added to each well carefully without disturbing the monolayer. The medium can be replaced with fresh medium after 6-16 h. However, this is only recommended if necessary.

4.3.3. Transfection using Lipofectamine LTX plus

Plasmid DNA was suspended in ½ volume Opti-MEM per well and Plus reagent (2 µl Plus reagent per 1 µg plasmid DNA) was added to the DNA solution. In parallel, Lipofectamine LTX transfection reagent (2 µl transfection reagent per 1 µg plasmid DNA) was suspended in ½ volume Opti-MEM for each well. Both suspensions were mixed 1:1. After incubation at RT for 5 min, 1 volume transfection mix was added to each well carefully without disturbing the monolayer. The medium can be replaced with fresh medium after 6-8 h. However, this is not mandatory. Transfection with Lipofectamine LTX plus was used to transfect HeLa and HeLa GL cells.

4.4. siRNA mediated knock down

To knock down endogenous proteins, cells were transfected with siRNA using Lipofectamine RNAiMAX. The cells were seeded to reach a confluency of 60-80 % for transfection (e.g. 75,000 HeLa GL cells per well in 400 µl DMEMxxx seeded the day before transfection). siRNA was diluted in ½ volume of Opti-MEM per well, and in parallel, RNAiMAX reagent was diluted in ½ volume of Opti-MEM per well. The solutions were mixed 1:1 and incubated at RT for 5 min. One volume transfection mix was carefully added to each well without disturbing the monolayer. The cells were further processed for analysis 48-72 h post-transfection. Scaling for different plate sizes is listed in Table 7.

Table 7: siRNA transfection in different plate sizes

Plate size	siRNA amount per well	RNAiMAX reagent per well	Total volume transfection-mix per well
96-well	0.8 pmol	0.25 µl	9 µl
48-well	2.9 pmol	0.87 µl	30 µl
24-well	5.0 pmol	1.50 µl	50 µl
12-well	9.2 pmol	2.76 µl	100 µl
6-well	25.3 pmol	7.58 µl	250 µl

4.5. Generation of transgenic cell lines

4.5.1. 3rd generation lentiviral particles

HEK293T cells were seeded in 6-well plates in 2 ml DMEMxxx using 900,000 cells per well and cultured overnight. The cells were transfected with pBOB-eGFP-LC3B (1.75 µg per well) and the three helper plasmids pMDLg (0.87 µg per well), pRSV-Rev (0.44 µg per well), pMD2.G (0.5 µg per well) using PEI transfection as described in section 4.3.1. 4-6 h after the transfection, the medium was replaced with 2 ml DMEMxxx. 48 h after the transfection, the lentiviral particles were harvested by taking the supernatant, pelleting the cell debris by centrifugation (2,500 g for 3 min), and filtering the supernatants through 0.45 µm filters. The cleared lentiviral stocks were stored at -80 °C.

4.5.2. Transduction of target cell lines and FACS sorting into clonal cell lines

The target cell lines (e.g. HEK293T or HeLa) were seeded in 6-well plates in 1.7 ml medium using 1 million cells per well. 300 µl lentiviral stock was added to the target cells, followed by culturing for 72 h. The transduced cells were washed with PBS once and detached using trypsin (37 °C for 5 min). The cells were then washed again by adding 1 ml PBS, pelleting the cells by centrifugation (300 g for 3 min), and discarding the supernatant. Next, the cells were suspended in 1 ml PBS and sorted by fluorescence activated cell sorting (FACS). Cells showing a medium eGFP-LC3B expression were sorted into 96-well F-bottom plates containing 200 µl DMEMxxx targeting one cell per well. The single cells were expanded into clonal cell lines, and reporter expression was verified before preparing cryo-stocks for storage at -80 °C.

4.6. Fluorescence microscopy

To visually assess reporter expression in clonal cell lines growing in 12-well plates, eGFP expression was visualized using a fluorescence microscope, and images of the brightfield and eGFP signal were recorded with the attached camera.

4.7. Whole cell lysates (WCL)

To generate WCL, cells were detached either via trypsin (37 °C for 5 min) or by scratching and collected in 1.5 ml reaction tubes in PBS. The cells were pelleted by centrifugation (4°C, 300 g for 3 min) and the supernatant was discarded. Next, the cells were washed with cold PBS by adding 1 ml cold PBS, pelleting by centrifugation (4°C, 300 g for 3 min), and discarding the supernatant. 100-300 µl TM-lysis buffer was added to the cells. They were vortexed for 20 s and incubated on ice for 10 min. Then, the lysates were cleared by centrifugation (4°C, 20,000 g for 20 min). The cleared supernatants were carefully transferred to a 1.5 ml reaction tube without disturbing the cell debris in the pellet. The protein concentrations of the lysates were measured using the Pierce Rapid Gold BCA Protein Assay Kit according to the manufacturer's instructions and adjusted. For Western blot analysis, 6x loading dye and dithiothreitol (DTT) stock solution were added to a final concentration of 1x and 0.1 M, respectively, and the WCL were stored at -20 °C.

4.8. Sodium dodecyl sulfate polyacrylamide gel electrophoresis (SDS-PAGE)

WCLs were heated to 95 °C for 10 min to denature the contained proteins. A NuPAGE 4 to 12 % Bis-Tris gel was placed into a running chamber filled with MES-SDS running buffer as per instructions. The WCLs were loaded into the pockets of the gel at 5-25 µg protein per lane. The gels were then run at constant voltage (80 V) for 2 h.

4.9. Western blot

The separated proteins were transferred from the Bis-Tris gel onto a PVDF-membrane by Western blotting. Whatman filter paper stacks (6 sheets per stack) and a PVDF-membrane were cut to size. The PVDF-membrane was first briefly activated in 100 % methanol for 1 min and then equilibrated in 1x semi dry blot transfer buffer. The Whatman filter paper stacks were equilibrated in 1x semi dry blot transfer buffer for at least 10 min as well. The NuPAGE 4 to 12 % Bis-Tris gel was removed from the chamber and the plastic housing and equilibrated in 1x semi dry blot transfer buffer for at least 10 min. After equilibration, a

western blot sandwich was assembled by placing a Whatman filter paper stack on the anode of the PerfectBlue SemiDry Blotter followed by the PVDF-membrane, the gel and a second Whatman filter paper stack. To avoid the formation of bubbles and remove excess transfer buffer a roller was used to even out the assembled sandwich. Next, the cathode lid was placed onto the sandwich and fixed in place. To avoid short circuits by excess transfer buffer, the blotter was tilted to one side, allowing the buffer to flow into the side channel. Blotting was performed at a constant voltage (30 V) for 30 min.

4.10. Staining and immunodetection

After blotting, the PVDF-membrane was fully dried at 37 °C for 10 min. It was then reactivated in 100 % methanol for 1 min and washed in PBS for 5 min. Next, the PVDF-membrane was stained using the Revert 700 total protein stain kit according to the manufacturer's instructions. After measuring total protein and de-staining, the PVDF-membrane was blocked in 25 ml Blocker Casein in PBS for 1 h at RT. Following blocking, the PVDF-membrane was incubated with the primary antibody (see Table 8) diluted in PBS-T with 0.1 % casein for 1.5 h at RT or at 4 °C overnight on a rotator. Subsequently, the PVDF-membrane was washed three times with PBS-T for 5 min and then incubated in IRDye secondary antibody diluted 1:20,000 in PBS-T with 0.1 % Casein for 0.5 h, followed by three washing steps with PBS-T. The fluorescent antibodies were then detected using an LI-COR odyssey and the Image Studio software. Quantification and image processing were performed using the Image Studio lite software.

Table 8: Dilution of antibodies for Western blot and fluorescence microcopy staining.

Antibody	**Dilution in Western blot**	**Dilution in confocal microscopy**
anti-GFP	1:1,000	
anti-LC3	1:200	
anti-β-actin	1:5,000	
anti-p62	1:1,000	
anti-FLAG	1:10,000	1:400
anti-Beclin-1	1:1,000	
anti-ULK1	1:1,000	
anti-HA	1:1,000	1:200
anti-V5	1:1,000	1:200
anti-CK2α	1:1,000	
anti-CK2α'	1:1,000	
anti-Strep II	1:1,000	1:200
anti-LAPM1		1:200
anti-rabbit-AF647		1:400
anti-mouse-AF647		1:400
anti-rabbit-AF568		1:400
anti-mouse-AF568		1:400
anti-mouse-AF488		1:400

4.11. Confocal laser scanning microscopy

To enhance adherence to the coverslips, they can be coated with poly-L-lysine by incubating them with poly-L-Lysine solution at 37 °C for 30 min followed by drying them at 37 °C for 5 min. The cells were seeded on glass coverslips in 24-well plates in 500 µl medium at approximately 100,000 cells per well. The cells were then transfected or treated according to the respective experiment (as indicated in the figures). 24-72 h after seeding, the cells were prepared for microscopic analysis. To this end, the cells were carefully washed twice with ice-cold PBS and fixed in 4 % paraformaldehyde (PFA) in PBS for 20 min at RT. Next, the cells were washed three times with PBS, and blocked and permeabilized by incubating them in 0.5 % Triton X-100, 5 % FBS in PBS for 30 min at RT. The cells were then washed twice using PBS followed by incubation with 150 µl primary antibody (see Table 8) diluted in PBS at 4 °C for 2 h. After incubation, the cells were washed three times with PBS and incubated with 150 µl secondary antibody (see Table 8) and 4',6-Diamidino-2-Phenylindole, Dihydrochloride (DAPI) (1:1,000) diluted in PBS at 4 °C for 2 h. Finally, the cells were washed three times with PBS and once with deionized water. The glass coverslips were mounted on microscopy slides using self-hardening Mowiol mounting medium. After drying at 4 °C overnight, the samples were analyzed using a Zeiss LSM 710 confocal microscope. The Images were processed using the ImageJ software.

4.12. Quantification of autophagy in confocal microscopy images

To quantify autophagy in images acquired in confocal microscopy, the autophagosome area per cell was analyzed. HeLa GL or HEK293T GL cells were treated as described in section 4.11, and the acquired images were analyzed in ImageJ. First, the GFP channel was separated from the other channels. Next, the background was subtracted using a rolling ball radius of 3, and the image was smoothed. An automatic threshold was applied to the image using the "Moments" threshold algorithm and assuming a dark background. Finally, the area of a cell was selected by hand, and the particles inside the area were analyzed using the "analyze particles" function. The total area of the particles was used as a measure to estimate autophagy. To give robust results, at least 30 individual cells were analyzed per sample. Instead of selecting the area of individual cells, the entire image can be analyzed for GFP particle area. In those cases, multiple images were analyzed, and it was assured that cell density was consistent between the different images. The macros used with (Fiji Is Just) ImageJ 2.3.0 are shown in Table 9.

Table 9: ImageJ macros used for the quantification of autophagosome pixel area.

```
macro "Process [q]" //q as the hotkey
{
      run("Split Channels"); //split channels
      close(); //close first additional channel
      close(); //close second additional channel
      run("Subtract Background...", "rolling=3");//subtract background
      run("Smooth"); //smooth background
      run("Threshold...");
      setAutoThreshold("Moments dark"); //apply Threshold
}

macro "Analyze particles [w]" //w as the hotkey
{
      run("Analyze Particles...", "clear summarize"); //analyze
      particles and display summary
}
```

4.13. Quantification of total and acidified autophagosomes in confocal microscopy

HEK293T mCherry-eGFP-LC3B cells were grown on poly-L-lysine coated coverslips in 24-well plates and transiently transfected using PEI, as described in section 4.3.1. The cells were treated and stained for the transfected proteins, as described in section 4.11. In the acquired images, puncta showing both mCherry and eGFP fluorescence (autophagosomes) and puncta showing only mCherry fluorescence (acidified autophagosomes/ autolysosomes) were counted. Their sum was calculated to obtain the total number of autophagosomes, and the ratio of acidified to non-acidified autophagosomes was evaluated.

4.14. Colocalization analysis in confocal microscopy

HEK293T GL cells were seeded for confocal microscopy analysis and transiently transfected using TransIT-LT1 transfection as described in section 4.3.2. The cells were stained for the transfected proteins and LAMP1, as described in section 4.11. The pictures were analyzed for colocalization of eGFP-LC3B and LAMP1 with the Huygens Professional software using the Colocalization Analyzer Advanced module. The correct channels were selected for analysis, the threshold was estimated using the Costes method, and a transfected cell was selected as the region of interest. Finally, the colocalization was computed, and the Pearson coefficient was recorded as a measure of colocalization.

4.15. Reverse transfection of cells – 96-well format

HEK293T GL cells were transiently transfected in 96-well format using reverse transfection with PEI. To this end, 140 ng plasmid DNA was suspended in 8.5 µl Opti-MEM per well in a 96-well F-bottom plate. 0.325 µg PEI (2.5 µg PEI per 1 µg plasmid DNA) was diluted in 8.5 µl Opti-MEM per well. Both solutions were combined 1:1 and mixed by vortexing. After incubation of the transfection mix at RT for 20 min, 45,000 detached HEK293T GL cells in 83 µl DMEMxxx were added to each well and gently mixed. The next day, the medium was replaced with 100 µl fresh DMEMxxx. 48 h post-transfection, the cells were harvested for further analysis.

4.16. Rapid quantification of autophagosomes by flow cytometry – 96-well format

After treatment or transfection of GL reporter cells in 96-well format, the cells were harvested by removing the medium and detaching them using 50 µl trypsin per well (37 °C for 5 min). The detached cells were suspended in 100 µl FBS supplemented medium to inactivate the trypsin and transferred to 96-well V-bottom plates. Following centrifugation (4 °C, 300 g for 3 min), the supernatant was discarded. The cells were washed by suspending them in 150 µl PBS supplemented with 1 % FBS, pelleting them by centrifugation (4 °C, 300 g for 3 min), and discarding the supernatant. The cells were then suspended in 100 µl PBS containing 0.05 % saponin and incubated at 4 °C for 10 min. Subsequently, the cells were washed twice as before. Next, the cells were fixed by incubating them in 100 µl 4 % PFA in PBS at RT for 30 min. The cells were then pelleted by centrifugation (4 °C, 300 g for 3 min), the supernatant was discarded, and the cells were suspended in 100 µl PBS supplemented with 1 % FBS and stored at 4 °C until analysis. Following fixation, the cells

could be stained by incubating them in 50 µl PBS supplemented with the primary antibody (anti-FLAG 1:400, anti-V5 1:200; anti-HA 1:200) at RT for 30 min. The cells were then washed as before and incubated in 50 µl PBS supplemented with the secondary antibody (anti-mouse-AF647 1:400; anti-rabbit-AF647 1:400) at RT for 30 min. After washing, the stained cells were suspended in 100 µl PBS supplemented with 1 % FBS and stored at 4 °C until analysis.

4.17. Comparing fixation methods for quantification of autophagy

To compare fixation methods, 50,000 HeLa GL cells per well were seeded in a 96-well F-bottom plate. The next day, the cells were treated with Rapamycin (1 µM) or Chloroquine (10 µM) for 4 h and then treated as described in section 4.16, stopping before the fixation step. The cells were then fixed with one of three methods: (I) The cells were left without fixation. (II) The cells were fixed by incubation in 100 µl 1 % PFA in PBS at RT for 20 min. They were then pelleted by centrifugation (4 °C, 300 g for 3 min), the supernatant was discarded, and the cells were suspended in 100 µl PBS supplemented with 1 % FBS for analysis. (III) The cells were fixed by incubation in 100 µl -20 °C, 100 % methanol at -20 °C for 20 min. They were then pelleted by centrifugation (4 °C, 300 g for 3 min), the supernatant was discarded, and the cells were suspended in 100 µl PBS supplemented with 1 % FBS for analysis. All samples were analyzed immediately after fixation using a FACSCanto II.

4.18. Quantification of autophagosomes by flow cytometry – 24-well format

After treatment or transfection in 24-well format, the cells were harvested by removing the medium and detaching them using 100 µl trypsin per well (37 °C for 5 min). The detached cells were suspended in 500 µl FBS supplemented medium to inactivate the trypsin and transferred to round bottom tubes. Following centrifugation (4 °C, 300 g for 3 min), the supernatant was discarded, and the cells were washed by suspending them in 1 ml PBS supplemented with 1 % FBS, pelleting them by centrifugation (4 °C, 300 g for 3 min) and discarding the supernatant. Subsequently, the cells were suspended in 100 µl PBS containing 0.05 % saponin and incubated at 4 °C for 10-20 min. Then, the cells were washed twice as before. The cells were fixed by incubating them in 100 µl 4 % PFA in PBS at RT for 30 min. The cells were then pelleted by centrifugation (4 °C, 300 g for 3 min), the supernatant was discarded, and the cells were suspended in 100 µl PBS supplemented with 1 % FBS and stored at 4 °C until analysis. After fixation, the cells can be stained by incubating them in 50

µl PBS supplemented with the primary antibody (anti-FLAG 1:400, anti-V5 1:200; anti-HA 1:200) at RT for 30 min. The cells were then washed as before and incubated in 50 µl PBS supplemented with the secondary antibody (anti-mouse-AF647 1:400; anti-rabbit-AF647 1:400) at RT for 30 min. After a washing step, the cells were suspended in 100 µl PBS supplemented with 1 % FBS and stored at 4 °C until analysis.

4.19. Quantification of autophagosome acidification by flow cytometry

Autophagosome acidification was monitored in flow cytometry using HEK293T mCherry-eGFP-LC3B reporter cells. The cells were transfected using PEI as described in section 4.3.1 and treated as specified in the figure. The cells were prepared for measurement as described in section 4.16. The mCherry and eGFP MFI were measured using a Cytoflex LX flow cytometer. The quotient of eGFP MFI/mCherry MFI was used as a measure for autophagosome acidification.

4.20. Quantification of acidic organelles by flow cytometry

HEK293T cells were transfected using PEI as described in section 4.3.1. The controls were treated for 4 h with Bafilomycin A1 (100 nM), and the cells were stained with Lysotracker Deep Red (50 nM) for 2 h immediately before harvesting. 48 h post-transfection, the cells were detached in PBS, pelleted by centrifugation (4 °C, 300 g for 3 min), and suspended in PBS supplemented with 1 % FBS. The MFI of the Lysotracker Deep Red was measured using a FACSCanto II flow cytometer, and the average MFI of the empty vector control was subtracted from all samples.

4.21. RT-qPCR

SARS-CoV-2 N transcript levels were determined as a measure of virus yield. Supernatants of SARS-CoV-2 infected Calu-3 cells were collected 48 h post-infection. Total RNA was isolated using the Viral RNA Mini Kit according to the manufacturer's instructions. The primers targeting SARS-CoV-2 N (N-Forward, N-Probe, N-Reverse) were purchased from Biomers and dissolved in RNase-free water to a concentration of 10 µM. Synthetic SARS-CoV-2 RNA was used as a quantitative standard to obtain viral copy numbers. RT-qPCR reactions were performed using TaqMan Fast Virus 1-Step Master Mix and a StepOnePlus Real-Time PCR System (96-well format, fast mode), as shown in Table 10 and Table 11. All reactions were run in duplicates.

Table 10: RT-qPCR reaction setup.

Reagent	**Volume per reaction**
RNase free water	7.5 µl
TaqMan Fast Virus 1-Step (4X)	5 µl
Primer fwd (10 µM)	1 µl
Primer rev (10 µM)	1 µl
Probe (10 µM)	0.5 µl
RNA sample	5 µl

Table 11: RT-qPCR temperature steps.

Temperature	**Time (mm:ss)**	**# of cycles**
50 °C	05:00	1
95 °C	00:20	1
95 °C	00:05	40
60 °C	00:30	

4.22. Assessing cell viability by intracellular ATP levels

Calu-3 cells were seeded in 96-well F-bottom plates in 100 µl medium using 10,000 cells per well. The next day, the cells were treated with dilution series of autophagy modulating drugs and incubated for 8 h before the medium was replaced with fresh medium. Two days post-treatment, the cells were lysed in passive lysis buffer, and the metabolic activity was measured using the CellTiter-Glo Luminescent Cell Viability Assay according to the manufacturer's instructions and an Orion II microplate Luminometer. The procedure was selected to match the equivalent virus experiments.

4.23. Co-immunoprecipitation

To identify interaction partners and confirm their interaction, co-immunoprecipitation was performed. To this end, HEK293T cells were transiently transfected with the indicated expression plasmids using PEI, as described in section 4.3.1. 48 h post-transfection, the cells were harvested in ice-cold PBS and lysed in ice-cold TM-lysis buffer. The lysates were vortexed and incubated on ice for 10 min. Next, the lysates were cleared by centrifugation (4 °C, 15,000 g for 20 min), and the protein concentration of the lysates was determined using the Pierce Rapid Gold BCA Protein Assay Kit as per instructions. The protein concentrations were adjusted, and input samples were taken for later Western blot analysis. To prepare the magnetic beads, they were washed twice with ice-cold TM-lysis buffer using a magnetic rack and added to the cleared lysates. The lysates were incubated on the beads at 4 °C for 4 h on a rotor. Next, the supernatant was removed from the beads using a magnetic rack, and the beads were washed 5 times by adding ice-cold TM-lysis buffer, vortexing the beads for 1 min, and discarding the supernatant using a magnetic rack. Then, 100 µl of 1x SDS loading buffer (6x Loading dye diluted in TM-lysis buffer) was added to the beads, and the samples were heated to 95 °C for 10 min. The samples were then stored at -20 °C. When applicable, mass spectrometric analysis was performed by Sebastian Wiese at the Core Unit Mass Spectrometry and Proteomics at Ulm University. The proteins contained in the samples were identified, and their abundance was quantified using label-free quantification.

4.24. Measuring CK2 activity

CK2 activity was measured using the CycLex CK2 (Casein kinase II) Kinase Assay/Inhibitor Screening Kit. To this end, HEK293T cells were transiently transfected using PEI as described in section 4.3.1 in 6-well plates. 48 h post-transfection, the cells were lysed in 100 µl TM-lysis buffer, and the lysates were cleared by centrifugation (4 °C, 20,000 g for 20 min). The protein concentration of the lysates was measured using the Pierce Rapid Gold BCA Protein Assay Kit as per instructions and adjusted. Then, 10 µl cell lysate was transferred to the assay plate per well, and 10 µl TM-lysis buffer was added to the control wells. Next, 10 µl of CX-4945 (final conc. 25 µM) in TM-lysis buffer was added to the respective wells, and 10 µl TM-lysis buffer was added to the other wells. 80 µl of kinase buffer was added to all wells and the plate was incubated at 30 °C for 30 min. After the incubation, the wells were washed five times with 200 µl wash buffer, and then 100 µl of the HRP-conjugated antibody solution was added to each well. After incubation at RT for 30 min, the wells were washed five times with 200 µl wash buffer, and 100 µl substrate

reagent was added to each well. Following incubation at RT for 5-15 min, 100 µl stop solution was added to the wells, and the absorption at 450 nm was measured using an Orion II microplate Luminometer.

4.25. *In silico* prediction of putative CK2 phosphorylation sites

Using the Eukaryotic Linear Motif resource for Functional Sites in Proteins[94] putative CK2 phosphorylation sites in the amino acid sequences of TRIM2, TRIM3 and TRIM71 were identified. Among the predicted sites, 3 were chosen for closer investigation. The first one was conserved in TRIM2 and TRIM3 and located in the RING domain of the TRIMs. It was further predicted to be poorly accessible. The second putative phosphorylation site was chosen as it is conserved in TRIM2 and TRIM3 with a high score. It was located close to the RING domain. The final putative phosphorylation site was chosen as it had a high score and was conserved in both TRIM2 and TRIM3. The site was located in the NHL repeats and the corresponding serine was also found in TRIM71. There were no other putative phosphorylation sites in the TRIMs that were both highly scored and found in more than one of the TRIMs.

4.26. Statistical and bioinformatic analysis

Data were collected at least in triplicates (biological triplicates) for all flow cytometry-based approaches and with at least 30 replicates (cells) for fluorescence confocal microscopy-based approaches as indicated. For the relative comparison of two samples, statistical differences were assessed by unpaired t-test with Welch's correction. Results were graphed by Graph Pad Prism 9 and are displayed as means ± standard error of the mean (SEM) with individual values shown. P-values ≤ 0.05 were considered statistically significant. A p-value between 0.05 and 0.01 is annotated with *, p-values between 0.01 and 0.001 with **, and p-values below 0.001 with ***.

5. Results

5.1. Establishing a reporter system for rapid quantification of changes in autophagy

5.1.1. Construction of autophagy reporter cell lines and establishing of the autophagy reporter assay

Autophagosome-associated LC3B-II is a hallmark of autophagy and is commonly used to measure autophagosome abundance and, in extension, autophagic flux[170]. To generate reporter cell lines for rapid quantification of changes in autophagy utilizing this hallmark, we constructed HeLa and HEK293T cells stably expressing eGFP-LC3B (GL). HeLa cells were chosen as they are commonly used in the field of autophagy research[87] and HEK293T cells, as they are readily transfectable. A cassette coding for an eGFP-LC3B fusion protein under the control of a CMV promoter was inserted into the genome of the parental cells using a third-generation lentiviral delivery system[41] (Fig. 4A). Following the transduction of the target cell line, individual cells showing a medium eGFP-LC3B fluorescence were sorted into 96-well plates using FACS and grown into clonal cell lines. Expression of the reporter was confirmed in fluorescence microscopy (Fig. 4B) and via Western blot analysis using anti-LC3 and anti-GFP antibodies (Fig. 4C). In confocal microscopy, the eGFP-LC3B expressing cell lines showed an eGFP background and clear eGFP puncta (autophagosomes) in the cytoplasm (Fig. 4D). Degradation of p62 is a hallmark of autophagy[128], and protein levels in the generated reporter cell lines and their respective parental cell lines were determined by Western blot (Fig. 4E). The absence of changes in p62 levels between parental and eGFP-LC3B expressing cells indicates that basal autophagy was not altered in a major way by the introduction of the reporter expression cassette. To verify that autophagy behaves as expected upon modulation, the GL reporter cells were treated with commonly used autophagy modulatory drugs, and the response was analyzed[87]: Rapamycin inhibits mTORC1[148] and thereby increases autophagy induction in the cell, and concurrently the observed number of autophagosomes. Bafilomycin A1 inhibits the vacuolar type H^+-ATPase (V-ATPase)[88], thereby preventing the acidification of lysosomes and leading to the accumulation of autophagosomes/autolysosomes. Chloroquine accumulates in lysosomes and increases their pH[68], inhibiting the degradation of autophagic cargo and leading to the accumulation of autophagosomes/autolysosomes. In HeLa GL and HEK293T GL cells treated with Rapamycin (1 μM, overnight), more eGFP-LC3B puncta (=autophagosomes)

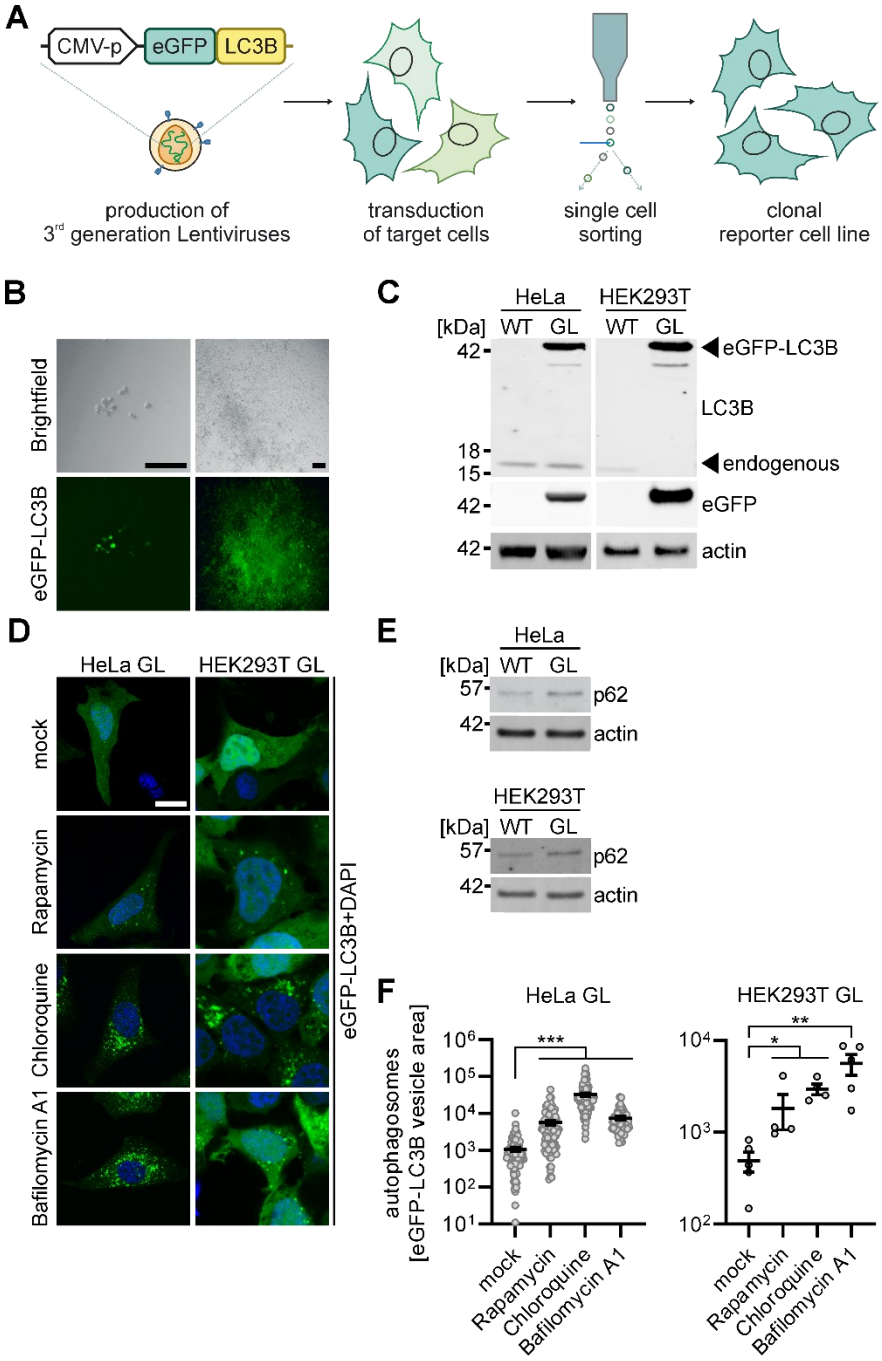


Figure 4: Generation of autophagy reporter cell lines. A) Schematic depiction of the generation of eGFP-LC3B reporter cell lines. An expression cassette for eGFP-LC3B was inserted into the genome of 3rd generation lentiviral particles which were used to transduce target cells. Single cells with a medium reporter expression were sorted into 96-well plates by FACS. The cells were expanded into clonal reporter cell lines. **B)** Brightfield and eGFP images of HeLa GL cells shortly after sorting and after expansion. Scale bar, 100 µm. **C)** Comparison of HeLa and HEK293T wildtype (WT) and GL cells. Immunoblotting shows expression of the eGFP-LC3B reporter and endogenous LC3B. **D)** Representative confocal microscopy images of HeLa GL and HEK293T GL cells either left untreated or treated with Rapamycin (1 µM), Chloroquine (10 µM) or Bafilomycin A1 (2.5 µM) overnight. Scale bar, 10 µm. **E)** Comparison of p62 levels in HeLa and HEK293T wildtype (WT) and GL cells by immunodetection. **F)** Quantification of samples shown in (D). For HeLa GL

cells the autophagosome (eGFP puncta) area per cell was quantified and for HEK293T GL cells the autophagosome (eGFP puncta) area was quantified for entire images with similar cell densities. Data are shown as mean ± SEM, n=49-102 (HeLa GL) and n=4-5 (HEK293T GL). Statistical significance of differences compared to the mock control was assessed using unpaired t-test with Welch's correction. *$p \leq 0.05$, **$p \leq 0.01$, ***$p \leq 0.001$. All experiments generating the shown data were performed and analyzed by myself. Data shown in figure panels B-F are modified from (Koepke et al., 2020)[91] (CC BY 4.0, https://creativecommons.org/licenses/by/4.0/).

were visible in the cytoplasm, as expected for increased autophagic flux. In line, a strong accumulation of autophagosomes was observed in cells from both reporter cell lines treated with either Chloroquine (10 µM, overnight) or Bafilomycin A1 (2.5 µM, overnight) (Fig. 4D). I used ImageJ and a custom macro to isolate and quantify the eGFP-LC3B puncta area. While the HEK293T GL cells were evenly distributed across the different images, this was not the case for the HeLa GL cells. Thus, the eGFP-puncta area per cell was quantified for the HeLa GL cells and the eGFP-puncta area for the entire image for the HEK293T GL cells. The quantification confirmed the visually observed phenotypes in both the HeLa GL and HEK293T GL cell lines for all three drug treatments (Fig. 4F). As measured in flow cytometry, the overall levels of eGFP-LC3B in the cells did not change significantly upon autophagy induction with Rapamycin (2 µM, 4 h) (Fig. 5A). Thus, to achieve rapid quantification of autophagosomes using MFI analysis by flow cytometry on a single cell level, the signal for membrane-associated eGFP-LC3B-II had to be isolated. To this end, cytosolic eGFP-LC3B/LC3B-I was removed from the cells by permeabilization with 0.05 % saponin in PBS and two subsequent washing steps, retaining only the membrane-associated eGFP-LC3B-II in the cells. The resulting eGFP MFI is then proportional to the number of autophagosomes. Consequently, treatment with Rapamycin (2 µM, 4 h) led to an eGFP MFI increase in the treated cells (Fig. 5A). The total eGFP signal was reduced by this treatment as background in the form of the surplus reporter was removed, and the size and granularity of the cells were altered as well (Fig. 5B). To improve stability of the treated cells and retain signal intensity in storage, we compared two fixation methods. Fixation with either methanol or paraformaldehyde retained the relative differences between untreated samples and samples treated with Rapamycin (1 µM, 4 h) or Chloroquine (10 µM, 4 h) (Fig. 5C). However, methanol fixation reduced the absolute eGFP-LC3B-II MFI. In contrast, paraformaldehyde did not affect the assay's sensitivity (Fig. 5C), indicating it as a preferred fixation method.

Taken together, I successfully generated autophagy reporter cell lines stably expressing eGFP-LC3B and verified that the transgene does not impact autophagy. To enable rapid quantification of autophagosomes, a flow cytometry-based method that quantifies the autophagosome bound eGFP-LC3B-II was established using stable cell lines.

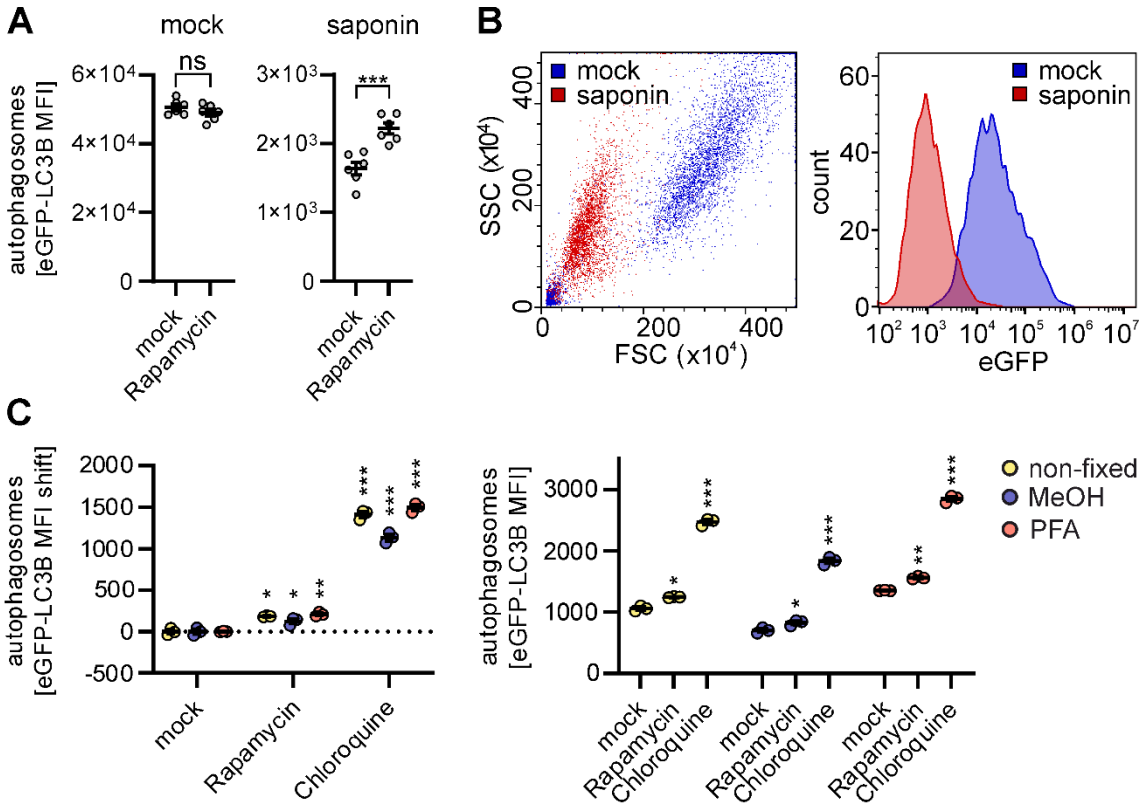


Figure 5: Establishing a flow cytometry-based assay to rapidly measure changes in autophagy. A) Left panel: eGFP-LC3B MFI of HeLa GL cells either left untreated or treated with Rapamycin (2 µM, 4 h). Right panel: eGFP-LC3B MFI of HeLa GL cells either left untreated or treated with Rapamycin (2 µM, 4 h) after treatment with 0.05 % saponin in PBS and subsequent washout. Data are shown as mean ± SEM, n=6. **B)** HeLa GL cells were either left untreated (mock, blue) or treated with 0.05 % saponin in PBS and subsequently washed out (saponin, red) and analyzed in flow cytometry. Left panel: changes in sideward scatter (SSC) and forward scatter (FSC). Right panel: shift of the eGFP fluorescence intensity. **C)** HeLa GL cells were either left untreated or treated with Rapamycin (1 µM, 4 h) or Chloroquine (10 µM, 4 h), treated with 0.05 % saponin in PBS and subsequently washed out. The cells were then either left untreated or fixed with methanol or PFA and analyzed in flow cytometry. Left panel: eGFP-LC3B-II MFI shift with the background (respective mock control) subtracted. Right panel: eGFP-LC3B-II MFI. Data are shown as mean ± SEM, n=3. Statistical significance of differences compared to the mock control was assessed using unpaired t-test with Welch's correction. *$p \leq 0.05$, **$p \leq 0.01$, ***$p \leq 0.001$, ns=not significant. All experiments generating the shown data were performed and analyzed by myself. Data shown in figure panels A-C are modified from (Koepke et al., 2020)[91] (CC BY 4.0, https://creativecommons.org/licenses/by/4.0/).

5.1.2. Application of the autophagy reporter assay

Rapamycin, Chloroquine, and Bafilomycin A1 are commonly used autophagy modulating compounds of which Rapamycin and Chloroquine are FDA-approved drugs with immunosuppressant properties[149,203]. We used them to verify the sensitivity and specificity of the flow cytometry-based assay. We treated HeLa GL and HEK293T GL cells with increasing concentrations of the three drugs and analyzed the cells in the reporter assay. I fitted curves (sigmoidal fit for Fig. 6A: left and right and B: middle and right; Hyperbola fit for Fig. 6A: middle, fits were chosen by the best coefficient of determination and plausibility) to calculate the required concentration to achieve a signal increase above 2x standard deviation (SD) of the mock control (Fig. 6A,B, red dotted line). For HeLa GL cells (Fig. 6A) the 2xSD concentrations were 61 nM for Rapamycin, 30 nM for Chloroquine and 32 nM for Bafilomycin A1. In HEK293T GL cells (Fig. 6B), treatment with 586 nM Chloroquine or 32 nM Bafilomycin A1 was calculated to achieve a signal above 2x SD of the mock control. Due to the limited range, no plausible fit was achieved for Rapamycin on HEK293T GL cells, but we observed that all concentrations down to 15.6 nM were sufficient to increase the signal above 2x SD of the mock control. These results further highlight the sensitivity of the reporter assay, as changes in autophagy by treatment with compounds at nM concentrations could be measured.

In addition to evaluating compound-screening approaches, I monitored the modulation of autophagy by overexpressed or depleted cellular proteins using the reporter assay. HeLa GL and HEK293T GL cells were transiently transfected with a construct expressing TRIM32, a known inducer of autophagic flux[34,35,166]. As TRIM32 is large enough (72 kDa) not to be removed during the saponin wash-out procedure, it was stained with antibodies to allow monitoring of autophagy modulation, specifically in TRIM32-expressing cells. In both cell lines, expression of TRIM32 led to a drastic increase in autophagosome number (Fig. 6C) compared to the vector control, demonstrating the applicability of the assay for this use. To assess the modulation of autophagy by cellular factors, core components of the autophagy machinery were depleted from HEK293T GL reporter cells by siRNA-mediated knock down. siRNAs targeting ULK1, ATG3, ATG4, ATG5, ATG7, ATG9, and ATG12 were employed. As expected, depletion of any of these factors resulted in a significant drop in the eGFP-LC3B-II MFI compared to the non-targeting control (Fig. 6D).

In summary, I confirmed that the flow cytometry-based reporter assay sensitively and accurately detects changes in autophagy mediated by treatment with compounds at nM concentrations and overexpression or depletion of cellular proteins.

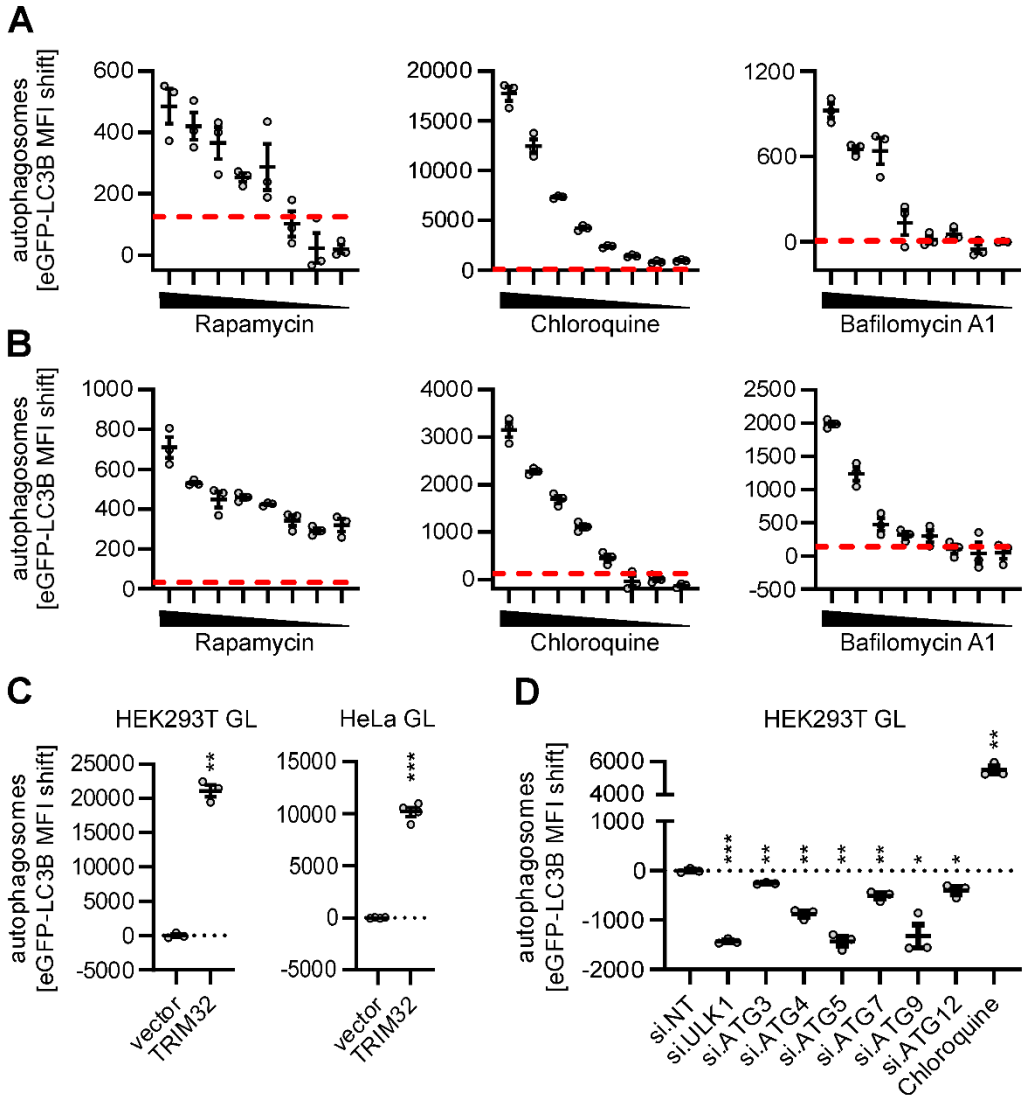


Figure 6: Application of the flow cytometry-based assay to measure changes in autophagy. eGFP-LC3B-II MFI shift of saponin treated and washed out **A)** HeLa GL and **B)** HEK293T GL cells treated with serial dilutions of Rapamycin (2 µM – 15 nM), Chloroquine (20 µM – 150 nM) or Bafilomycin A1 (625 nM – 5 nM) for 4 h. Red line: 2x SD of the untreated control. Data are shown as mean ± SEM, n=3. **C)** eGFP-LC3B-II MFI shift of flag-positive HeLa GL and HEK293T GL cells transfected with the indicated constructs, treated with saponin and washed out. Data are shown as mean ± SEM, n=3-4. **D)** eGFP-LC3B-II MFI shift of HEK293T GL cells that were transfected with the indicated siRNAs or treated with Chloroquine (10 µM, 4 h), treated with saponin and washed out. Data are shown as mean ± SEM, n=3. non-targeting siRNA (si.NT). Statistical significance of differences compared to the vector, untreated or si.NT control was assessed using unpaired t-test with Welch's correction. *$p \leq 0.05$, **$p \leq 0.01$, ***$p \leq 0.001$. The experiments generating the data shown in the figure panels A-B were performed and analyzed by Benjamin Winter. The experiments generating the data shown in the figure panels C-D were performed and analyzed by myself. Data shown in figure 6 are modified from (Koepke et al., 2020)[91] (CC BY 4.0, https://creativecommons.org/licenses/by/4.0/).

5.2. Manipulation of autophagy by SARS-CoV-2

Autophagy is an integral part of the human anti-viral innate immune defenses. Like virtually all successful viral pathogens, SARS-CoV-2, the causative agent of the COVID-19 pandemic, has evolved mechanisms to evade restriction by autophagy or hijack its machinery to benefit its replication[65,90,126].

5.2.1. Impact of autophagy on SARS-CoV-2

To understand how SARS-CoV-2 reacts to modulation of autophagy, Calu-3 cells were treated with Rapamycin or Bafilomycin A1 in increasing concentrations for 24 h and then infected with SARS-CoV-2 (MOI 0.05; strain: BetaCoV/France/IDF0372/2020). The concentrations for Rapamycin and Bafilomycin A1 were selected to ensure cell viability of over 70 % (Fig. 7A, bottom panel). 48 h post-infection, the copy number of SARS-CoV-2 N RNA was determined in the supernatants of the cells to quantify viral replication. Inhibition of autophagic degradation by Bafilomycin A1 maximally reduced the SARS-CoV-2 N RNA to 68 % compared to the untreated control (Fig. 7A, top panel). As the relatively modest impact of Bafilomycin A1 does not clearly exceed the effects the stimulation has on cell viability (down to 85-67 % viability at the same concentrations, selectivity index (SI)=1.25 at 0.5 nM), a clear anti-viral effect cannot be inferred from this data. Stimulation with Rapamycin, on the other hand, inhibits viral replication by over 2-fold (down to 36 % of the unstimulated control), exceeding the cytotoxic effects (74 % viability at the same concentrations, SI=2 at 0.5 µM). Thus, SARS-CoV-2 is mostly resistant to high autophagic flux and barely, if at all, affected by blocking autophagic turnover.

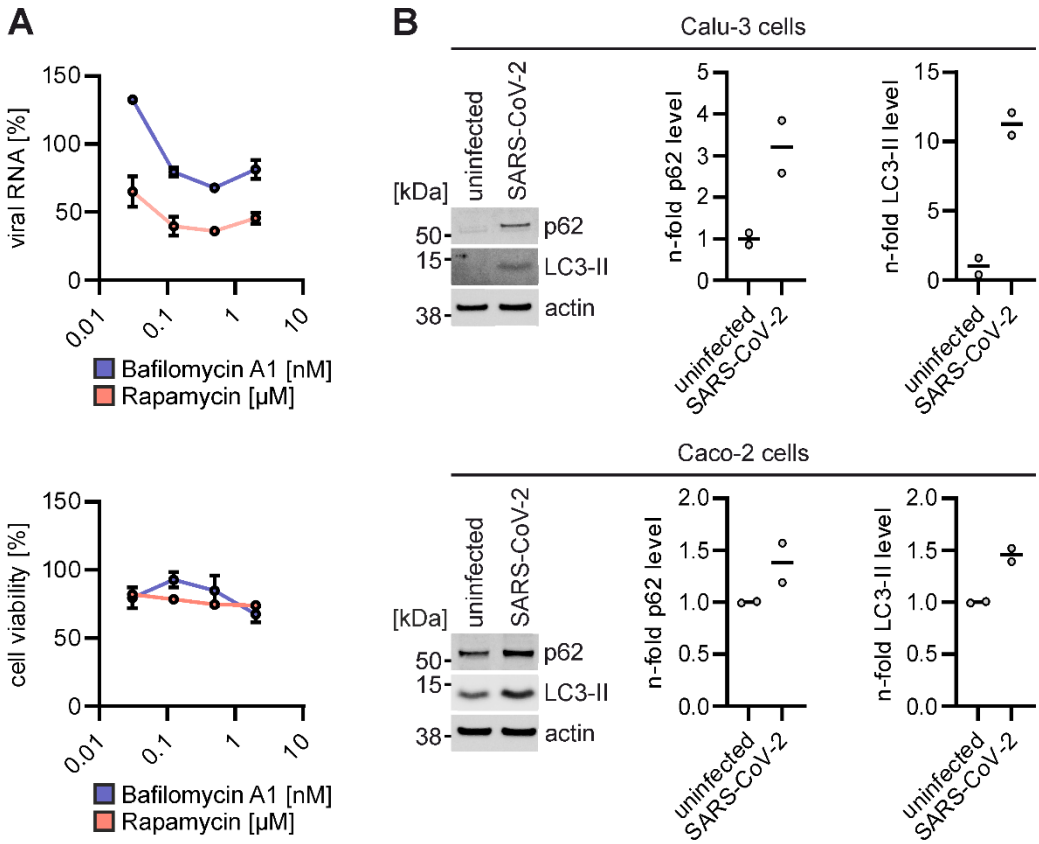


Figure 7: SARS-CoV-2 controls autophagy in infected cells. A) Calu-3 cells were treated with Bafilomycin A1 (2 - 0.031 nM) or Rapamycin (2 - 0.031 µM) for 24 h and either infected with SARS-CoV-2 (MOI 0.05, harvest 48 h post-infection, strain: BetaCoV/France/IDF0372/2020) or left uninfected and cultured for 48 h. Top panel: SARS-CoV-2 N RNA levels in the supernatants of infected cells normalized to the mock treated control. Bottom panel: relative cell viability of uninfected Calu-3 cells as assessed by intracellular ATP levels. Data are shown as mean ± SEM, n=3 **B)** Relative p62 and LC3-II levels (normalized to actin levels) in Calu-3 (top panel) or Caco-2 (bottom panel) cells infected with SARS-CoV-2 (MOI 0.05, Calu-3; MOI 1, Caco-2; both harvested 48 h post infection, strain: BetaCoV/France/IDF0372/2020) or uninfected. Representative immunoblots are shown. Data are shown as mean, n=2. The experiments generating the data shown in the figure panel A (top panel) were performed and analyzed by Rayhane Nchioua, and the experiments generating the data shown in the figure panels A (bottom panel) were performed and analyzed by Susanne Klute. The infection and sample preparation for the experiments in figure panel B were performed by Rayhane Nchioua, and the immunoblotting and analysis was performed by myself. Data shown in figure panels A-B are modified from (Hayn et al., 2021)[65] with permission from the copyright holder (CC BY-NC-ND 4.0, https://creativecommons.org/licenses/by-nc-nd/4.0/).

5.2.2. Impact of SARS-CoV-2 on autophagy

Low anti-viral effects of autophagy modulation suggested that SARS-CoV-2 evades restriction by autophagy. Thus, we determined the overall impact of a SARS-CoV-2 infection on autophagy. To this end, lung-derived Calu-3 cells and gut-derived Caco-2 cells were infected with SARS-CoV-2 (MOI 0.05, Calu-3; MOI 1, Caco-2; strain: BetaCoV/France/IDF0372/2020) and analyzed in Western blot 48 h post-infection. Levels of both the autophagy receptor p62 and the lipidated form of LC3, LC3-II, were increased in the infected cells compared to the uninfected control (Fig. 7B). This trend is consistent in both cell lines, albeit with varying magnitudes. Together, accumulation of p62 and increased LC3-II levels indicate that infection with SARS-CoV-2 impairs autophagic degradation and leads to an accumulation of autophagosomes in the infected cells.

5.2.3. A variety of SARS-CoV-2 proteins modulate autophagy

SARS-CoV-2 encodes a total of 15 ORFs that express 30 viral proteins[56] (Fig. 3). Their functions include forming the virion, facilitating viral replication, and shaping the host environment. However, which proteins manipulate autophagy was unclear. To elucidate this, 29 SARS-CoV-2 proteins were individually overexpressed in HEK293T GL cells, and 48 h post-transfection, the cells were treated to only retain the autophagosome associated eGFP-LC3B-II and analyzed in flow cytometry. In addition to analyzing the impact of the SARS-CoV-2 proteins on basal autophagy, I assessed their effects on autophagy under conditions of saturated induction of autophagy (Rapamycin, 1 μM) and saturated inhibition of the turnover of autophagosomes (Bafilomycin A1, 0.1 μM). These three conditions allow to infer whether an increase in eGFP-LC3B-II signal is likely caused by induction of autophagy (signal masked in the presence of Rapamycin) or accumulation of autophagosomes (signal masked in the presence of Bafilomycin A1). Expression of all constructs was verified in Western blot analysis (Fig. 8B). In total, 8 SARS-CoV-2 proteins significantly altered the basal autophagy (Fig. 8A). Of the non-structural proteins of SARS-CoV-2 Nsp2 and Nsp5 overexpression lead to a slight increase in autophagosome abundance at basal and induced (Rapamycin) autophagy levels. This effect was absent under Bafilomycin A1 treatment, suggesting that Nsp2 and Nsp5 caused an accumulation of autophagosomes. Nsp1 expressing cells displayed a moderate decrease in eGFP-LC3B-II signal at all three autophagy levels, suggesting that Nsp1 reduced induction of autophagy. However, Nsp1 imposes a general block of translation[172] – including translation of the reporter – which could be responsible for the observed reduction in eGFP signal. Indeed, its negative impact on

autophagy could not be verified in an orthogonal method as indicated by unchanged p62 levels in Western blot (Fig. 8C). Thus, it is likely that Nsp1 does not alter autophagy but rather interferes with reporter expression. At basal autophagy levels, Nsp15 overexpression led to the strongest reduction of the eGFP-LC3B-II signal amongst all SARS-CoV-2 proteins tested. Induction of autophagy by Rapamycin counteracted this, suggesting that Nsp15 may act on mTORC1 or an associated pathway. In accordance, treatment with Bafilomycin A1 barely affected the Nsp15 mediated reduction of autophagic flux. Among the structural proteins of SARS-CoV-2 E and M significantly increased autophagosome accumulation (Fig. 8A). Bafilomycin A1 treatment partially masked the effect of both proteins, suggesting that E and M impair the turnover of autophagosomes. Of the SARS-CoV-2 accessory proteins, cells expressing either ORF3a or ORF7a showed a potent increase in eGFP-LC3B-II signal similar in magnitude to the effects of E and M (Fig. 8A). For both accessory proteins, the signal increase was masked by treatment with Bafilomycin A1, suggesting that ORF3a and ORF7a impaired turnover of autophagosomes, leading to their accumulation.

Taken together, the SARS-CoV-2 proteins Nsp2, Nsp5, Nsp15, E, M, ORF3a, and ORF7a alter the abundance of autophagosomes and thus likely modulate autophagy.

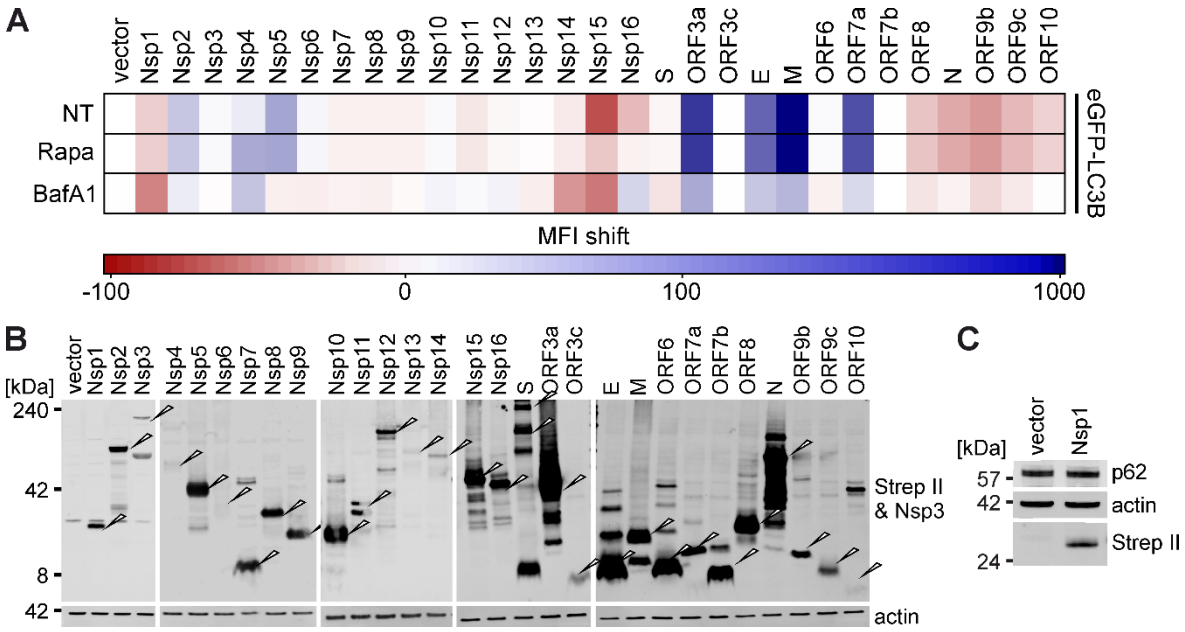


Figure 8: Impact of SARS-CoV-2 proteins on autophagy. A) HEK293T GL cells were transiently transfected with the indicated constructs and either left non-treated (NT) or treated with Rapamycin (Rapa, 1 µM, 4 h) or Bafilomycin A1 (BafA1, 0.1 µM, 4 h). The cells were treated with saponin, washed out and analyzed in flow cytometry 48 h post-transfection. Color represents the mean of n=4. The empty vector control is set to 0 (white). **B)** Immunoblot of HEK293T GL cells transfected with the indicated constructs. Viral proteins are highlighted by arrows at their expected weight. **C)** Immunoblot of HEK293T GL cells transfected with the indicated constructs. Statistical significance of differences compared to the vector control was assessed using unpaired t-test with Welch's correction. The experiments generating the data shown in the figure panel B were performed and analyzed in collaboration by Maximilian Hirschenberger and myself. The experiments generating the data shown in the figure panel A and C were performed and analyzed by myself. Data shown in figure panels A-B are modified from (Hayn et al., 2021)[65] with permission from the copyright holder (CC BY-NC-ND 4.0, https://creativecommons.org/licenses/by-nc-nd/4.0/).

5.2.4. Mechanistic analysis of SARS-CoV-2 proteins interfering with autophagy

Seven of the 29 SARS-CoV-2 proteins (Nsp2, Nsp5, Nsp15, E, M, ORF3a, and ORF7a) significantly regulated basal autophagy in the reporter assay. For further analysis, I focused on the five most potent modulators of autophagy, of which Nsp15 reduced autophagosome content, E, M, ORF3a, and ORF7a and prevented the turnover of autophagosomes. To analyze their impact on endogenous autophagy, these five SARS-CoV-2 proteins were individually overexpressed in HEK293T cells, and levels of endogenous autophagy markers were analyzed by Western blotting. Expression of the viral proteins was confirmed via their Strep II tag (Fig. 9A). In addition to the hallmarks of autophagy, p62 abundance and LC3B processing, protein levels of two core components of the autophagy initiation machinery, Beclin-1 and ULK1, which are frequently targeted by viruses[20,96,129,130,136,151], were analyzed. The expression of any of the five SARS-CoV-2 proteins did not change ULK1 or Beclin-1 levels significantly (Fig. 9A,D,E). Western blot analysis showed that Nsp15 overexpression led to an accumulation of p62 and had a trend toward decreased LC3B-II protein levels (Fig. 9A,B,C). Thus, Nsp15 most likely reduces autophagic flux by inhibiting the initiation of autophagy. Expression of ORF3a, E, and ORF7a led to increased levels of both p62 and LC3B-II (Fig. 9A,B,C). This suggests that these three SARS-CoV-2 proteins impair the degradation of autophagosomes and cause their accumulation. Finally, when overexpressing SARS-CoV-2 M, LC3B-II protein levels were increased, but p62 levels remained unchanged (Fig. 9A,B,C). Thus, autophagic flux seems to be unaffected by M expression, indicating that LC3B lipidation is increased independent of canonical autophagy. Using the HeLa GL reporter cells, autophagosomes can be visualized in fluorescence microscopy as eGFP-LC3B puncta. To determine the effect of the viral proteins on autophagosome count and morphology, I expressed SARS-CoV-2 Nsp15, E, M, ORF3a, and ORF7a in HeLa GL cells and analyzed them in confocal microscopy (Fig. 9F). Autophagosome area per cell was quantified by analyzing the images in ImageJ. Cells expressing Nsp15 contained less eGFP-LC3B puncta indicating reduced autophagic flux, thus confirming the previous results (Fig. 9F,G). Cells expressing E, ORF3a, or ORF7a contained more vesicle-like eGFP-puncta (=autophagosomes) than the control, confirming the results previously obtained in flow cytometry and western blot (Fig. 9F,G). Of these four SARS-CoV-2 proteins, only ORF7a partially localized to autophagosomes in the cells (Fig. 9F), whereas Nsp15, ORF3a, and E displayed a dispersed cytoplasmic localization. ORF3a, ORF7a, E and Nsp15 did not

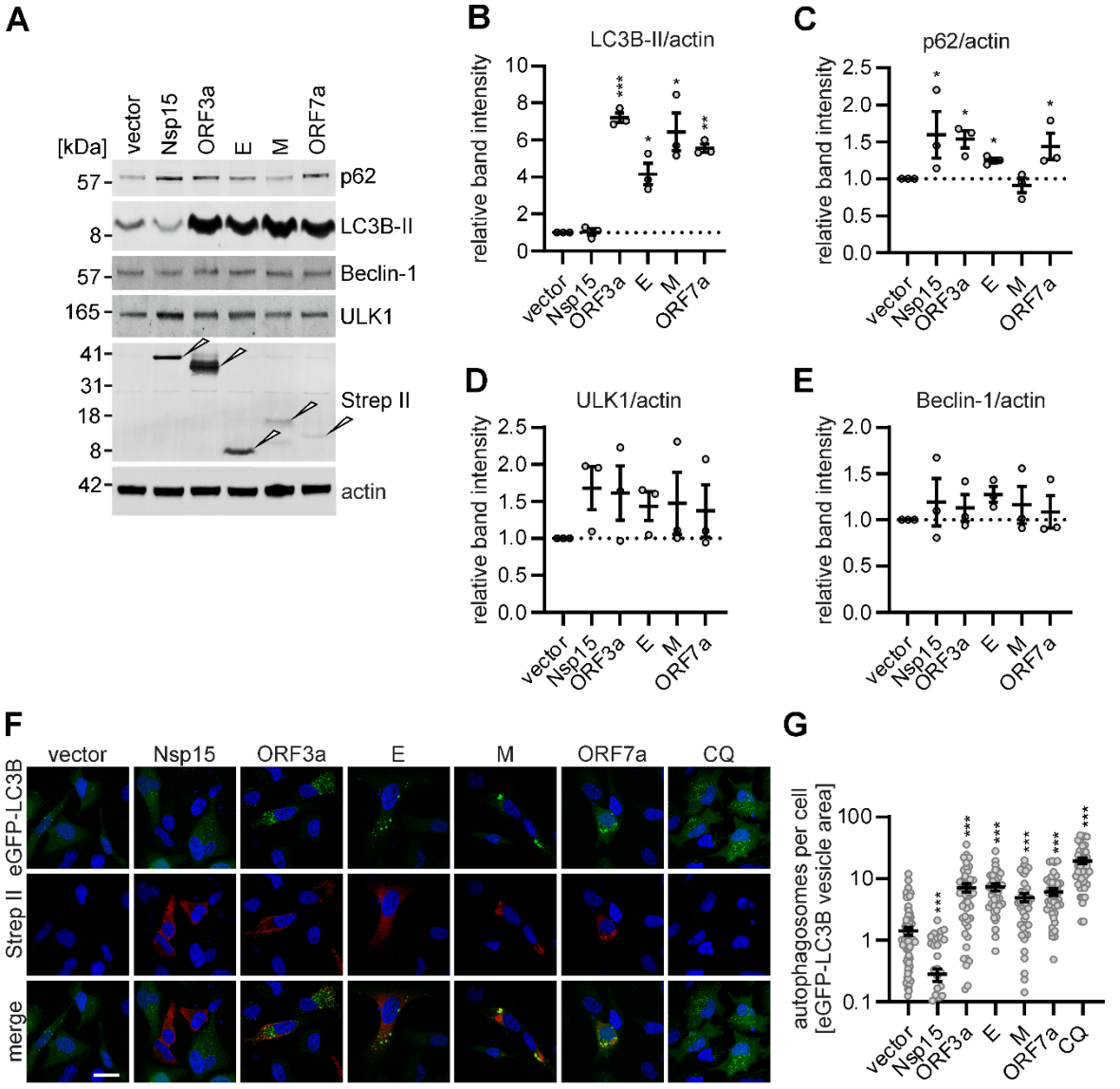


Figure 9: Proteins of SARS-CoV-2 inhibit induction of autophagy and suppress the turnover of autophagosomes. A) Representative immunoblots of HEK293T cells transiently transfected with the indicated constructs. Arrows highlight the viral proteins at their expected weight. Quantification of **B)** LC3B-II, **C)** p62, **D)** ULK1 and **E)** Beclin-1 levels in the samples shown in (A) normalized to actin. Data are shown as mean ± SEM, n=3. **F)** Representative confocal microscopy images of HeLa GL cells transiently transfected with the indicated constructs or treated with Chloroquine (10 µM, 4 h). eGFP-LC3B (green), Strep II (viral proteins, red) and DAPI (blue). Scale bar, 10 µm. **G)** Quantification of eGFP vesicle area per cell in the samples shown in (F). Data are shown as mean ± SEM, n=38-105. Statistical significance of differences compared to the vector control was assessed using unpaired t-test with Welch's correction. *$p \leq 0.05$, **$p \leq 0.01$, ***$p \leq 0.001$. The experiments generating the data shown in the figure were performed and analyzed by myself. Data shown in figure panels A-G are modified from (Hayn et al., 2021)[65] with permission from the copyright holder (CC BY-NC-ND 4.0, https://creativecommons.org/licenses/by-nc-nd/4.0/).

drastically change the morphology of autophagosomes. However, rather than increasing the number of eGFP-LC3B puncta in the cells, the expression of M led to a large non-vesicle-like accumulation of eGFP-LC3B in the perinuclear region (Fig. 9F).

In summary, the results indicate that SARS-CoV-2 uses Nsp15 to inhibit autophagy induction and ORF3a, E, and ORF7a to reduce the turnover of autophagosomes. The M protein of SARS-CoV-2 seems to target autophagic (LC3B-II positive) membranes to the perinuclear region but does not alter canonical autophagy.

5.2.5. ORF3a and ORF7a prevent autophagic turnover by perturbing the autophagosome-lysosome interplay

ORF3a and ORF7a both efficiently prevent autophagic flux and cause an accumulation of autophagosomes in the cells. To analyze their molecular mechanisms, we employed the fusion protein mCherry-eGFP-LC3B^{85,138} as a pH-sensitive reporter to study the acidification of autophagosomes upon fusion with lysosomes. At a neutral pH, fluorescence from both mCherry and eGFP are observed in the autophagosomes. However, upon acidification, the eGFP fluorescence is lost, while mCherry retains its fluorescent properties. HEK293T cells stably expressing mCherry-eGFP-LC3B were transfected with ORF3a or ORF7a expressing constructs. 48 h post-transfection, the cells were treated to retain only membrane-associated reporter, and eGFP and mCherry MFIs were quantified using flow cytometry. The quotient of the eGFP MFI divided by the mCherry MFI increased in a dose-dependent manner with increasing amounts of transfected ORF3a or ORF7a expressing constructs (Fig. 10A). As less eGFP fluorescence is quenched, this indicates that in the presence of ORF3a or ORF7a acidification of autophagosomes is reduced. Using confocal microscopy, I visualized and quantified the number of eGFP and/or mCherry positive puncta (=autophagosomes/autolysosomes). The total number of puncta per cell was increased in both ORF3a and ORF7a expressing cells (Fig. 10B,C). In line with the flow cytometry results, expression of either ORF3a or ORF7a decreased the relative amount of acidified autophagosomes (acidified autophagosomes: vector 70 %, ORF3a 28 %, ORF7a 18 %, Baf A1 17 %) (Fig. 10C). To corroborate these results, we used the dye Lysotracker Deep Red which allows specific labeling of acidic organelles. We transfected HEK293T cells with constructs expressing ORF3a or ORF7a, stained them with Lysotracker Deep Red, and analyzed them in flow cytometry. Cells expressing ORF3a showed a higher Lysotracker

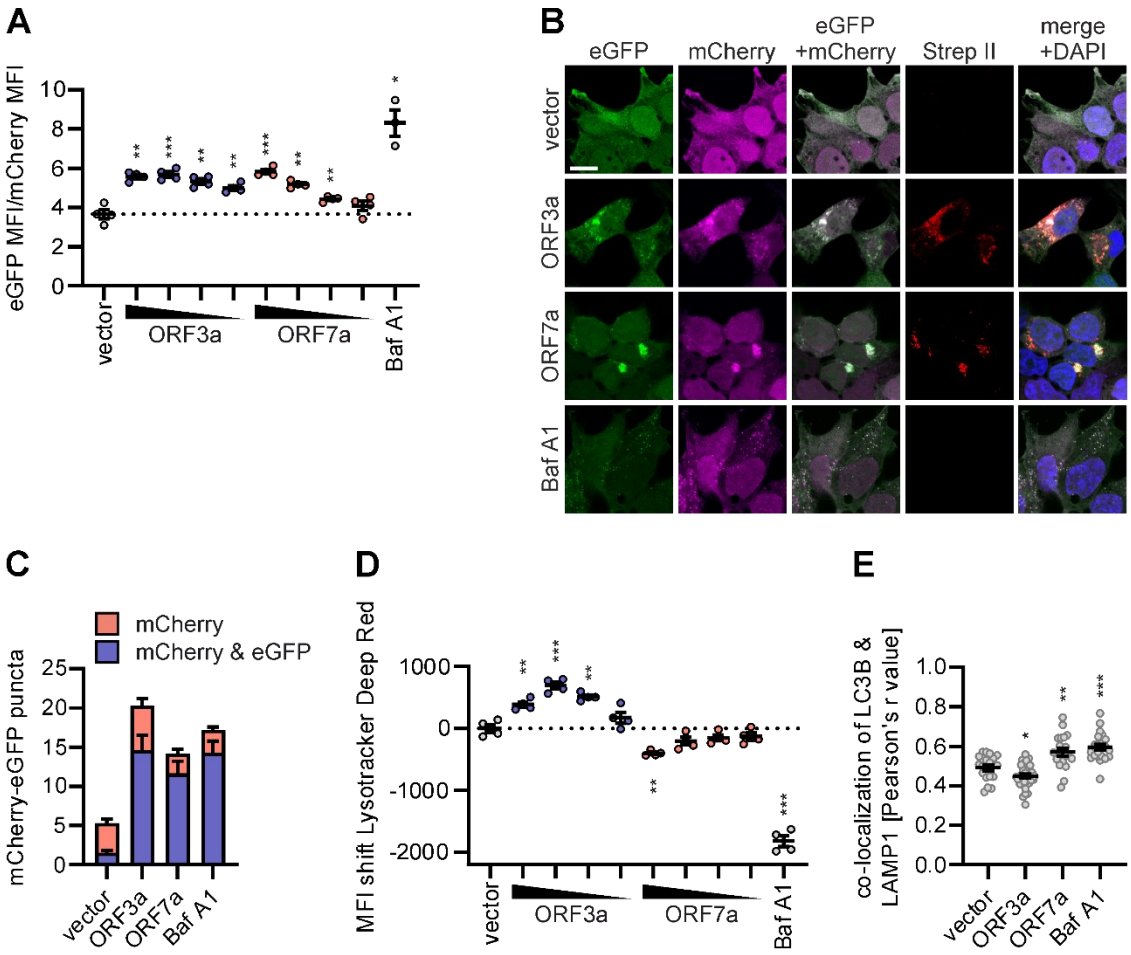


Figure 10: SARS-CoV-2 ORF3a and ORF7a use distinct mechanisms to prevent autophagic turnover. **A)** Ratio of eGFP MFI to mCherry MFI in HEK293T mCherry-eGFP-LC3B expressing cells transfected with the indicated constructs or treated with Bafilomycin A1 (0.1 µM, 8 h), treated with saponin and washed out. **B)** Representative confocal microscopy images. HEK293T GL cells were transfected with the indicated constructs or treated with Bafilomycin A1 (0.1 µM, 4 h). eGFP-LC3B (green), mCherry (magenta), Strep II (viral proteins, red) and DAPI (blue). Scale bar, 10 µm. **C)** Quantification of mCherry positive and eGFP-mCherry double positive puncta per cell in the samples shown in (B). Data are shown as mean indicated by the height of the bar + SEM, n=12-100. **D)** HEK293T cells were transfected with the indicated constructs or treated with Bafilomycin A1 (0.1 µM, 4 h). Lysotracker Deep Red MFI shift is shown with the vector control set to zero. Data are shown as mean ± SEM, n=4. **E)** Quantification of the co-localization of LAMP1 (anti-LAMP1 staining) and LC3B (eGFP-LC3B) in HeLa GL cells transfected with the indicated constructs or treated with Bafilomycin A1 (0.1 µM, 4 h). Transfected (Strep II positive) cells were analyzed. Data are shown as mean ± SEM, n=19-32. Statistical significance of differences compared to the vector control was assessed using unpaired t-test with Welch's correction. *$p \leq 0.05$, **$p \leq 0.01$, ***$p \leq 0.001$. The experiments generating the data shown in the figure panels A and D were performed in collaboration by Susanne Klute and myself, and the analysis was performed by myself. The experiments generating the data shown in the figure panel E were performed and analyzed by Maximilian Hirschenberger. The experiments generating the data shown in the figure panels B and C were performed and analyzed by myself. Data shown in figure panels A-E are modified from (Hayn et al., 2021)[65] with permission from the copyright holder (CC BY-NC-ND 4.0, https://creativecommons.org/licenses/by-nc-nd/4.0/).

signal, indicating increased amounts of acidic organelles, e.g. lysosomes or autolysosomes, that accumulate in the cells (Fig. 10D). In contrast, the Lysotracker signal decreased upon expression of ORF7a, suggesting that lysosome acidification is reduced in the presence of ORF7a (Fig. 10D). Next, we investigated whether autophagosomes were still fusing with lysosomes in the presence of the viral proteins. To assess this, HeLa GL cells were transfected with constructs expressing ORF3a or ORF7a, and we quantified colocalization of the autophagosome marker eGFP-LC3B and the lysosome marker LAMP1[17] using the Huygens Professional software. Expression of ORF3a led to a reduction of the co-localization (Fig. 10E), indicating reduced fusion, while expression of ORF7a had the opposite effect, increasing co-localization of eGFP-LC3B and LAMP1.

Taken together, both ORF3a and ORF7a of SARS-CoV-2 led to an accumulation of autophagosomes inside the cell and prevented their acidification. However, ORF3a achieved this by inhibiting autophagosome-lysosome-fusion, while ORF7a reduced the acidification of lysosomes and, subsequently autolysosomes.

5.3. TRIM proteins inhibit autophagy induction

Autophagy is a tightly regulated cellular process. Members of the highly diverse family of TRIM proteins comprising 80 different members are known to regulate autophagy positively[64,116,163,164]. However, the role and mechanism of TRIMs that negatively regulate autophagy remained elusive.

5.3.1. Filamin-NHL TRIM proteins reduce autophagic flux

In a previous study on the impact of TRIM proteins on autophagy, few TRIMs that reduce autophagic flux were identified[163]. Amongst them were the three filamin-NHL containing TRIM proteins: TRIM2, TRIM3, and TRIM71. These are characterized by a C-terminal filamin domain followed by multiple NHL repeats. Their close relatives are TRIM32, harboring only the NHL repeats, TRIM45, with only the filamin domain, and TRIM56 lacking both specific domains at its C-terminus[154] (Fig. 11A). Transient transfection of HEK293T GL cells with constructs expressing FLAG-tagged versions of these TRIM proteins revealed that only TRIM2, TRIM3, and TRIM71 reduced the eGFP-LC3B-II MFI, indicating lower numbers of autophagosomes per cell (Fig. 11B). The eGFP-LC3B-II MFI remained unaltered in cells expressing TRIM45 while expression of TRIM32 or TRIM56, both known to be associated with induction of autophagy[34,35,166,175], led to an increase in autophagosomes per cell (Fig. 11B). Expression of all constructs was confirmed in Western

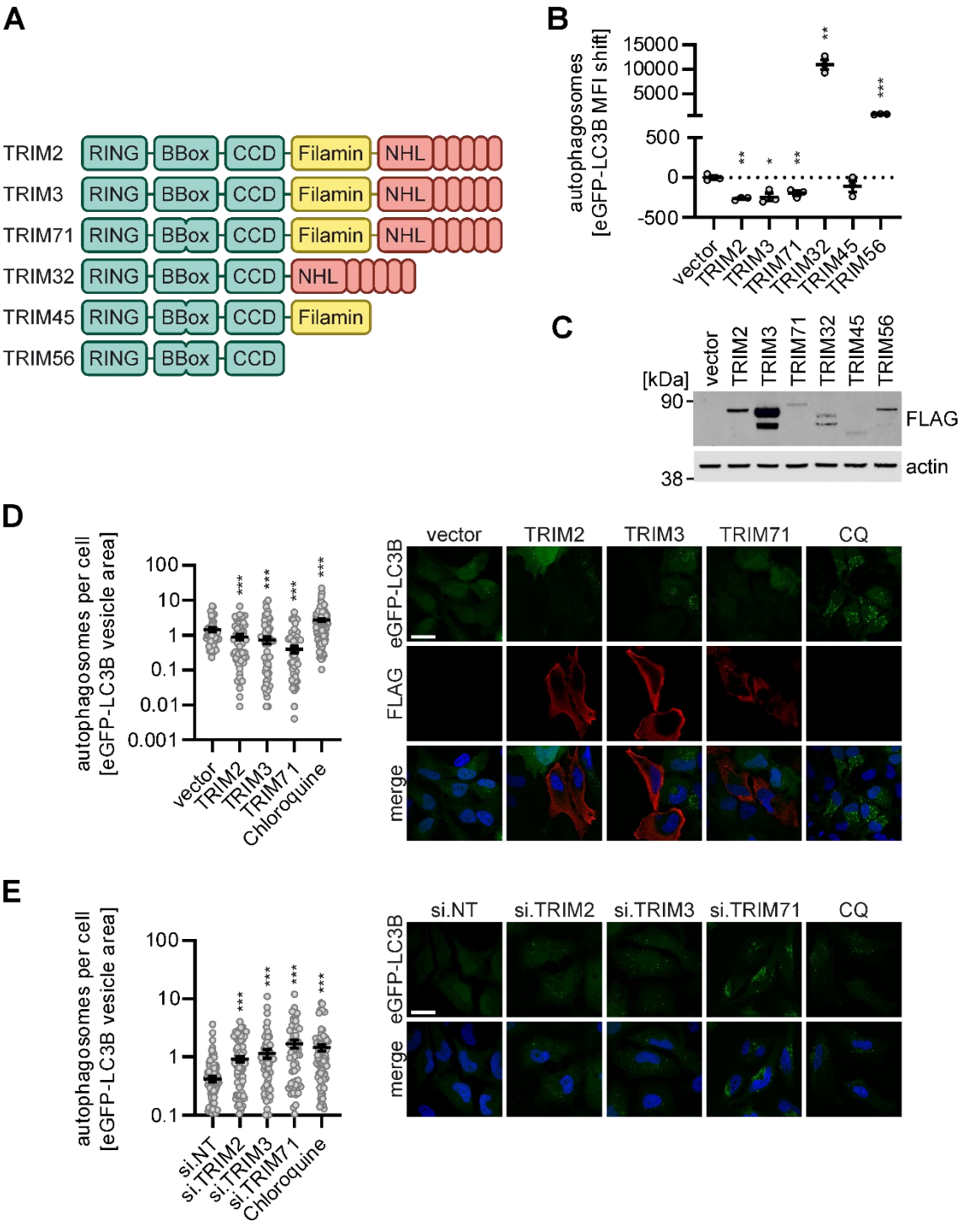


Figure 11: TRIM2, TRIM3 and TRIM71 inhibit autophagy. A) Schematic depiction of the domain organization of TRIM2, TRIM3 and TRIM71 and their close relatives. **B)** eGFP-LC3B-II MFI shift of HEKT293T GL cells transfected with the indicated constructs, treated with saponin, washed out and stained with an anti-FLAG antibody. Data are shown as mean ± SEM, n=3. **C)** Immunoblot of HEK293T GL cells transfected with the indicated constructs. **D)** HeLa GL cells were transfected with the indicated constructs or treated with Chloroquine (10 µM, overnight) and analyzed in confocal microscopy. Representative images and quantification of eGFP-LC3B vesicle area per cell are shown. eGFP-LC3B (green), FLAG (TRIMs, red), DAPI (blue). Scale bar, 10 µm. Data are shown as mean ± SEM, n=61-139. **E)** HeLa GL cells were transfected with

the indicated siRNAs or treated with Chloroquine (10 µM, overnight) and analyzed in confocal microscopy. Representative images and quantification of eGFP-LC3B vesicle area per cell are shown. eGFP-LC3B (green), DAPI (blue). Scale bar, 10 µm. Data are shown as mean ± SEM, n=61-117. Statistical significance of differences compared to the vector or si.NT control was assessed using unpaired t-test with Welch's correction. *p ≤ 0.05, **p ≤ 0.01, ***p ≤ 0.001. The experiments generating the data shown in the figure were performed and analyzed by myself.

blot (Fig. 11C). To corroborate these finding, I transiently transfected HeLa GL cells with constructs expressing TRIM2, TRIM3, and TRIM71 and analyzed eGFP-LC3B puncta formation in confocal microscopy. Cells expressing the filamin-NHL TRIMs contained fewer autophagosomes compared to the control (Fig. 11D), which was confirmed by determining the average pixel area of autophagosomes per cell using ImageJ.

To investigate the effects of filamin-NHL TRIMs at endogenous levels, I used siRNA-mediated knock down. HeLa GL cells depleted of TRIM2, TRIM3, or TRIM71 contained increased numbers of autophagosomes as observed in confocal microscopy (Fig. 11E). Quantification of the autophagosome area per cell in ImageJ also showed significantly reduced autophagosome area in the TRIM-depleted cells.

In summary, the filamin-NHL TRIMs (TRIM2, TRIM3, and TRIM71) reduce the induction of autophagy at an endogenous level. As their close relatives TRIM32, TRIM45, and TRIM56 do not exert this function, at least the filamin domain and the NHL repeats seem to be required for autophagy inhibition.

5.3.2. Casein kinase II interacts with filamin-NHL TRIMs

To investigate the molecular mechanism underlying the filamin-NHL TRIM-mediated inhibition of autophagy induction, interaction partners of TRIM2 and TRIM3 were identified. To this end, FLAG-tagged versions of TRIM2 and TRIM3 lacking the RING domain (ΔRING) were large-scale purified and putative interaction partners identified using mass spectrometry (MS). Truncated mutants of TRIM2 and TRIM3 lacking the enzymatic ubiquitin ligase RING domain were used to increase the chances of retaining functional interaction partners that would potentially be released after processing. Also, protein-protein interaction is often mediated by the C-terminal domain in TRIMs. Fold enrichment analysis comparing interaction partners of TRIM2ΔRING and TRIM3ΔRING revealed that parts of CK2 (CK2α, CK2α') are prominent binding partners (Fig. 12A). Notably, CK2 has previously been associated with dysregulated autophagy but has been ascribed a conflicting role, to mediate both inhibitory and inducing functions[83,140,182]. The CK2 complex consists

of the two catalytic subunits CK2α and CK2α', and the regulatory subunit CK2β. All three subunits of CK2 were enriched in the pulldowns of TRIM2ΔRING and TRIM3ΔRING, while none or substantially less was detected in the controls (Fig. 12B), indicating specific interaction of the TRIMs with the endogenous CK2 complex. To verify this, co-immunoprecipitation experiments co-expressing TRIM2, TRIM3, or TRIM71 with the tagged versions of the three subunits of CK2, CK2α, CK2α', or CK2β, in pairs were conducted. Western blot analysis showed that CK2α was co-purified with TRIM2, TRIM3, and TRIM71, with some background binding in the control (Fig. 12C). As the CK2α levels were constant in the input and the observed CK2α signal is above background in all three TRIM samples (Fig. 12C), specific binding of CK2α to the filamin-NHL TRIMs was confirmed. For CK2α', the signal did not surpass background, thus not confirming specific interaction with the filamin-NHL TRIMs (Fig. 12C). CK2β did not show any background binding in the control, but specific binding to TRIM3 and TRIM71 (Fig. 12C). Interaction between the filamin-NHL TRIMs and CK2 inside the cell could be precluded by localization to different compartments. To examine this, filamin-NHL TRIMs and CK2 subunits were expressed in HeLa cells and their localization was analyzed in confocal microscopy. TRIM2, TRIM3, and TRIM71 were all localized almost exclusively to the cytoplasm. TRIM2 and TRIM3 showed a dispersed signal in the cytoplasm, while TRIM71 additionally formed puncta (Fig. 12D, the entire panel with all subpanel is shown in SFig. 1). The components of the CK2 complex mainly localized to the nucleus. However, they were also found in the cytoplasm with varying intensity. CK2α was least abundant in the cytoplasm, while CK2α' and CK2β showed a stronger dispersed signal in the cytoplasm. CK2β additionally formed puncta in the cytoplasm (Fig. 12D). Overexpression of all CK2 subunits together closely resembled the localization observed for CK2β with high nuclear and intermediate cytoplasmic signals and distinct puncta-like accumulations (Fig. 12D). Notably, neither the localization of the CK2 subunits nor the TRIMs were altered by their co-expression (SFig. 1). However, both TRIMs and the components of the CK2 complex co-localize in the cytoplasm of cells.

Taken together, the results indicate that all three filamin-NHL TRIMs (TRIM2, TRIM3, and TRIM71) can interact with the CK2 complex in the cytosol.

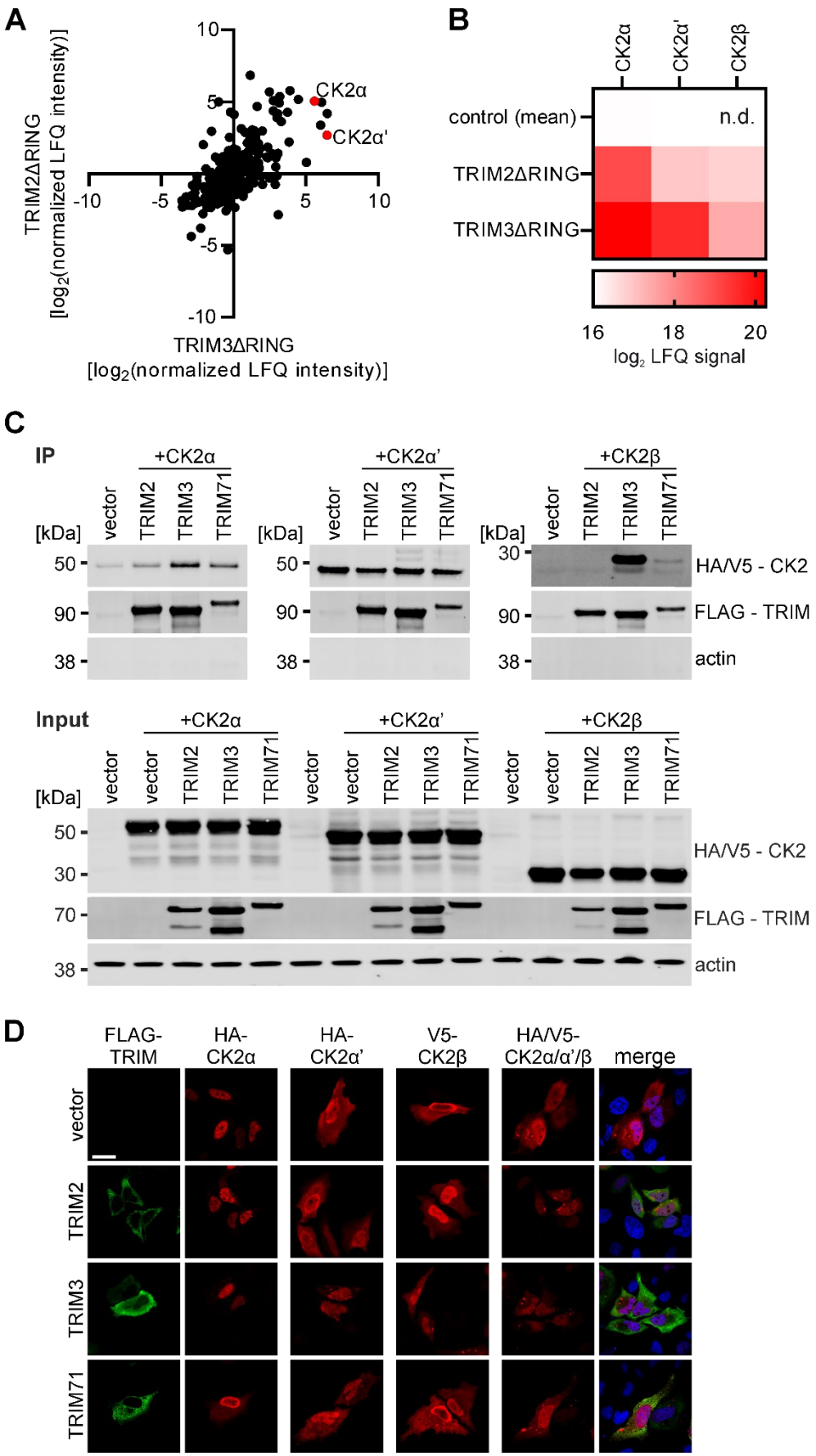

A
TRIM2ΔRING [log2(normalized LFQ intensity)]
TRIM3ΔRING [log2(normalized LFQ intensity)]
CK2α
CK2α'
B
CK2α
CK2α'
CK2β
control (mean)
TRIM2ΔRING
TRIM3ΔRING
n.d.
log2 LFQ signal
C
IP
Input
+CK2α
+CK2α'
+CK2β
vector
TRIM2
TRIM3
TRIM71
[kDa]
HA/V5 - CK2
FLAG - TRIM
actin
D
FLAG-TRIM
HA-CK2α
HA-CK2α'
V5-CK2β
HA/V5-CK2α/α'/β
merge
vector
TRIM2
TRIM3
TRIM71

Figure 12: CK2 is a potent interaction partner of the filamin-NHL TRIMs. A) HEK293T cells transfected with the indicated constructs were lysed and subjected to co-immunoprecipitation enriching TRIM2ΔRING or TRIM3ΔRING. The samples were analyzed in mass spectrometry. Fold enrichment over the control samples is shown and the CK2α subunits are highlighted in red. n=1. **B)** Label free quantification data from (A) indicating abundance of the indicated proteins (top) in the indicated samples (left). Color indicates abundance ranging from $\leq 2^{16}$ (white) up to over 2^{20} (red). n=1, n.d.=not detected. **C)** Immunoblot of co-immunoprecipitation (enriching the FLAG-tagged TRIMs) of HEK293T cells transfected with the indicated constructs. Top panel: co-immunoprecipitation indicating (co-) enrichment. Bottom panel: Input before co-immunoprecipitation. **D)** Representative confocal microscopy images of HeLa cells transfected with the indicated constructs. FLAG (TRIMs, green), HA and V5 (CK2 subunits, red), DAPI (blue). The full panel is shown in Suppl. Fig. 1. Scale bar, 10 µm. The experiments generating the data shown in figure panels A and B were performed and analyzed in collaboration with the Core Unit Mass Spectrometry and Proteomics at ulm university which took over mass spectrometry analysis and interpretation/quantification, and by myself for sample generation and final analysis. The experiments generating the data shown in figure panels C and D were performed and analyzed by myself.

5.3.3. The Casein kinase II activity inhibits autophagy

To characterize the impact of CK2 on autophagy, the active subunits CK2α and CK2α', and the CK2 complex were expressed in HEK293T GL cells. The cells were simultaneously stimulated with Bafilomycin A1 to allow the accumulation of autophagosomes. Expression of both active subunits of CK2 alone and the complex reduced the number of autophagosomes as indicated by the decreased eGFP-LC3B-II MFI (Fig. 13A). In line with this, inhibition of CK2, using CX-4945, led to a dose-dependent increase in the eGFP-LC3B-II signal (Fig. 13B), suggesting that CK2 inhibits autophagy at endogenous expression levels. To clarify the hierarchy between the TRIMs and CK2, we examined whether CK2 is active upstream or downstream of the TRIM proteins. First, we assessed whether CK2 is stabilized or activated by the filamin-NHL TRIMs (CK2 acts downstream). Upon expression of TRIM2, TRIM3, or TRIM71 in HEK293T cells, I did not observe changes in endogenous CK2α or CK2α' levels as measured in Western blot (Fig. 13C). Using a CK2 activity assay to measure CK2 activity in the lysates of HEK293T cells transfected with constructs expressing the filamin-NHL TRIMs or the CK2 subunits, TRIM-mediated changes in the activity of endogenous CK2 were not observed. As expected, the CK2 inhibitor CX-4945 decreased activity of endogenous and overexpressed CK2, serving as a control (Fig. 13D). Sequence analysis of the filamin-NHL TRIMs revealed one putative CK2 phosphorylation site in the NHL repeats, shared by TRIM2, TRIM3, and TRIM71 and two putative phosphorylation sites in or near the RING domain of TRIM2, and TRIM3 (Fig. 13E). To investigate whether CK2 phosphorylation of the filamin-NHL TRIMs at these

sites might influence their autophagy inhibiting activity, which would indicate CK2 acting upstream of the TRIMs, I generated serine to alanine mutants of TRIM3 for each site. When overexpressing these TRIM3 mutants in HeLa GL cells, TRIM3 WT as well as its two mutants with altered phosphorylation sites in or near the RING domain, reduced the autophagosome area per cell to the same degree. The third mutant with the deficient phosphorylation site in the NHL repeats, however, reduced autophagy to a significantly lesser degree than wildtype TRIM3 (Fig. 13F). Along these lines, when expressing the mutants in HEK293T GL cells and measuring changes in autophagosome number in flow cytometry, I observed that again only the TRIM3 mutant with the altered NHL phosphorylation site showed impaired inhibition of autophagy.

In summary, CK2 inhibits endogenous autophagy, likely by acting upstream of TRIM2, 3, and 71. CK2 is neither stabilized nor activated by the filamin-NHL TRIMs but in turn, might activate the TRIMs by phosphorylating a site in their NHL repeats to enhance TRIM-mediated inhibition of autophagy.

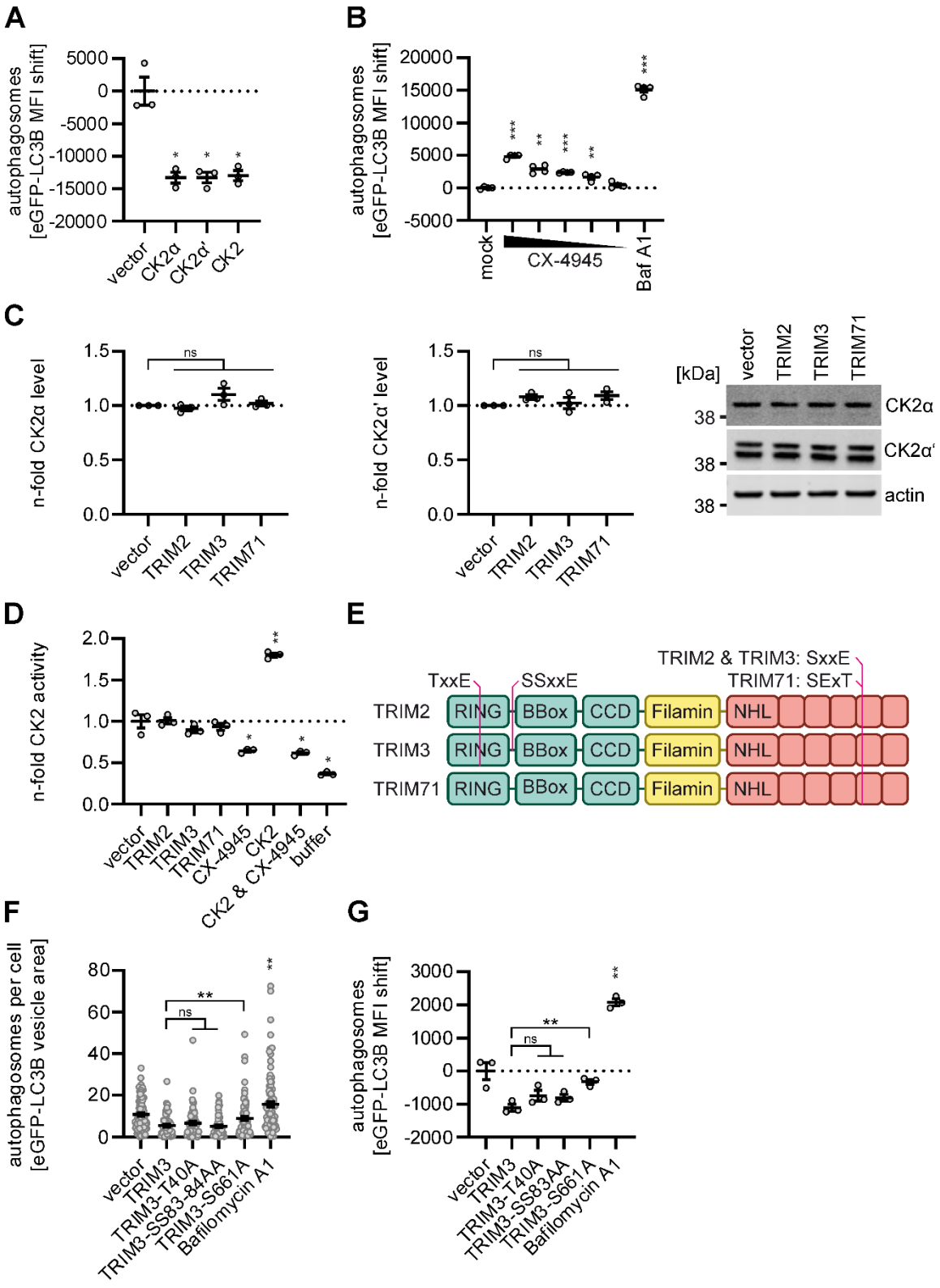


Figure 13: CK2 possibly phosphorylates TRIM3 to inhibit autophagy. A) eGFP-LC3B-II MFI shift of HEK293T GL cells transfected with the indicated constructs (CK2: equal amounts (µg DNA) of constructs expressing CK2α, CK2α' or CK2β) and treated with Bafilomycin A1 (0.25 µM, 4 h). The cells were treated with saponin and washed out. Data are shown as mean ± SEM, n=3. **B)** eGFP-LC3B-II MFI shift of HEK293T GL cells either left untreated or treated with CX-4945 (50-1.5625 µM, 4 h) or Bafilomycin A1

(Baf A1, 0.1 µM, 4 h), treated with saponin and washed out. Data are shown as mean ± SEM, n=4. **C)** HEK293T cells were transfected with the indicated constructs and analyzed in Western blot. CK2α and CK2α' levels were normalized to total protein content and the vector control. Representative immunoblots are shown. Data are shown as mean ± SEM, n=3. **D)** Relative CK2 activity levels of HEK293T cells transfected with the indicated constructs (CK2: equal amounts (µg DNA) of constructs expressing CK2α, CK2α' or CK2β), as analyzed in the CK2 activity assay either left untreated or treated with CX-4945 (25 µM). Data are shown as mean ± SEM, n=3. **E)** Schematic depiction of the domain organization of TRIM2, TRIM3 and TRIM71, and the position of the predicted CK2 phosphorylation sites including the simplified amino acid sequence. **F)** eGFP-LC3B vesicle area per cell of HeLa GL cells transfected with the indicated constructs and analyzed in confocal microscopy. The positive control was additionally treated with Bafilomycin A1 (0.1 µM, 4 h). Data are shown as mean ± SEM, n=59-113. **G)** eGFP-LC3B-II MFI shift of HEK293T GL cells transfected with the indicated constructs, treated with saponin and washed out. The positive control was treated with Bafilomycin A1 (0.1 µM, 4 h). Data are shown as mean ± SEM, n=3. Statistical significance of differences compared to the vector or mock control, or TRIM3 was assessed using unpaired t-test with Welch's correction. *$p \leq 0.05$, **$p \leq 0.01$, ***$p \leq 0.001$. The experiments generating the data shown in figure panel D were performed and analyzed by Helene Hönigsperger. The experiments generating the data shown in figure panels A-C and F-G were performed and analyzed by myself.

6. Discussion

In this thesis, I established an improved high throughput method to quantify changes in autophagy using flow cytometry, as published in Scientific Reports[91]. I used this technique to discover novel viral and cellular autophagy regulatory factors. My assays identify Nsp2, Nsp5, Nsp15, E, ORF3a, and ORF7a of SARS-CoV-2 as viral modulators of autophagy and defined the underlying mechanisms of ORF3a and ORF7a that allow SARS-CoV-2 to evade restriction by autophagy, as published in Cell Reports[65] and Autophagy[90]. Further, I revealed that the cellular filamin-NHL TRIMs TRIM2, TRIM3, and TRIM71 act as inhibitors of autophagy induction and propose the CK2-TRIM2/3/71 axis as a novel regulatory pathway of autophagy.

6.1. High throughput quantification of autophagy

To enable rapid quantification of changes in autophagy, I aimed to establish a method that makes use of commonly available equipment and is suited for the acquisition of large sample numbers. While an established repertoire of methods is available in the field of autophagy (a comprehensive overview is given in Klionsky et al., "Guidelines for the use and interpretation of assays for monitoring autophagy (4th edition)"[87]), many of these methods are laborious or require specialized equipment and proprietary software. To meet our aims, we improved on existing methods[43,81] and established a reporter assay that utilizes flow cytometry with a high-throughput sampler and the association of LC3B-II with autophagosomes to measure changes in autophagy (Fig. 4, Fig. 5, Fig. 6)[91]. The use of flow cytometry allows rapid acquisition of samples while retaining information about the inherent heterogeneity of autophagy, even allowing comparison of autophagy in individual cells (Fig. 5B). The sensitivity of the reporter assay is increased through isolation of the eGFP-LC3B-II signal, which is associated with autophagosomes, from the background by saponin treatment and washout (Fig. 5A). To avoid downsides stemming from co-transfection of multiple constructs such as differences in transfection rates and reporter expression[167], we generated multiple cell lines constitutively expressing the eGFP-LC3B reporter based on HEK293T and HeLa cells (Fig. 4A-D). These are readily transfectable and commonly used within the field respectively. Notably, despite overexpressing one of the core proteins of the autophagy machinery – LC3B – the basal autophagic flux remains similar (Fig. 4E), indicating that overexpression of LC3B - per se - does not increase autophagic flux.

Other approaches to measure autophagy in a high throughput manner use for example the mCherry-eGFP-LC3B reporter protein which is employed in similar setups as our eGFP-LC3B protocol but with the additional benefit of providing mechanistic insight[85,138]. As mCherry fluorescence is more resistant to acidic pH than eGFP fluorescence, the maturation of autophagosomes can be visualized by monitoring their acidification (loss of eGFP fluorescence but not mCherry fluorescence). This system suffers from a considerable background in flow cytometry, and additional treatments like permeabilization or fixation can influence the readout. In addition, changes in autophagy that prevent acidification or alterations at the very beginning of the cascade are harder to pick up. Early high throughput approaches to measure changes in autophagy were based on the degradation of tagged LC3 reporter proteins. These reporters can be fusion proteins with fluorescent proteins[32,161] or luciferases[127], which allow a readout through flow cytometry or luciferase activity. While such approaches can be cheap and rapid, they suffer from high background. A system more optimized for high-throughput analysis uses an eGFP-LC3-RFP-LC3ΔG reporter[53,80]. It relies on the degradation of eGFP-LC3B but additionally incorporates the nonfunctional RFP-LC3ΔG as an internal control. This allows measuring autophagic flux directly and the accumulation of effects over time, facilitating higher sensitivity. Degradation of the autophagy receptor p62 is another commonly used hallmark of autophagic flux[97]. However, constant high expression of a p62 reporter protein can lead to its aggregation and influence autophagy and measurement[87]. Thus, the use of a doxycycline-inducible or similar system is recommended, increasing the complexity and cost of the system. In addition, a reporter system based on p62 will only record p62-involving specific autophagy, none of the other autophagy receptors, or bulk autophagy.

All approaches mentioned - including our method - are limited to genetically modified or transfected cell lines. One way to apply high throughput autophagy quantification to primary cells is to stain them with anti-LC3 or anti-p62 antibodies. These approaches, while important for validation, are prohibitively expensive when considering large sample sizes. Another possibility is to monitor the amount of autophagy-associated organelles in the cells using for example, acridine orange[157] or Cyto-ID[57] dyes. Acridine orange stains acidic organelles and has the benefits of low cost and suitability for high throughput measurement. However, the dye lacks specificity for autophagosomes and, thus, autophagy. Cyto-ID, on the other hand, is more specific for autophagosomes and allows the staining of different stages in autophagosomal maturation. While Cyto-ID is valuable in the study of autophagy

in primary cells, its application in high throughput analysis is unfavorable due to its high cost. Finally, most high throughput autophagy screenings are performed using automated fluorescence microscopy and automated image analysis quantifying eGFP-LC3 puncta in cells[12,66,77,105,173,174,198]. While such approaches make use of a well-established system and enable the acquisition and evaluation of large sample numbers, they require specialized equipment and proprietary software which are not widely available.

In summary, we established and improved a method for rapid quantification of changes in autophagy[91]. The use of flow cytometry makes it widely available and allows the acquisition of large sample sizes. By isolating the eGFP-LC3B-II fluorescence from the background, the method achieves high sensitivity using a robust hallmark of autophagy to measure the autophagosome content of individual cells. The method can be applied to different cell types by generating new reporter cell lines in a similar fashion[91] and can even be adapted for primary cells by using anti-LC3 antibodies.

6.2. Limitations of LC3B processing-based autophagy screening systems

Quantification of eGFP-LC3B-II in flow cytometry has some pitfalls that need to be considered when employing it as a readout for screening. Like with any autophagy quantification method relying solely on the processing of LC3B, increased levels of autophagic flux and inhibition of the turnover of autophagosomes are hard to distinguish, as both lead to elevated LC3B-II levels[91]. To circumvent this, simultaneous stimulation with saturating amounts of Bafilomycin A1 can be used to mask effects that block autophagic turnover and highlight effects that induce autophagic flux. Hits can further be validated and characterized using a mCherry-eGFP-LC3B reporter to observe the acidification of autophagosomes, and co-localization analysis of autophagosomal and lysosomal markers can help identify defects in the fusion step. Lipidation of LC3B could further be linked to a pathway separate from autophagy, like LC3-associated phagocytosis[150] rather than canonical autophagy. Thus, it is highly recommended to verify the initial screening hits and establish physiological relevance using an orthogonal method. For example, p62 degradation can be measured in Western blot to allow differentiation between induction of autophagic flux, a block of the turnover of autophagosomes, and LC3-associated pathways (which generally do not alter p62 levels). Ideally, endogenous protein levels are measured in primary human cells as the cancer cells used in screening approaches often have dysregulated basal

autophagy. Autophagosomes can further be identified in fluorescence microscopy or electron microscopy, as LC3B-positive puncta or double-membrane vesicles, respectively. To definitively link an observed phenotype to autophagy, its dependence on core proteins of the autophagy machinery, such as ATG5, ATG12, or ATG16L[52], can be demonstrated using cells lacking one or multiple of these factors. Finally, the processing of LC3B-I to LC3B-II can be visualized and quantified using Western blotting, as LC3B-II has a shorter retention time than LC3B and LC3B-I.

Taken together, the main limitations of the reporter assay are the differentiation between induction of autophagic flux and a block of autophagosome turnover, the definitive association of the observed effect with autophagy, and the determination of physiological relevance. Thus, hits identified using this system require additional verification, ideally in primary cells using endogenous readouts.

6.3. The interplay between SARS-CoV-2 and autophagy

Autophagy is a double-edged sword in viral infections[26], having both pro-viral and anti-viral roles. To combat infection, autophagy degrades viral components and exposes PAMPs to PRRs, triggering further anti-viral signaling[103]. However, viruses have evolved strategies to evade restriction by autophagy and, in some cases, even hijack parts of the autophagy machinery to benefit their own replication, for example, by using them in the establishment of a replication compartment[7,16,200]. Thus, both inhibition and activation of autophagy can be anti-viral, and the response of a virus towards autophagy is highly virus-species specific. SARS-CoV-2 is known to be inhibited by Chloroquine, an autophagy modulating drug, *in vitro*[109]. However, this might rather be linked to Chloroquine's impact on the endosomal entry than the induced block of autophagosome degradation. According to our data, SARS-CoV-2 is mostly resistant to restriction by induction of autophagy, as indicated by a mere 2-fold reduction of replication in the presence of Rapamycin, which elevates autophagic flux. Autophagy induction is even less potent at inhibiting SARS-CoV-2 replication when performed later in infection[65]. In line with this, SARS-CoV-2 controls autophagy in infected cells efficiently as indicated by increased LC3B-II and p62 levels, which argue that degradation of autophagosomes and thus inhibition is blocked (Fig. 7). Other coronaviruses, such as the highly pathogenic severe acute respiratory syndrome coronavirus type 1 (SARS-CoV-1) and middle east respiratory syndrome-related coronavirus (MERS-CoV), have also been shown to inhibit the turnover of autophagosomes[24]. SARS-CoV-1 is published to use its ORF9b and Nsp6 proteins to inhibit the turnover of autophagosomes, leading to their

accumulation[30,158] and MERS-CoV infection is described to cause an accumulation of autophagosomes, while its replication is inhibited by autophagy[50]. Taken together, control of autophagy is conserved to other coronaviruses, at least the related SARS-CoV-1 and MERS-CoV. Further, coronaviruses[58,146] and other viruses, including flaviviruses[16,29,61,143] and poliovirus[8], have been described to exploit autophagy for their replication. Some of these viruses, such as ZIKV[107] and IAV[114], are known to induce autophagy to boost their replication. The block and prevent strategy we observed for SARS-CoV-2 is also employed by HPIV3, which inhibits the fusion of autophagosomes and lysosomes using its phosphoprotein P[36]. HSV-1[136] and HCMV[20,130] both encode proteins that block Beclin-1 to simultaneously reduce the induction of autophagy and the fusion of autophagosomes with lysosomes.

To decipher how SARS-CoV-2 manipulates autophagy, I analyzed the impact of 29 of its proteins on autophagy[65,90]. Notably, structural, non-structural, and accessory proteins of SARS-CoV-2 did modulate autophagy (Fig. 8). Evolution of such a diverse counteraction of autophagy highlights the importance of this defense pathway. The SARS-CoV-2 proteins Nsp2, Nsp5, Nsp15, ORF3a, ORF7a, E, and M significantly altered autophagy, with the latter five being the most potent.

The non-structural protein Nsp15 inhibits the induction of autophagy, potentially by affecting mTORC1 signaling (Fig. 8, Fig. 9), as its effects are negated by mTOR inhibition. If mTORC1 activity is influenced by Nsp15, this effect might either be directly aimed at evading restriction by autophagy or it might primarily push the infected cell to favor biosynthesis of proteins and lipids to improve viral replication by activation of mTORC1[9] or both. Nsp15 is a prime example of the versatility of viral proteins. In addition to potentially favoring viral replication and inhibiting innate immunity via mTORC1, Nsp15 confers an endonuclease function[84]. Of note, if the enzymatic activity of Nsp15 is important for its impact on autophagy, it could be targeted with inhibitors to combat viral replication by reactivating autophagy. Its endonuclease activity is further suggested to remove viral RNA to avoid detection by PRRs[59]. Thus, inhibition of the enzymatic activity of Nsp15 could potentially boost both the interferon response and autophagy to mount a twin-track response that could effectively combat viral infection and limit inflammation via autophagy[33].

The E protein is a structural protein of SARS-CoV-2 and thus is part of the virion. E is a viroporin with ion channel activity and has been shown to suppress inflammasome activation

and potentially disrupt tight junctions[18,155,188]. Our data shows that SARS-CoV-2 E further blocks the turnover of autophagosomes and thus prevents autophagic degradation (Fig. 8, Fig. 9). As the incoming virus is especially vulnerable to autophagy[65], the E protein could prevent restriction by autophagy immediately after entry. Thus, in future studies, it will be of great interest to pinpoint the specific motif in E conferring autophagy modulation and to analyze its impact on incoming virion stability in the presence of elevated autophagic flux and on viral fitness. Other viruses are also known to modulate autophagy with their structural proteins or proteins that are incorporated into the virion. For example, HIV-1 env has been described to activate the mTOR pathway in dendritic cells, shutting down autophagy[10] and IAV uses its M2 ion channel in the process of entering a target cell and to target LC3 to the cell surface to improve its replication[7].

Accessory proteins of viruses usually shape the host environment to favor replication and prevent restriction by innate immunity. SARS-CoV-2 encodes ten accessory proteins. Of these, ORF3a and ORF7a potently inhibit autophagic degradation, which is why I investigated the underlying molecular mechanisms in more detail. While both proteins have a similar function -preventing autophagic turnover- and lead to the accumulation of autophagosomes (Fig. 8, Fig. 9) they use distinct mechanisms. ORF3a inhibits the fusion of autophagosomes and lysosomes to prevent their degradation (Fig. 10). This was confirmed in a recent publication by Miao and colleagues[126], which shows that SARS-CoV-2 ORF3a sequesters core components of the HOPS complex which is crucially involved in the fusion of autophagosomes and lysosomes. The step is targeted by other viruses, such as HPIV3, which uses its P protein to bind to SNAP29 and block assembly of the trans-SNARE complex, which mediates membrane fusion[36]. ORF7a, on the other hand, inhibits the acidification of autolysosomes to prevent restriction by autophagy (Fig. 10). In addition to preventing degradation of viral components, deacidification of lysosomes could play a major role in the egress of SARS-CoV-2. It is described that β-coronaviruses, such as SARS-CoV-2, use a lysosomal route for egress[54], therefore requiring deacidified lysosomes. It is tempting to speculate that not only ORF7a is important for viral egress by decreasing the lysosomal pH but that ORF3a also modulates lysosome trafficking.

While Nsp15, ORF3a, ORF7a, and E seem to impact canonical autophagy, including the degradation of p62, this is not the case for the M protein of SARS-CoV-2 (Fig. 9A-C). M is a structural protein and is critically involved in the viral infection cycle. It is further described to antagonize interferon induction and induce mitochondrial apoptosis[118,169,192]. Here, I

observed a redirecting and accumulation of autophagic or rather LC3B-II decorated membranes to the perinuclear space where they co-localized with M (Fig. 9). It is well established that coronaviruses and other RNA viruses rely on double-membrane vesicles, also found as LC3B-positive autophagosomes, as a site for genome replication[8,58]. In the case of the β-coronavirus MHV, colocalization of this replication compartment with LC3 has been described[146]. Thus, it is intriguing to speculate that M contributes to the recruitment of membrane structures that are LC3B positive to be used as part of the viral replication compartment or that it is involved in shaping membrane trafficking for the virus.

Whereas SARS-CoV-2 Nsp15 inhibits early steps in autophagy, E, ORF3a, and ORF7a inhibit late steps. While it seems unintuitive, such a two-pronged strategy to inhibit both induction of autophagy and its degradative steps is observed with other viruses as well. HSV-1, HCMV, and HIV-1, all target Beclin-1[20,96,130,136] with a similar effect, suggesting this combination might be required to control autophagy and exploit it effectively.

Notably, these SARS-CoV-2 proteins all confer multiple functions. In addition to their effects on autophagy, they confer, for example, endonuclease activity (Nsp15[84]), act as an ion channel (E[155]), or antagonize interferon induction (M[169]) and interferon signaling (ORF3a[181] and ORF7a[186]). This suggests that the autophagy modulating functions are non-redundant and rather have evolved to enable the virus to synergistically control or exploit different aspects of autophagy and associated pathways. Such multi-functionality is common among viral proteins and also applicable for most (if not all) other proteins of SARS-CoV-2. For example, its structural proteins, which are crucial parts of the virion, are also involved in antagonizing innate immunity[65]. Nsp3 confers functions including autoproteolytic cleaving of other Nsps[62], aiding in the assembly of the replication compartment[2], and preventing the activation of the PRR MDA5 via de-ISGylation[108].

While I characterized the 5 top modulators of autophagy employed by SARS-CoV-2 in greater detail, more viral proteins showed marginal/slight autophagy modulating potential in the screen (Nsp2 and Nsp5 showing significant modulation and others displaying trends) (Fig. 8). Thus, it is highly likely that more proteins of SARS-CoV-2 will be confirmed to modulate the autophagy pathway in future studies. In addition, my experimental approach using overexpression of single proteins may have missed some viral autophagy modulating mechanisms. For example, the expression of the proteins from transfected constructs does not mimic the expression levels of the SARS-CoV-2 proteins in the viral context leaving

open the possibility that the importance of individual proteins is under- or overestimated. Thus, verification of the observed effects on autophagy in the viral context is of high interest for future studies. Further, in the screening setting, I expressed the viral proteins separately. While this allows attributing an observed effect to a specific protein, it misses effects conferred by multi-protein complexes. For example, Nsp3, Nsp4, and Nsp6 of SARS-CoV-1 are known to be critical for the formation of the replication organelle, which might involve parts of the autophagic machinery as a source for DMVs[2] and in the case of SARS-CoV-2 M is potentially involved too. Neither Nsp3 nor Nsp4 nor Nsp6 alone were picked up in my approach. Finally, any effects on autophagy or effects that avoid restriction by autophagy which are not mediated by the viral proteins but instead for example, RNA products like miRNAs or spatial separation, will not be detected.

In summary, SARS-CoV-2 uses at least 4 of its proteins, Nsp15, E, ORF3a, and ORF7a, to tightly control autophagy and potentially its M protein to exploit autophagy and benefit its replication. While the mechanisms of ORF3a and ORF7a were clarified, the molecular details of Nsp2, Nsp5, Nsp15, and E are still unclear[65,90]. In addition, other proteins may contribute to autophagy evasion by SARS-CoV-2 as well.

6.4. Filamin-NHL TRIMs and CK2 inhibit autophagy

While viruses need to counteract or evade innate immune responses like autophagy, the host has to tightly control these pathways to maintain immune homeostasis as well, even in the absence of an infection. This is especially important for a digestive process like autophagy, which is not only involved in anti-viral/anti-microbial processes but critically controls nutrient availability, protein stability, and organelle turnover in the cell[103]. Unsurprisingly, dysregulation of autophagy is observed in many malignancies like cancers and neurodegenerative diseases[103]. To identify host proteins that mediate the control of autophagy, we looked into the highly diverse family of TRIM proteins, which are well-known to modulate innate immune processes. Several TRIM proteins were previously identified to induce autophagy[163]. However, none have yet been characterized that limit autophagy. I identified the filamin-NHL containing TRIMs TRIM2, TRIM3, and TRIM71 as inhibitors of autophagy induction (Fig. 11). Their filamin domain contains an immunoglobulin (Ig)-like fold, a common motif that is known to mediate interactions with other proteins[48,60,168], and the NHL repeats are found in a large number of eukaryotic and prokaryotic proteins[42,55,162] and are known to confer RNA binding[95,113]. Such RNA binding could be important for autophagy inhibition, as some long non-coding RNAs have been

described to activate autophagy[14,72,174,180]. These three TRIM proteins, but not their close relatives TRIM32, TRIM45, and TRIM56, that lack either one or two of the C-terminal domains, reduce autophagy levels. Curiously, while TRIM45 (containing just the filamin domain) does not affect autophagy, TRIM32[34,35,166] (containing only the NHL repeats) and TRIM56[175] (lacking both domains) increase autophagy levels, suggesting that a synergistic interaction between the two domains as well as the conserved region of the TRIMs is required to mediate inhibition of autophagy. While the precise function of the NHL repeats and the filamin domain in this context remains elusive, truncation of the NHL repeats in TRIM3 leads to a switch of its effect on autophagy from inhibitory to activatory (unpublished data, not shown), highlighting its importance. It is possible that the TRIMs target autophagy-modulating RNAs with their NHL repeats to inhibit autophagy.

To elucidate the molecular mechanism underlying filamin-NHL TRIM-mediated autophagy inhibition, I identified interaction partners of TRIM2 and TRIM3. Among them, CK2 stood out, as the entire tetrameric complex comprised of two active (CK2α and CK2α', two subunits per complex) and one regulatory subunit (CK2β, two subunits per complex) showed potent interaction with both TRIM2 and TRIM3 (Fig. 12A,B). CK2 is a constitutively active Ser/Thr protein kinase that interacts with a plethora of pathways with targets that are involved in gene expression, signaling, viral replication, and more[124,147]. While CK2 has been described to alter autophagy, its role in the regulation of the pathway is discussed as both inducing and inhibitory functionality have been attributed to it[83,140,176,182]. Using co-immunoprecipitation, I confirmed the interaction of overexpressed TRIMs and CK2 subunits, albeit with background binding of the CK2α and CK2α' subunits to the beads. By using harsher conditions during washing, e.g. by increasing the salt concentration and the number of washing steps, or by using a different substrate for the co-immunoprecipitation, this background binding may be decreased. While I also observed some background binding in the initial co-immunoprecipitation using TRIM2ΔRING and TRIM3ΔRING as bait for the endogenous CK2α and CK2α' subunit, a potent co-enrichment with the TRIMs was observed in both cases, arguing for interaction between TRIMs and CK2. In accordance with the literature[45], I found both CK2 and the filamin-NHL TRIMs in the cytoplasm, allowing for a potential functional interaction in the cell (Fig. 12C,D). While I did not observe a specific colocalization of the TRIMs and CK2, the dissociation of the substrate after processing by the interaction partner could be responsible for this. To circumvent this, experiments using CK2 inhibitors while analyzing colocalization are of interest. Of note,

expression of CK2, like the filamin-NHL TRIMs, inhibits induction of autophagy and vice versa, the pharmacological inhibition of CK2 increases autophagic flux, arguing for a potential functional link of the interaction partners (Fig. 13A,B).

Using the primary sequence in *in silico* analysis, I identified three sites in the filamin-NHL TRIMs that could serve as putative phosphorylation sites of CK2 (Fig. 13E). Two of the sites are located at the N-terminus and conserved in TRIM2 and TRIM3, with one of them falling into the catalytic RING domain and the other one being located in close proximity to it. Both N-terminal, putative phosphorylation sites have the potential to influence the catalytic activity of the TRIMs and thus their inhibition of autophagy. The third putative CK2 phosphorylation site is located in the fifth NHL repeat and conserved for TRIM2 and TRIM3. TRIM71 shares a serine at the same location, however, it has altered adjacent amino acids. In TRIM2 and TRIM3, the site corresponds to the CK2 target site (SxxE) with a serine or threonine at position n and an acidic residue (D or E) at position n+3[123,124]. In TRIM71, the S at position n is conserved, however, the glutamic acid is moved to position n+1, and threonine is present at position n+3 (SExT). While it is not standard, CK2 phosphorylation can occur when acidic residues are present at positions other than n+3, but there is usually more than one acidic residue present in these cases. A phosphorylated residue at position n+3 has also been described to favor CK2 phosphorylation. Thus, phosphorylation of TRIM71 at this residue is possible. Upon initial investigation using alanine mutants of TRIM3, I observed that only mutation of the putative phosphorylation site in the NHL repeats reduces the inhibitory effect of TRIM3 on autophagy. This hints at a potential enhancing phosphorylation of TRIM3 by CK2 at this position. However, experiments confirming the phosphorylation of the filamin-NHL TRIMs by CK2 are required before a definitive statement can be made. As the C-terminal domains of TRIMs are mainly responsible for substrate specificity, phosphorylation of the serine in the NHL repeats could influence substrate binding or the interplay between the domains to impact the autophagy modulating properties.

In Summary, I identified the filamin-NHL TRIMs TRIM2, TRIM3, and TRIM71, as well as CK2 as inhibitors of autophagy induction. Further, I propose the CK2-TRIM axis as a novel autophagy modulating pathway in which CK2 interacts with the TRIMs and phosphorylates them to inhibit autophagy.

6.5. Outlook

Our knowledge of the regulation of autophagy and its interaction with viral pathogens constantly expands. However, many open questions remain. By understanding the viral antagonism of autophagy and solving its specific regulation, we will hopefully be able to finetune this pathway to be most effective at combating viral infection.

6.5.1. Evolution of autophagy antagonism by SARS-CoV-2

To understand more about the autophagy antagonism by SARS-CoV-2, we aim to investigate its evolution. For one, we are going to compare the autophagy modulating SARS-CoV-2 proteins I identified to their homologs in the common cold coronaviruses, which have been circulating in the human population for decades[67,144,179,183] and are considered to be endemic. This comparison could give insight into the specific adaptations to the human host as well as the relation between autophagy antagonism and disease severity. Further, we want to examine how autophagy antagonism has been shaped by evolution over the course of the current COVID-19 pandemic by investigating the changes to autophagy antagonism and resistance of the variants of concern. This could give insights into adaptations specific to the human host and establish the autophagy antagonism's relevance for viral fitness.

6.5.2. Modulation of virus-induced autophagy and inflammation via the novel CK2-TRIM axis

While I found hints that CK2 phosphorylates TRIM3 to inhibit autophagy, this interaction needs to be further investigated. The next step is to analyze the phosphorylation status of TRIM3 and its mutants at the predicted CK2 phosphorylation sites e.g. via mass spectrometry. Additionally, I plan to assess the importance of the filamin-NHL TRIMs in viral infection. I will investigate whether viruses have evolved to hijack these proteins to influence autophagy in their favor. In addition, pharmaceutical modulation of the CK2-TRIM axis could be a novel, broadly active approach to combat viruses that are restricted by autophagy, such as HIV-1[117,131] and MERS[50]. Inversely, exogenous activation of the filamin-NHL TRIMs to reduce autophagy levels could be used to treat infections with autophagy-dependent viruses, like influenza A[200]. To facilitate the modulation of this novel axis, we want to identify peptides or small molecules targeting the filamin-NHL TRIMs. Such drugs specifically modulating autophagy via the filamin-NHL TRIMs would have great potential in therapeutic approaches even beyond viral infections by allowing the rebalancing of dysregulated autophagy. However, it needs to be considered that targeting CK2 in

therapeutic approaches is a less autophagy-focused approach due to the wide variety of pathways influenced by CK2. Interestingly, inhibition of CK2 has been identified as a potential treatment option for SARS-CoV-2 infection[11]. The treatment of severe COVID-19 patients with the CK2 inhibitor CX-4945 is currently under clinical investigation[178]. How increased autophagy levels caused by the inhibition of CK2 contribute to the anti-SARS-CoV-2 effect of CX-4945 remains to be elucidated. Inhibition of CK2 is further being investigated in the treatment of multiple cancers[121,152] and seems promising in combination with other established treatments to achieve a synergistic effect and reduce severe side effects[31].

6.5.3. Beyond virology – autophagy modulation in bacterial infections, cancer, and neurodegenerative diseases

Modulating autophagy in therapeutic settings is not limited to the treatment of viral infections. For one, autophagy restricts bacterial[69,137] and fungal[137] pathogens, and thus, induction of autophagy can combat the associated malignancies. Further, a rebalancing of dysregulated autophagy in cancers[122] and neurodegenerative diseases[125] could be part of future treatments. While the potential of autophagy modulation as a treatment is immense, the interplay between autophagy and disease needs to be thoroughly investigated. Only when this interaction is sufficiently well understood can autophagy be modulated in a way that maximizes counteraction of the pathogen or disease mechanism while minimizing detrimental effects caused by its dysregulation.

7. Summary

Autophagy is an auto-digestive process targeting cytoplasmic cargo for lysosomal degradation. It is crucial for maintaining cellular homeostasis, and dysregulation of autophagy is associated with a number of malignancies, including cancer and neurodegenerative diseases. Notably, autophagy plays an emerging role in anti-viral innate immune defenses. However, successful viral pathogens have evolved mechanisms to avoid restriction by autophagy. For example, the pandemic coronavirus SARS-CoV-2 suppresses autophagic turnover in infected cells, but the viral determinants responsible were unknown. To investigate which proteins of SARS-CoV-2 counteract autophagy, I established a method to rapidly and accurately quantify changes in autophagic flux using flow cytometry[91]. I analyzed the impact of 29 proteins of SARS-CoV-2 on autophagy and identified Non-structural protein 2 (Nsp2), Nsp5, Nsp15, envelope (E), membrane (M), ORF3a and ORF7a as candidate autophagy antagonists[65,90]. The five most potent modulators (Nsp15, E, M, ORF3a and ORF7a) were subsequently explored in more detail. We found that Nsp15 inhibits the induction of autophagy, likely via mTORC1, whereas E, ORF3a, and ORF7a inhibit turnover of autophagosomes. Mechanistically, ORF3a inhibits the fusion of autophagosomes and lysosomes, and ORF7a prevents the acidification of (auto-)lysosomes. Finally, M redirects autophagic membranes to the perinuclear space but does not impact autophagic flux. The reporter system to analyze the impact of proteins on autophagy was also applied to discover novel cellular proteins that regulate autophagy. Here, I identified three members of the tripartite motif (TRIM) protein family, TRIM2, 3, and 71, as novel inhibitors of autophagic flux. My data shows that these TRIMs use their filamin-NHL domain to reduce autophagy induction. CK2 was found to be a major interaction partner of TRIM2/3 and 71 which also regulates autophagy. Overexpression of CK2 reduces autophagic flux, conversely inhibition of CK2 activates autophagy. *In silico*, we identified a putative CK2 phosphorylation site in the NHL repeats of the TRIMs. Strikingly, mutation of this site reduced the functionality of TRIM3, suggesting that CK2 activates filamin-NHL TRIMs by phosphorylation in their NHL domain to inhibit autophagy.

In summary, I established a method for rapid quantification of changes in autophagy[91], allowing me to define novel viral and host autophagy regulating proteins. Characterization of autophagy antagonists of SARS-CoV-2 gave insight on how this pathogen avoids restriction by autophagy[65,90]. In addition, my data proposes the cellular CK2-TRIM2/3/71 axis as a novel autophagy inhibiting pathway to maintain autophagy homeostasis.

8. References

(1) Ampofo E, Sokolowsky T, Götz C, Montenarh M: Functional Interaction of Protein Kinase CK2 and Activating Transcription Factor 4 (ATF4), a Key Player in the Cellular Stress Response. Biochimica et Biophysica Acta (BBA) - Molecular Cell Research 1833 439–451 (2013)

(2) Angelini M M, Akhlaghpour M, Neuman B W, Buchmeier M J: Severe Acute Respiratory Syndrome Coronavirus Nonstructural Proteins 3, 4, and 6 Induce Double-Membrane Vesicles. mBio 4 e00524-13 (2013)

(3) Bae J S, Park S-H, Kim K M, Kwon K S, Kim C Y, Lee H K, Park B-H, Park H S, Lee H, Moon W S, Chung M J, Sylvester K G, Jang K Y: CK2α Phosphorylates DBC1 and Is Involved in the Progression of Gastric Carcinoma and Predicts Poor Survival of Gastric Carcinoma Patients. International Journal of Cancer 136 797–809 (2015)

(4) Baginska J, Viry E, Berchem G, Poli A, Noman M Z, van Moer K, Medves S, Zimmer J, Oudin A, Niclou S P, Bleackley R C, Goping I S, Chouaib S, Janji B: Granzyme B Degradation by Autophagy Decreases Tumor Cell Susceptibility to Natural Killer-Mediated Lysis under Hypoxia. Proceedings of the National Academy of Sciences 110 17450–17455 (2013)

(5) Balastik M, Ferraguti F, Pires-da Silva A, Lee T H, Alvarez-Bolado G, Lu K P, Gruss P: Deficiency in Ubiquitin Ligase TRIM2 Causes Accumulation of Neurofilament Light Chain and Neurodegeneration. Proc. Natl. Acad. Sci. U.S.A. 105 12016–12021 (2008)

(6) Barz S, Kriegenburg F, Sánchez-Martín P, Kraft C: Small but Mighty: Atg8s and Rabs in Membrane Dynamics during Autophagy. Biochimica et Biophysica Acta (BBA) - Molecular Cell Research 1868 119064 (2021)

(7) Beale R, Wise H, Stuart A, Ravenhill B J, Digard P, Randow F: A LC3-Interacting Motif in the Influenza A Virus M2 Protein Is Required to Subvert Autophagy and Maintain Virion Stability. Cell Host & Microbe 15 239–247 (2014)

(8) Belov G A, Nair V, Hansen B T, Hoyt F H, Fischer E R, Ehrenfeld E: Complex Dynamic Development of Poliovirus Membranous Replication Complexes. J Virol 86 302–312 (2012)

(9) Ben-Sahra I, Manning B D: MTORC1 Signaling and the Metabolic Control of Cell Growth. Current Opinion in Cell Biology 45 72–82 (2017)

(10) Blanchet F P, Moris A, Nikolic D S, Lehmann M, Cardinaud S, Stalder R, Garcia E, Dinkins C, Leuba F, Wu L, Schwartz O, Deretic V, Piguet V: Human Immunodeficiency Virus-1 Inhibition of Immunoamphisomes in Dendritic Cells Impairs Early Innate and Adaptive Immune Responses. Immunity 32 654–669 (2010)

(11) Bouhaddou M, Memon D, Meyer B, White K M, Rezelj V V, Correa Marrero M, Polacco B J, Melnyk J E, Ulferts S, Kaake R M, Batra J, Richards A L, Stevenson E, Gordon D E, Rojc A, Obernier K, Fabius J M, Soucheray M, Miorin L, Moreno E, Koh C, Tran Q D, Hardy A, Robinot R, Vallet T, Nilsson-Payant B E, Hernandez-Armenta C, Dunham A, Weigang S, Knerr J, Modak M, Quintero D, Zhou Y, Dugourd A, Valdeolivas A, Patil T, Li Q, Hüttenhain R, Cakir M, Muralidharan M, Kim M, Jang G, Tutuncuoglu B, Hiatt J, Guo J Z, Xu J, Bouhaddou S, Mathy C J P, Gaulton A, Manners E J, Félix E, Shi Y, Goff M, Lim J K, McBride T, O'Neal M C, Cai Y, Chang J C J, Broadhurst D J, Klippsten S, De wit E, Leach A R, Kortemme T, Shoichet B, Ott M, Saez-Rodriguez J, tenOever B R, Mullins R D, Fischer E R, Kochs G, Grosse R, García-Sastre A, Vignuzzi M, Johnson J R, Shokat K M, Swaney

D L, Beltrao P, Krogan N J: The Global Phosphorylation Landscape of SARS-CoV-2 Infection. Cell 182 685-712.e19 (2020)

(12) Bravo-San Pedro J M, Pietrocola F, Sica V, Izzo V, Sauvat A, Kepp O, Maiuri M C, Kroemer G, Galluzzi L: High-Throughput Quantification of GFP-LC3+ Dots by Automated Fluorescence Microscopy. In *Methods in Enzymology*; Elsevier, 2017; Vol. 587, pp 71–86

(13) Brencicova E, Diebold S S: Nucleic Acids and Endosomal Pattern Recognition: How to Tell Friend from Foe? Front Cell Infect Microbiol 3 37 (2013)

(14) Cai Q, Wang S, Jin L, Weng M, Zhou D, Wang J, Tang Z, Quan Z: Long Non-Coding RNA GBCDRlnc1 Induces Chemoresistance of Gallbladder Cancer Cells by Activating Autophagy. Molecular Cancer 18 82 (2019)

(15) Cairns D M, Dulko D, Griffiths J K, Golan Y, Cohen T, Trinquart L, Price L L, Beaulac K R, Selker H P: Efficacy of Niclosamide vs Placebo in SARS-CoV-2 Respiratory Viral Clearance, Viral Shedding, and Duration of Symptoms Among Patients With Mild to Moderate COVID-19: A Phase 2 Randomized Clinical Trial. JAMA Network Open 5 e2144942 (2022)

(16) Cao B, Parnell L A, Diamond M S, Mysorekar I U: Inhibition of Autophagy Limits Vertical Transmission of Zika Virus in Pregnant Mice. Journal of Experimental Medicine 214 2303–2313 (2017)

(17) Carlsson S R, Fukuda M: The Lysosomal Membrane Glycoprotein Lamp-1 Is Transported to Lysosomes by Two Alternative Pathways. Archives of Biochemistry and Biophysics 296 630–639 (1992)

(18) Chai J, Cai Y, Pang C, Wang L, McSweeney S, Shanklin J, Liu Q: Structural Basis for SARS-CoV-2 Envelope Protein Recognition of Human Cell Junction Protein PALS1. Nat Commun 12 3433 (2021)

(19) Chang H-M, Martinez N J, Thornton J E, Hagan J P, Nguyen K D, Gregory R I: Trim71 Cooperates with MicroRNAs to Repress Cdkn1a Expression and Promote Embryonic Stem Cell Proliferation. Nat Commun 3 923 (2012)

(20) Chaumorcel M, Lussignol M, Mouna L, Cavignac Y, Fahie K, Cotte-Laffitte J, Geballe A, Brune W, Beau I, Codogno P, Esclatine A: The Human Cytomegalovirus Protein TRS1 Inhibits Autophagy via Its Interaction with Beclin 1. J Virol 86 2571–2584 (2012)

(21) Chavez-Dominguez R, Perez-Medina M, Lopez-Gonzalez J S, Galicia-Velasco M, Aguilar-Cazares D: The Double-Edge Sword of Autophagy in Cancer: From Tumor Suppression to Pro-Tumor Activity. Frontiers in Oncology 10 (2020)

(22) Chen D, Zheng Q, Sun L, Ji M, Li Y, Deng H, Zhang H: ORF3a of SARS-CoV-2 Promotes Lysosomal Exocytosis-Mediated Viral Egress. Developmental Cell 56 3250-3263.e5 (2021)

(23) Chen G, Kong J, Tucker-Burden C, Anand M, Rong Y, Rahman F, Moreno C S, Van Meir E G, Hadjipanayis C G, Brat D J: Human Brat Ortholog TRIM3 Is a Tumor Suppressor That Regulates Asymmetric Cell Division in Glioblastoma. Cancer Research 74 4536–4548 (2014)

(24) Chen X, Wang K, Xing Y, Tu J, Yang X, Zhao Q, Li K, Chen Z: Coronavirus Membrane-Associated Papain-like Proteases Induce Autophagy through Interacting with Beclin1 to Negatively Regulate Antiviral Innate Immunity. Protein Cell 5 912–927 (2014)

(25) Chen Y, Hao Q, Wang J, Li J, Huang C, Zhang Y, Wu X, Lu H, Zhou X: Ubiquitin Ligase TRIM71 Suppresses Ovarian Tumorigenesis by Degrading Mutant P53. Cell Death Dis 10 1–14 (2019)

(26) Choi Y, Bowman J W, Jung J U: Autophagy during Viral Infection — a Double-Edged Sword. Nat Rev Microbiol 16 341–354 (2018)
(27) Chon H J, Bae K J, Lee Y, Kim J: The Casein Kinase 2 Inhibitor, CX-4945, as an Anti-Cancer Drug in Treatment of Human Hematological Malignancies. Front. Pharmacol. 6 (2015)
(28) Commissioner O of the: *Coronavirus (COVID-19) Update: FDA Revokes Emergency Use Authorization for Chloroquine and Hydroxychloroquine*. FDA. https://www.fda.gov/news-events/press-announcements/coronavirus-covid-19-update-fda-revokes-emergency-use-authorization-chloroquine-and (accessed 2022-07-01)
(29) Cortese M, Goellner S, Acosta E G, Neufeldt C J, Oleksiuk O, Lampe M, Haselmann U, Funaya C, Schieber N, Ronchi P, Schorb M, Pruunsild P, Schwab Y, Chatel-Chaix L, Ruggieri A, Bartenschlager R: Ultrastructural Characterization of Zika Virus Replication Factories. Cell Reports 18 2113–2123 (2017)
(30) Cottam E M, Whelband M C, Wileman T: Coronavirus NSP6 Restricts Autophagosome Expansion. Autophagy 10 1426–1441 (2014)
(31) D'Amore C, Borgo C, Sarno S, Salvi M: Role of CK2 Inhibitor CX-4945 in Anti-Cancer Combination Therapy – Potential Clinical Relevance. Cell Oncol. 43 1003–1016 (2020)
(32) Deitersen J, Berning L, Stuhldreier F, Ceccacci S, Schlütermann D, Friedrich A, Wu W, Sun Y, Böhler P, Berleth N, Mendiburo M J, Seggewiß S, Anand R, Reichert A S, Monti M C, Proksch P, Stork B: High-Throughput Screening for Natural Compound-Based Autophagy Modulators Reveals Novel Chemotherapeutic Mode of Action for Arzanol. Cell Death Dis 12 560 (2021)
(33) Deretic V, Saitoh T, Akira S: Autophagy in Infection, Inflammation and Immunity. Nat Rev Immunol 13 722–737 (2013)
(34) Di Rienzo M, Antonioli M, Fusco C, Liu Y, Mari M, Orhon I, Refolo G, Germani F, Corazzari M, Romagnoli A, Ciccosanti F, Mandriani B, Pellico M T, De La Torre R, Ding H, Dentice M, Neri M, Ferlini A, Reggiori F, Kulesz-Martin M, Piacentini M, Merla G, Fimia G M: Autophagy Induction in Atrophic Muscle Cells Requires ULK1 Activation by TRIM32 through Unanchored K63-Linked Polyubiquitin Chains. Sci. Adv. 5 eaau8857 (2019)
(35) Di Rienzo M, Piacentini M, Fimia G M: A TRIM32-AMBRA1-ULK1 Complex Initiates the Autophagy Response in Atrophic Muscle Cells. Autophagy 15 1674–1676 (2019)
(36) Ding B, Zhang G, Yang X, Zhang S, Chen L, Yan Q, Xu M, Banerjee A K, Chen M: Phosphoprotein of Human Parainfluenza Virus Type 3 Blocks Autophagosome-Lysosome Fusion to Increase Virus Production. Cell Host & Microbe 15 564–577 (2014)
(37) Dixit D, Sharma V, Ghosh S, Mehta V S, Sen E: Inhibition of Casein Kinase-2 Induces P53-Dependent Cell Cycle Arrest and Sensitizes Glioblastoma Cells to Tumor Necrosis Factor (TNFα)-Induced Apoptosis through SIRT1 Inhibition. Cell Death Dis 3 e271–e271 (2012)
(38) Dong W, Luo B, Qiu C, Jiang X, Shen B, Zhang L, Liu W, Zhang W: TRIM3 Attenuates Apoptosis in Parkinson's Disease via Activating PI3K/AKT Signal Pathway. Aging 13 735–749 (2021)
(39) Dotan I, Ziv E, Dafni N, Beckman J S, McCann R O, Glover C V C, Canaani D: Functional Conservation between the Human, Nematode, and Yeast CK2 Cell Cycle Genes. Biochemical and Biophysical Research Communications 288 603–609 (2001)

(40) Drożdżal S, Rosik J, Lechowicz K, Machaj F, Szostak B, Przybyciński J, Lorzadeh S, Kotfis K, Ghavami S, Łos M J: An Update on Drugs with Therapeutic Potential for SARS-CoV-2 (COVID-19) Treatment. Drug Resistance Updates 59 100794 (2021)
(41) Dull T, Zufferey R, Kelly M, Mandel R J, Nguyen M, Trono D, Naldini L: A Third-Generation Lentivirus Vector with a Conditional Packaging System. J Virol 72 8463–8471 (1998)
(42) Edwards T A, Wilkinson B D, Wharton R P, Aggarwal A K: Model of the Brain Tumor–Pumilio Translation Repressor Complex. Genes Dev. 17 2508–2513 (2003)
(43) Eng K E, Panas M D, Hedestam G B K, McInerney G M: A Novel Quantitative Flow Cytometry-Based Assay for Autophagy. Autophagy 6 634–641 (2010)
(44) Eskelinen E-L, Reggiori F, Baba M, Kovács A L, Seglen P O: Seeing Is Believing: The Impact of Electron Microscopy on Autophagy Research. Autophagy 7 935–956 (2011)
(45) Faust M, Montenarh M: Subcellular Localization of Protein Kinase CK2. Cell Tissue Res 301 329–340 (2000)
(46) Ferrer-Font L, Villamañan L, Arias-Ramos N, Vilardell J, Plana M, Ruzzene M, Pinna L, Itarte E, Arús C, Candiota A: Targeting Protein Kinase CK2: Evaluating CX-4945 Potential for GL261 Glioblastoma Therapy in Immunocompetent Mice. Pharmaceuticals 10 24 (2017)
(47) Fu B, Wang L, Ding H, Schwamborn J C, Li S, Dorf M E: TRIM32 Senses and Restricts Influenza A Virus by Ubiquitination of PB1 Polymerase. PLoS Pathog 11 e1004960 (2015)
(48) Fucini P, Renner C, Herberhold C, Noegel A A, Holak T A: The Repeating Segments of the F-Actin Cross-Linking Gelation Factor (ABP-120) Have an Immunoglobulin-like Fold. Nat Struct Biol 4 223–230 (1997)
(49) Garcia-Beltran W F, Lam E C, St. Denis K, Nitido A D, Garcia Z H, Hauser B M, Feldman J, Pavlovic M N, Gregory D J, Poznansky M C, Sigal A, Schmidt A G, Iafrate A J, Naranbhai V, Balazs A B: Multiple SARS-CoV-2 Variants Escape Neutralization by Vaccine-Induced Humoral Immunity. Cell 184 2372-2383.e9 (2021)
(50) Gassen N C, Niemeyer D, Muth D, Corman V M, Martinelli S, Gassen A, Hafner K, Papies J, Mösbauer K, Zellner A, Zannas A S, Herrmann A, Holsboer F, Brack-Werner R, Boshart M, Müller-Myhsok B, Drosten C, Müller M A, Rein T: SKP2 Attenuates Autophagy through Beclin1-Ubiquitination and Its Inhibition Reduces MERS-Coronavirus Infection. Nat Commun 10 5770 (2019)
(51) Gassen N C, Papies J, Bajaj T, Emanuel J, Dethloff F, Chua R L, Trimpert J, Heinemann N, Niemeyer C, Weege F, Hönzke K, Aschman T, Heinz D E, Weckmann K, Ebert T, Zellner A, Lennarz M, Wyler E, Schroeder S, Richter A, Niemeyer D, Hoffmann K, Meyer T F, Heppner F L, Corman V M, Landthaler M, Hocke A C, Morkel M, Osterrieder N, Conrad C, Eils R, Radbruch H, Giavalisco P, Drosten C, Müller M A: SARS-CoV-2-Mediated Dysregulation of Metabolism and Autophagy Uncovers Host-Targeting Antivirals. Nat Commun 12 3818 (2021)
(52) Geng J, Klionsky D J: The Atg8 and Atg12 Ubiquitin-like Conjugation Systems in Macroautophagy. EMBO Rep 9 859–864 (2008)
(53) Geng J, Klionsky D J: Direct Quantification of Autophagic Flux by a Single Molecule-Based Probe. Autophagy 13 639–641 (2017)
(54) Ghosh S, Dellibovi-Ragheb T A, Kerviel A, Pak E, Qiu Q, Fisher M, Takvorian P M, Bleck C, Hsu V W, Fehr A R, Perlman S, Achar S R, Straus M R, Whittaker G R, de Haan C A M, Kehrl J, Altan-Bonnet G, Altan-Bonnet N: β-Coronaviruses Use

Lysosomes for Egress Instead of the Biosynthetic Secretory Pathway. Cell 183 1520-1535.e14 (2020)

(55) Good M C, Greenstein A E, Young T A, Ng H-L, Alber T: Sensor Domain of the Mycobacterium Tuberculosis Receptor Ser/Thr Protein Kinase, PknD, Forms a Highly Symmetric β Propeller. Journal of Molecular Biology 339 459–469 (2004)

(56) Gordon D E, Jang G M, Bouhaddou M, Xu J, Obernier K, White K M, O'Meara M J, Rezelj V V, Guo J Z, Swaney D L, Tummino T A, Hüttenhain R, Kaake R M, Richards A L, Tutuncuoglu B, Foussard H, Batra J, Haas K, Modak M, Kim M, Haas P, Polacco B J, Braberg H, Fabius J M, Eckhardt M, Soucheray M, Bennett M J, Cakir M, McGregor M J, Li Q, Meyer B, Roesch F, Vallet T, Mac Kain A, Miorin L, Moreno E, Naing Z Z C, Zhou Y, Peng S, Shi Y, Zhang Z, Shen W, Kirby I T, Melnyk J E, Chorba J S, Lou K, Dai S A, Barrio-Hernandez I, Memon D, Hernandez-Armenta C, Lyu J, Mathy C J P, Perica T, Pilla K B, Ganesan S J, Saltzberg D J, Rakesh R, Liu X, Rosenthal S B, Calviello L, Venkataramanan S, Liboy-Lugo J, Lin Y, Huang X-P, Liu Y, Wankowicz S A, Bohn M, Safari M, Ugur F S, Koh C, Savar N S, Tran Q D, Shengjuler D, Fletcher S J, O'Neal M C, Cai Y, Chang J C J, Broadhurst D J, Klippsten S, Sharp P P, Wenzell N A, Kuzuoglu-Ozturk D, Wang H-Y, Trenker R, Young J M, Cavero D A, Hiatt J, Roth T L, Rathore U, Subramanian A, Noack J, Hubert M, Stroud R M, Frankel A D, Rosenberg O S, Verba K A, Agard D A, Ott M, Emerman M, Jura N, von Zastrow M, Verdin E, Ashworth A, Schwartz O, d'Enfert C, Mukherjee S, Jacobson M, Malik H S, Fujimori D G, Ideker T, Craik C S, Floor S N, Fraser J S, Gross J D, Sali A, Roth B L, Ruggero D, Taunton J, Kortemme T, Beltrao P, Vignuzzi M, García-Sastre A, Shokat K M, Shoichet B K, Krogan N J: A SARS-CoV-2 Protein Interaction Map Reveals Targets for Drug Repurposing. Nature 583 459–468 (2020)

(57) Guo S, Liang Y, Murphy S F, Huang A, Shen H, Kelly D F, Sobrado P, Sheng Z: A Rapid and High Content Assay That Measures Cyto-ID-Stained Autophagic Compartments and Estimates Autophagy Flux with Potential Clinical Applications. Autophagy 11 560–572 (2015)

(58) de Haan C A M, Reggiori F: Are Nidoviruses Hijacking the Autophagy Machinery? Autophagy 4 276–279 (2008)

(59) Hackbart M, Deng X, Baker S C: Coronavirus Endoribonuclease Targets Viral Polyuridine Sequences to Evade Activating Host Sensors. Proc. Natl. Acad. Sci. U.S.A. 117 8094–8103 (2020)

(60) Halaby D M, Poupon A, Mornon J-P: The Immunoglobulin Fold Family: Sequence Analysis and 3D Structure Comparisons. Protein Engineering, Design and Selection 12 563–571 (1999)

(61) Hamel R, Dejarnac O, Wichit S, Ekchariyawat P, Neyret A, Luplertlop N, Perera-Lecoin M, Surasombatpattana P, Talignani L, Thomas F, Cao-Lormeau V-M, Choumet V, Briant L, Desprès P, Amara A, Yssel H, Missé D: Biology of Zika Virus Infection in Human Skin Cells. J Virol 89 8880–8896 (2015)

(62) Harcourt B H, Jukneliene D, Kanjanahaluethai A, Bechill J, Severson K M, Smith C M, Rota P A, Baker S C: Identification of Severe Acute Respiratory Syndrome Coronavirus Replicase Products and Characterization of Papain-Like Protease Activity. Journal of Virology 78 13600–13612 (2004)

(63) Hashimoto A, Gao C, Mastio J, Kossenkov A, Abrams S I, Purandare A V, Desilva H, Wee S, Hunt J, Jure-Kunkel M, Gabrilovich D I: Inhibition of Casein Kinase 2 Disrupts Differentiation of Myeloid Cells in Cancer and Enhances the Efficacy of Immunotherapy in Mice. Cancer Research 78 5644–5655 (2018)

(64) Hatakeyama S: TRIM Family Proteins: Roles in Autophagy, Immunity, and Carcinogenesis. Trends in Biochemical Sciences 42 297–311 (2017)
(65) Hayn M, Hirschenberger M, Koepke L, Nchioua R, Straub J H, Klute S, Hunszinger V, Zech F, Prelli Bozzo C, Aftab W, Christensen M H, Conzelmann C, Müller J A, Srinivasachar Badarinarayan S, Stürzel C M, Forne I, Stenger S, Conzelmann K-K, Münch J, Schmidt F I, Sauter D, Imhof A, Kirchhoff F, Sparrer K M J: Systematic Functional Analysis of SARS-CoV-2 Proteins Uncovers Viral Innate Immune Antagonists and Remaining Vulnerabilities. Cell Reports 35 109126 (2021)
(66) He P, Peng Z, Luo Y, Wang L, Yu P, Deng W, An Y, Shi T, Ma D: High-Throughput Functional Screening for Autophagy-Related Genes and Identification of TM9SF1 as an Autophagosome-Inducing Gene. Autophagy 5 52–60 (2009)
(67) van der Hoek L, Pyrc K, Jebbink M F, Vermeulen-Oost W, Berkhout R J M, Wolthers K C, Wertheim-van Dillen P M E, Kaandorp J, Spaargaren J, Berkhout B: Identification of a New Human Coronavirus. Nat Med 10 368–373 (2004)
(68) Homewood C A, Warhurst D C, Peters W, Baggaley V C: Lysosomes, PH and the Anti-Malarial Action of Chloroquine. Nature 235 50–52 (1972)
(69) Huang J, Brumell J H: Bacteria–Autophagy Interplay: A Battle for Survival. Nat Rev Microbiol 12 101–114 (2014)
(70) Huang X-Q, Zhang X-F, Xia J-H, Chao J, Pan Q-Z, Zhao J-J, Zhou Z-Q, Chen C-L, Tang Y, Weng D-S, Zhang J-H, Xia J-C: Tripartite Motif-Containing 3 (TRIM3) Inhibits Tumor Growth and Metastasis of Liver Cancer. Chin J Cancer 36 77 (2017)
(71) Husain A, Byrareddy S N: Rapamycin as a Potential Repurpose Drug Candidate for the Treatment of COVID-19. Chemico-Biological Interactions 331 109282 (2020)
(72) Hwang H J, Ha H, Lee B S, Kim B H, Song H K, Kim Y K: LC3B Is an RNA-Binding Protein to Trigger Rapid MRNA Degradation during Autophagy. Nat Commun 13 1436 (2022)
(73) Itakura E, Kishi C, Inoue K, Mizushima N: Beclin 1 Forms Two Distinct Phosphatidylinositol 3-Kinase Complexes with Mammalian Atg14 and UVRAG. MBoC 19 5360–5372 (2008)
(74) Jang D E, Song J, Park J-W, Yoon S-H, Bae Y-S: Protein Kinase CK2 Activates Nrf2 via Autophagic Degradation of Keap1 and Activation of AMPK in Human Cancer Cells. BMB Rep 53 272–277 (2020)
(75) Jena K K, Kolapalli S P, Mehto S, Nath P, Das B, Sahoo P K, Ahad A, Syed G H, Raghav S K, Senapati S, Chauhan S, Chauhan S: TRIM16 Controls Assembly and Degradation of Protein Aggregates by Modulating the P62-NRF2 Axis and Autophagy. EMBO J 37 (2018)
(76) Jiang P, Nishimura T, Sakamaki Y, Itakura E, Hatta T, Natsume T, Mizushima N: The HOPS Complex Mediates Autophagosome–Lysosome Fusion through Interaction with Syntaxin 17. Mol Biol Cell 25 1327–1337 (2014)
(77) Joachim J, Jiang M, McKnight N C, Howell M, Tooze S A: High-Throughput Screening Approaches to Identify Regulators of Mammalian Autophagy. Methods 75 96–104 (2015)
(78) Kabeya Y, Mizushima N, Ueno T, Yamamoto A, Kirisako T, Noda T, Kominami E, Ohsumi Y, Yoshimori T: LC3, a Mammalian Homologue of Yeast Apg8p, Is Localized in Autophagosome Membranes after Processing. EMBO J 19 5720–5728 (2000)
(79) Kahn F, Bonander C, Moghaddassi M, Rasmussen M, Malmqvist U, Inghammar M, Björk J: Risk of Severe COVID-19 from the Delta and Omicron Variants in Relation to Vaccination Status, Sex, Age and Comorbidities – Surveillance Results from Southern Sweden, July 2021 to January 2022. Euro Surveill 27 2200121 (2022)

(80) Kaizuka T, Morishita H, Hama Y, Tsukamoto S, Matsui T, Toyota Y, Kodama A, Ishihara T, Mizushima T, Mizushima N: An Autophagic Flux Probe That Releases an Internal Control. Molecular Cell 64 835–849 (2016)

(81) Kaminskyy V, Abdi A, Zhivotovsky B: A Quantitative Assay for the Monitoring of Autophagosome Accumulation in Different Phases of the Cell Cycle. Autophagy 7 83–90 (2011)

(82) Khan M M, Strack S, Wild F, Hanashima A, Gasch A, Brohm K, Reischl M, Carnio S, Labeit D, Sandri M, Labeit S, Rudolf R: Role of Autophagy, SQSTM1, SH3GLB1, and TRIM63 in the Turnover of Nicotinic Acetylcholine Receptors. Autophagy 10 123–136 (2014)

(83) Kim J, Park M, Ryu B J, Kim S H: The Protein Kinase 2 Inhibitor CX-4945 Induces Autophagy in Human Cancer Cell Lines. Bulletin of the Korean Chemical Society 35 2985–2989 (2014)

(84) Kim Y, Jedrzejczak R, Maltseva N I, Wilamowski M, Endres M, Godzik A, Michalska K, Joachimiak A: Crystal Structure of Nsp15 Endoribonuclease NendoU from SARS-CoV-2. Protein Science 29 1596–1605 (2020)

(85) Kimura S, Noda T, Yoshimori T: Dissection of the Autophagosome Maturation Process by a Novel Reporter Protein, Tandem Fluorescent-Tagged LC3. Autophagy 3 452–460 (2007)

(86) Kimura T, Jain A, Choi S W, Mandell M A, Schroder K, Johansen T, Deretic V: TRIM-Mediated Precision Autophagy Targets Cytoplasmic Regulators of Innate Immunity. Journal of Cell Biology 210 973–989 (2015)

(87) Klionsky D J, Abdel-Aziz A K, Abdelfatah S, Abdellatif M, Abdoli A, Abel S, Abeliovich H, Abildgaard M H, Abudu Y P, Acevedo-Arozena A, Adamopoulos I E, Adeli K, Adolph T E, Adornetto A, Aflaki E, Agam G, Agarwal A, Aggarwal B B, Agnello M, Agostinis P, Agrewala J N, Agrotis A, Aguilar P V, Ahmad S T, Ahmed Z M, Ahumada-Castro U, Aits S, Aizawa S, Akkoc Y, Akoumianaki T, Akpinar H A, Al-Abd A M, Al-Akra L, Al-Gharaibeh A, Alaoui-Jamali M A, Alberti S, Alcocer-Gómez E, Alessandri C, Ali M, Alim Al-Bari M A, Aliwaini S, Alizadeh J, Almacellas E, Almasan A, Alonso A, Alonso G D, Altan-Bonnet N, Altieri D C, Álvarez É M C, Alves S, Alves da Costa C, Alzaharna M M, Amadio M, Amantini C, Amaral C, Ambrosio S, Amer A O, Ammanathan V, An Z, Andersen S U, Andrabi S A, Andrade-Silva M, Andres A M, Angelini S, Ann D, Anozie U C, Ansari M Y, Antas P, Antebi A, Antón Z, Anwar T, Apetoh L, Apostolova N, Araki T, Araki Y, Arasaki K, Araújo W L, Araya J, Arden C, Arévalo M-A, Arguelles S, Arias E, Arikkath J, Arimoto H, Ariosa A R, Armstrong-James D, Arnauné-Pelloquin L, Aroca A, Arroyo D S, Arsov I, Artero R, Asaro D M L, Aschner M, Ashrafizadeh M, Ashur-Fabian O, Atanasov A G, Au A K, Auberger P, Auner H W, Aurelian L, Autelli R, Avagliano L, Ávalos Y, Aveic S, Aveleira C A, Avin-Wittenberg T, Aydin Y, Ayton S, Ayyadevara S, Azzopardi M, Baba M, Backer J M, Backues S K, Bae D-H, Bae O-N, Bae S H, Baehrecke E H, Baek A, Baek S-H, Baek S H, Bagetta G, Bagniewska-Zadworna A, Bai H, Bai J, Bai X, Bai Y, Bairagi N, Baksi S, Balbi T, Baldari C T, Balduini W, Ballabio A, Ballester M, Balazadeh S, Balzan R, Bandopadhyay R, Banerjee S, Banerjee S, Bánréti Á, Bao Y, Baptista M S, Baracca A, Barbati C, Bargiela A, Barilà D, Barlow P G, Barmada S J, Barreiro E, Barreto G E, Bartek J, Bartel B, Bartolome A, Barve G R, Basagoudanavar S H, Bassham D C, Bast R C, Basu A, Batoko H, Batten I, Baulieu E E, Baumgarner B L, Bayry J, Beale R, Beau I, Beaumatin F, Bechara L R G, Beck G R, Beers M F, Begun J, Behrends C, Behrens G M N, Bei R, Bejarano E, Bel S, Behl C, Belaid A, Belgareh-Touzé N, Bellarosa C, Belleudi F, Belló Pérez M, Bello-Morales R, Beltran J S de O, Beltran

S, Benbrook D M, Bendorius M, Benitez B A, Benito-Cuesta I, Bensalem J, Berchtold M W, Berezowska S, Bergamaschi D, Bergami M, Bergmann A, Berliocchi L, Berlioz-Torrent C, Bernard A, Berthoux L, Besirli C G, Besteiro S, Betin V M, Beyaert R, Bezbradica J S, Bhaskar K, Bhatia-Kissova I, Bhattacharya R, Bhattacharya S, Bhattacharyya S, Bhuiyan Md S, Bhutia S K, Bi L, Bi X, Biden T J, Bijian K, Billes V A, Binart N, Bincoletto C, Birgisdottir A B, Bjorkoy G, Blanco G, Blas-Garcia A, Blasiak J, Blomgran R, Blomgren K, Blum J S, Boada-Romero E, Boban M, Boesze-Battaglia K, Boeuf P, Boland B, Bomont P, Bonaldo P, Bonam S R, Bonfili L, Bonifacino J S, Boone B A, Bootman M D, Bordi M, Borner C, Bornhauser B C, Borthakur G, Bosch J, Bose S, Botana L M, Botas J, Boulanger C M, Boulton M E, Bourdenx M, Bourgeois B, Bourke N M, Bousquet G, Boya P, Bozhkov P V, Bozi L H M, Bozkurt T O, Brackney D E, Brandts C H, Braun R J, Braus G H, Bravo-Sagua R, Bravo-San Pedro J M, Brest P, Bringer M-A, Briones-Herrera A, Broaddus V C, Brodersen P, Brodsky J L, Brody S L, Bronson P G, Bronstein J M, Brown C N, Brown R E, Brum P C, Brumell J H, Brunetti-Pierri N, Bruno D, Bryson-Richardson R J, Bucci C, Buchrieser C, Bueno M, Buitrago-Molina L E, Buraschi S, Buch S, Buchan J R, Buckingham E M, Budak H, Budini M, Bultynck G, Burada F, Burgoyne J R, Burón M I, Bustos V, Büttner S, Butturini E, Byrd A, Cabas I, Cabrera-Benitez S, Cadwell K, Cai J, Cai L, Cai Q, Cairó M, Calbet J A, Caldwell G A, Caldwell K A, Call J A, Calvani R, Calvo A C, Calvo-Rubio Barrera M, Camara N O, Camonis J H, Camougrand N, Campanella M, Campbell E M, Campbell-Valois F-X, Campello S, Campesi I, Campos J C, Camuzard O, Cancino J, Candido de Almeida D, Canesi L, Caniggia I, Canonico B, Cantí C, Cao B, Caraglia M, Caramés B, Carchman E H, Cardenal-Muñoz E, Cardenas C, Cardenas L, Cardoso S M, Carew J S, Carle G F, Carleton G, Carloni S, Carmona-Gutierrez D, Carneiro L A, Carnevali O, Carosi J M, Carra S, Carrier A, Carrier L, Carroll B, Carter A B, Carvalho A N, Casanova M, Casas C, Casas J, Cassioli C, Castillo E F, Castillo K, Castillo-Lluva S, Castoldi F, Castori M, Castro A F, Castro-Caldas M, Castro-Hernandez J, Castro-Obregon S, Catz S D, Cavadas C, Cavaliere F, Cavallini G, Cavinato M, Cayuela M L, Cebollada Rica P, Cecarini V, Cecconi F, Cechowska-Pasko M, Cenci S, Ceperuelo-Mallafré V, Cerqueira J J, Cerutti J M, Cervia D, Cetintas V B, Cetrullo S, Chae H-J, Chagin A S, Chai C-Y, Chakrabarti G, Chakrabarti O, Chakraborty T, Chakraborty T, Chami M, Chamilos G, Chan D W, Chan E Y W, Chan E D, Chan H Y E, Chan H H, Chan H, Chan M T V, Chan Y S, Chandra P K, Chang C-P, Chang C, Chang H-C, Chang K, Chao J, Chapman T, Charlet-Berguerand N, Chatterjee S, Chaube S K, Chaudhary A, Chauhan S, Chaum E, Checler F, Cheetham M E, Chen C-S, Chen G-C, Chen J-F, Chen L L, Chen L, Chen L, Chen M, Chen M-K, Chen N, Chen Q, Chen R-H, Chen S, Chen W, Chen W, Chen X-M, Chen X-W, Chen X, Chen Y, Chen Y-G, Chen Y, Chen Y, Chen Y-J, Chen Y-Q, Chen Z S, Chen Z, Chen Z-H, Chen Z J, Chen Z, Cheng H, Cheng J, Cheng S-Y, Cheng W, Cheng X, Cheng X-T, Cheng Y, Cheng Z, Chen Z, Cheong H, Cheong J K, Chernyak B V, Cherry S, Cheung C F R, Cheung C H A, Cheung K-H, Chevet E, Chi R J, Chiang A K S, Chiaradonna F, Chiarelli R, Chiariello M, Chica N, Chiocca S, Chiong M, Chiou S-H, Chiramel A I, Chiurchiù V, Cho D-H, Choe S-K, Choi A M K, Choi M E, Choudhury K R, Chow N S, Chu C T, Chua J P, Chua J J E, Chung H, Chung K P, Chung S, Chung S-H, Chung Y-L, Cianfanelli V, Ciechomska I A, Cifuentes M, Cinque L, Cirak S, Cirone M, Clague M J, Clarke R, Clementi E, Coccia E M, Codogno P, Cohen E, Cohen M M, Colasanti T, Colasuonno F, Colbert R A, Colell A, Čolić M, Coll N S, Collins M O, Colombo M I, Colón-Ramos D A, Combaret L, Comincini S, Cominetti M R,

Consiglio A, Conte A, Conti F, Contu V R, Cookson M R, Coombs K M, Coppens I, Corasaniti M T, Corkery D P, Cordes N, Cortese K, Costa M do C, Costantino S, Costelli P, Coto-Montes A, Crack P J, Crespo J L, Criollo A, Crippa V, Cristofani R, Csizmadia T, Cuadrado A, Cui B, Cui J, Cui Y, Cui Y, Culetto E, Cumino A C, Cybulsky A V, Czaja M J, Czuczwar S J, D'Adamo S, D'Amelio M, D'Arcangelo D, D'Lugos A C, D'Orazi G, da Silva J A, Dafsari H S, Dagda R K, Dagdas Y, Daglia M, Dai X, Dai Y, Dai Y, Dal Col J, Dalhaimer P, Dalla Valle L, Dallenga T, Dalmasso G, Damme M, Dando I, Dantuma N P, Darling A L, Das H, Dasarathy S, Dasari S K, Dash S, Daumke O, Dauphinee A N, Davies J S, Dávila V A, Davis R J, Davis T, Dayalan Naidu S, De Amicis F, De Bosscher K, De Felice F, De Franceschi L, De Leonibus C, de Mattos Barbosa M G, De Meyer G R Y, De Milito A, De Nunzio C, De Palma C, De Santi M, De Virgilio C, De Zio D, Debnath J, DeBosch B J, Decuypere J-P, Deehan M A, Deflorian G, DeGregori J, Dehay B, Del Rio G, Delaney J R, Delbridge L M D, Delorme-Axford E, Delpino M V, Demarchi F, Dembitz V, Demers N D, Deng H, Deng Z, Dengjel J, Dent P, Denton D, DePamphilis M L, Der C J, Deretic V, Descoteaux A, Devis L, Devkota S, Devuyst O, Dewson G, Dharmasivam M, Dhiman R, di Bernardo D, Di Cristina M, Di Domenico F, Di Fazio P, Di Fonzo A, Di Guardo G, Di Guglielmo G M, Di Leo L, Di Malta C, Di Nardo A, Di Rienzo M, Di Sano F, Diallinas G, Diao J, Diaz-Araya G, Díaz-Laviada I, Dickinson J M, Diederich M, Dieudé M, Dikic I, Ding S, Ding W-X, Dini L, Dinić J, Dinic M, Dinkova-Kostova A T, Dionne M S, Distler J H W, Diwan A, Dixon I M C, Djavaheri-Mergny M, Dobrinski I, Dobrovinskaya O, Dobrowolski R, Dobson R C J, Đokić J, Dokmeci Emre S, Donadelli M, Dong B, Dong X, Dong Z, Dorn G W, Dotsch V, Dou H, Dou J, Dowaidar M, Dridi S, Drucker L, Du A, Du C, Du G, Du H-N, Du L-L, du Toit A, Duan S-B, Duan X, Duarte S P, Dubrovska A, Dunlop E A, Dupont N, Durán R V, Dwarakanath B S, Dyshlovoy S A, Ebrahimi-Fakhari D, Eckhart L, Edelstein C L, Efferth T, Eftekharpour E, Eichinger L, Eid N, Eisenberg T, Eissa N T, Eissa S, Ejarque M, El Andaloussi A, El-Hage N, El-Naggar S, Eleuteri A M, El-Shafey E S, Elgendy M, Eliopoulos A G, Elizalde M M, Elks P M, Elsasser H-P, Elsherbiny E S, Emerling B M, Emre N C T, Eng C H, Engedal N, Engelbrecht A-M, Engelsen A S T, Enserink J M, Escalante R, Esclatine A, Escobar-Henriques M, Eskelinen E-L, Espert L, Eusebio M-O, Fabrias G, Fabrizi C, Facchiano A, Facchiano F, Fadeel B, Fader C, Faesen A C, Fairlie W D, Falcó A, Falkenburger B H, Fan D, Fan J, Fan Y, Fang E F, Fang Y, Fang Y, Fanto M, Farfel-Becker T, Faure M, Fazeli G, Fedele A O, Feldman A M, Feng D, Feng J, Feng L, Feng Y, Feng Y, Feng W, Fenz Araujo T, Ferguson T A, Fernández Á F, Fernandez-Checa J C, Fernández-Veledo S, Fernie A R, Ferrante A W, Ferraresi A, Ferrari M F, Ferreira J C B, Ferro-Novick S, Figueras A, Filadi R, Filigheddu N, Filippi-Chiela E, Filomeni G, Fimia G M, Fineschi V, Finetti F, Finkbeiner S, Fisher E A, Fisher P B, Flamigni F, Fliesler S J, Flo T H, Florance I, Florey O, Florio T, Fodor E, Follo C, Fon E A, Forlino A, Fornai F, Fortini P, Fracassi A, Fraldi A, Franco B, Franco R, Franconi F, Frankel L B, Friedman S L, Fröhlich L F, Frühbeck G, Fuentes J M, Fujiki Y, Fujita N, Fujiwara Y, Fukuda M, Fulda S, Furic L, Furuya N, Fusco C, Gack M U, Gaffke L, Galadari S, Galasso A, Galindo M F, Gallolu Kankanamalage S, Galluzzi L, Galy V, Gammoh N, Gan B, Ganley I G, Gao F, Gao H, Gao M, Gao P, Gao S-J, Gao W, Gao X, Garcera A, Garcia M N, Garcia V E, García-Del Portillo F, Garcia-Escudero V, Garcia-Garcia A, Garcia-Macia M, García-Moreno D, Garcia-Ruiz C, García-Sanz P, Garg A D, Gargini R, Garofalo T, Garry R F, Gassen N C, Gatica D, Ge L, Ge W, Geiss-Friedlander R, Gelfi C, Genschik P, Gentle I E, Gerbino V, Gerhardt C,

Germain K, Germain M, Gewirtz D A, Ghasemipour Afshar E, Ghavami S, Ghigo A, Ghosh M, Giamas G, Giampietri C, Giatromanolaki A, Gibson G E, Gibson S B, Ginet V, Giniger E, Giorgi C, Girao H, Girardin S E, Giridharan M, Giuliano S, Giulivi C, Giuriato S, Giustiniani J, Gluschko A, Goder V, Goginashvili A, Golab J, Goldstone D C, Golebiewska A, Gomes L R, Gomez R, Gómez-Sánchez R, Gomez-Puerto M C, Gomez-Sintes R, Gong Q, Goni F M, González-Gallego J, Gonzalez-Hernandez T, Gonzalez-Polo R A, Gonzalez-Reyes J A, González-Rodríguez P, Goping I S, Gorbatyuk M S, Gorbunov N V, Görgülü K, Gorojod R M, Gorski S M, Goruppi S, Gotor C, Gottlieb R A, Gozes I, Gozuacik D, Graef M, Gräler M H, Granatiero V, Grasso D, Gray J P, Green D R, Greenhough A, Gregory S L, Griffin E F, Grinstaff M W, Gros F, Grose C, Gross A S, Gruber F, Grumati P, Grune T, Gu X, Guan J-L, Guardia C M, Guda K, Guerra F, Guerri C, Guha P, Guillén C, Gujar S, Gukovskaya A, Gukovsky I, Gunst J, Günther A, Guntur A R, Guo C, Guo C, Guo H, Guo L-W, Guo M, Gupta P, Gupta S K, Gupta S, Gupta V B, Gupta V, Gustafsson A B, Gutterman D D, H.B. R, Haapasalo A, Haber J E, Hać A, Hadano S, Hafrén A J, Haidar M, Hall B S, Halldén G, Hamacher-Brady A, Hamann A, Hamasaki M, Han W, Hansen M, Hanson P I, Hao Z, Harada M, Harhaji-Trajkovic L, Hariharan N, Haroon N, Harris J, Hasegawa T, Hasima Nagoor N, Haspel J A, Haucke V, Hawkins W D, Hay B A, Haynes C M, Hayrabedyan S B, Hays T S, He C, He Q, He R-R, He Y-W, He Y-Y, Heakal Y, Heberle A M, Hejtmancik J F, Helgason G V, Henkel V, Herb M, Hergovich A, Herman-Antosiewicz A, Hernández A, Hernandez C, Hernandez-Diaz S, Hernandez-Gea V, Herpin A, Herreros J, Hervás J H, Hesselson D, Hetz C, Heussler V T, Higuchi Y, Hilfiker S, Hill J A, Hlavacek W S, Ho E A, Ho I H T, Ho P W-L, Ho S-L, Ho W Y, Hobbs G A, Hochstrasser M, Hoet P H M, Hofius D, Hofman P, Höhn A, Holmberg C I, Hombrebueno J R, Yi-Ren Hong C-W H, Hooper L V, Hoppe T, Horos R, Hoshida Y, Hsin I-L, Hsu H-Y, Hu B, Hu D, Hu L-F, Hu M C, Hu R, Hu W, Hu Y-C, Hu Z-W, Hua F, Hua J, Hua Y, Huan C, Huang C, Huang C, Huang C, Huang C, Huang H, Huang K, Huang M L H, Huang R, Huang S, Huang T, Huang X, Huang Y J, Huber T B, Hubert V, Hubner C A, Hughes S M, Hughes W E, Humbert M, Hummer G, Hurley J H, Hussain S, Hussain S, Hussey P J, Hutabarat M, Hwang H-Y, Hwang S, Ieni A, Ikeda F, Imagawa Y, Imai Y, Imbriano C, Imoto M, Inman D M, Inoki K, Iovanna J, Iozzo R V, Ippolito G, Irazoqui J E, Iribarren P, Ishaq M, Ishikawa M, Ishimwe N, Isidoro C, Ismail N, Issazadeh-Navikas S, Itakura E, Ito D, Ivankovic D, Ivanova S, Iyer A K V, Izquierdo J M, Izumi M, Jäättelä M, Jabir M S, Jackson W T, Jacobo-Herrera N, Jacomin A-C, Jacquin E, Jadiya P, Jaeschke H, Jagannath C, Jakobi A J, Jakobsson J, Janji B, Jansen-Dürr P, Jansson P J, Jantsch J, Januszewski S, Jassey A, Jean S, Jeltsch-David H, Jendelova P, Jenny A, Jensen T E, Jessen N, Jewell J L, Ji J, Jia L, Jia R, Jiang L, Jiang Q, Jiang R, Jiang T, Jiang X, Jiang Y, Jimenez-Sanchez M, Jin E-J, Jin F, Jin H, Jin L, Jin L, Jin M, Jin S, Jo E-K, Joffre C, Johansen T, Johnson G V W, Johnston S A, Jokitalo E, Jolly M K, Joosten L A B, Jordan J, Joseph B, Ju D, Ju J-S, Ju J, Juárez E, Judith D, Juhász G, Jun Y, Jung C H, Jung S-C, Jung Y K, Jungbluth H, Jungverdorben J, Just S, Kaarniranta K, Kaasik A, Kabuta T, Kaganovich D, Kahana A, Kain R, Kajimura S, Kalamvoki M, Kalia M, Kalinowski D S, Kaludercic N, Kalvari I, Kaminska J, Kaminskyy V O, Kanamori H, Kanasaki K, Kang C, Kang R, Kang S S, Kaniyappan S, Kanki T, Kanneganti T-D, Kanthasamy A G, Kanthasamy A, Kantorow M, Kapuy O, Karamouzis M V, Karim Md R, Karmakar P, Katare R G, Kato M, Kaufmann S H E, Kauppinen A, Kaushal G P, Kaushik S, Kawasaki K, Kazan K, Ke P-Y, Keating D J, Keber U, Kehrl J H, Keller K E, Keller C W, Kemper J K, Kenific C M, Kepp

O, Kermorgant S, Kern A, Ketteler R, Keulers T G, Khalfin B, Khalil H, Khambu B, Khan S Y, Khandelwal V K M, Khandia R, Kho W, Khobrekar N V, Khuansuwan S, Khundadze M, Killackey S A, Kim D, Kim D R, Kim D-H, Kim D-E, Kim E Y, Kim E-K, Kim H-R, Kim H-S, Hyung-Ryong Kim, Kim J H, Kim J K, Kim J-H, Kim J, Kim J H, Kim K I, Kim P K, Kim S-J, Kimball S R, Kimchi A, Kimmelman A C, Kimura T, King M A, Kinghorn K J, Kinsey C G, Kirkin V, Kirshenbaum L A, Kiselev S L, Kishi S, Kitamoto K, Kitaoka Y, Kitazato K, Kitsis R N, Kittler J T, Kjaerulff O, Klein P S, Klopstock T, Klucken J, Knævelsrud H, Knorr R L, Ko B C B, Ko F, Ko J-L, Kobayashi H, Kobayashi S, Koch I, Koch J C, Koenig U, Kögel D, Koh Y H, Koike M, Kohlwein S D, Kocaturk N M, Komatsu M, König J, Kono T, Kopp B T, Korcsmaros T, Korkmaz G, Korolchuk V I, Korsnes M S, Koskela A, Kota J, Kotake Y, Kotler M L, Kou Y, Koukourakis M I, Koustas E, Kovacs A L, Kovács T, Koya D, Kozako T, Kraft C, Krainc D, Krämer H, Krasnodembskaya A D, Kretz-Remy C, Kroemer G, Ktistakis N T, Kuchitsu K, Kuenen S, Kuerschner L, Kukar T, Kumar A, Kumar A, Kumar D, Kumar D, Kumar S, Kume S, Kumsta C, Kundu C N, Kundu M, Kunnumakkara A B, Kurgan L, Kutateladze T G, Kutlu O, Kwak S, Kwon H J, Kwon T K, Kwon Y T, Kyrmizi I, La Spada A, Labonté P, Ladoire S, Laface I, Lafont F, Lagace D C, Lahiri V, Lai Z, Laird A S, Lakkaraju A, Lamark T, Lan S-H, Landajuela A, Lane D J R, Lane J D, Lang C H, Lange C, Langel Ü, Langer R, Lapaquette P, Laporte J, LaRusso N F, Lastres-Becker I, Lau W C Y, Laurie G W, Lavandero S, Law B Y K, Law H K, Layfield R, Le W, Le Stunff H, Leary A Y, Lebrun J-J, Leck L Y W, Leduc-Gaudet J-P, Lee C, Lee C-P, Lee D-H, Lee E B, Lee E F, Lee G M, Lee H-J, Lee H K, Lee J M, Lee J S, Lee J-A, Lee J-Y, Lee J H, Lee M, Lee M G, Lee M J, Lee M-S, Lee S Y, Lee S-J, Lee S Y, Lee S B, Lee W H, Lee Y-R, Lee Y, Lee Y, Lefebvre C, Legouis R, Lei Y L, Lei Y, Leikin S, Leitinger G, Lemus L, Leng S, Lenoir O, Lenz G, Lenz H J, Lenzi P, León Y, Leopoldino A M, Leschczyk C, Leskelä S, Letellier E, Leung C-T, Leung P S, Leventhal J S, Levine B, Lewis P A, Ley K, Li B, Li D-Q, Li J, Li J, Li J, Li K, Li L, Li M, Li M, Li M, Li M, Li M, Li P-L, Li M-Q, Li Q, Li S, Li T, Li W, Li W, Li X, Li Y-P, Li Y, Li Z, Li Z, Li Z, Lian J, Liang C, Liang Q, Liang W, Liang Y, Liang Y, Liao G, Liao L, Liao M, Liao Y-F, Librizzi M, Lie P P Y, Lilly M A, Lim H J, Lima T R R, Limana F, Lin C, Lin C-W, Lin D-S, Lin F-C, Lin J D, Lin K M, Lin K-H, Lin L-T, Lin P-H, Lin Q, Lin S, Lin S-J, Lin W, Lin X, Lin Y-X, Lin Y-S, Linden R, Lindner P, Ling S-C, Lingor P, Linnemann A K, Liou Y-C, Lipinski M M, Lipovšek S, Lira V A, Lisiak N, Liton P B, Liu C, Liu C-H, Liu C-F, Liu C H, Liu F, Liu H, Liu H-S, Liu H, Liu H, Liu J, Liu J, Liu J, Liu L, Liu L, Liu M, Liu Q, Liu W, Liu W, Liu X-H, Liu X, Liu X, Liu X, Liu X, Liu Y, Liu Y, Liu Y, Liu Y, Liu Y, Livingston J A, Lizard G, Lizcano J M, Ljubojevic-Holzer S, LLeonart M E, Llobet-Navàs D, Llorente A, Lo C H, Lobato-Márquez D, Long Q, Long Y C, Loos B, Loos J A, López M G, López-Doménech G, López-Guerrero J A, López-Jiménez A T, López-Pérez Ó, López-Valero I, Lorenowicz M J, Lorente M, Lorincz P, Lossi L, Lotersztajn S, Lovat P E, Lovell J F, Lovy A, Lőw P, Lu G, Lu H, Lu J-H, Lu J-J, Lu M, Lu S, Luciani A, Lucocq J M, Ludovico P, Luftig M A, Luhr M, Luis-Ravelo D, Lum J J, Luna-Dulcey L, Lund A H, Lund V K, Lünemann J D, Lüningschrör P, Luo H, Luo R, Luo S, Luo Z, Luparello C, Lüscher B, Luu L, Lyakhovich A, Lyamzaev K G, Lystad A H, Lytvynchuk L, Ma A C, Ma C, Ma M, Ma N-F, Ma Q-H, Ma X, Ma Y, Ma Z, MacDougald O A, Macian F, MacIntosh G C, MacKeigan J P, Macleod K F, Maday S, Madeo F, Madesh M, Madl T, Madrigal-Matute J, Maeda A, Maejima Y, Magarinos M, Mahavadi P, Maiani E, Maiese K, Maiti P, Maiuri M C, Majello B, Major M B, Makareeva E, Malik F,

Mallilankaraman K, Malorni W, Maloyan A, Mammadova N, Man G C W, Manai F, Mancias J D, Mandelkow E-M, Mandell M A, Manfredi A A, Manjili M H, Manjithaya R, Manque P, Manshian B B, Manzano R, Manzoni C, Mao K, Marchese C, Marchetti S, Marconi A M, Marcucci F, Mardente S, Mareninova O A, Margeta M, Mari M, Marinelli S, Marinelli O, Mariño G, Mariotto S, Marshall R S, Marten M R, Martens S, Martin A P J, Martin K R, Martin S, Martin S, Martín-Segura A, Martín-Acebes M A, Martin-Burriel I, Martin-Rincon M, Martin-Sanz P, Martina J A, Martinet W, Martinez A, Martinez A, Martinez J, Martinez Velazquez M, Martinez-Lopez N, Martinez-Vicente M, Martins D O, Martins J O, Martins W K, Martins-Marques T, Marzetti E, Masaldan S, Masclaux-Daubresse C, Mashek D G, Massa V, Massieu L, Masson G R, Masuelli L, Masyuk A I, Masyuk T V, Matarrese P, Matheu A, Matoba S, Matsuzaki S, Mattar P, Matte A, Mattoscio D, Mauriz J L, Mauthe M, Mauvezin C, Maverakis E, Maycotte P, Mayer J, Mazzoccoli G, Mazzoni C, Mazzulli J R, McCarty N, McDonald C, McGill M R, McKenna S L, McLaughlin B, McLoughlin F, McNiven M A, McWilliams T G, Mechta-Grigoriou F, Medeiros T C, Medina D L, Megeney L A, Megyeri K, Mehrpour M, Mehta J L, Meijer A J, Meijer A H, Mejlvang J, Meléndez A, Melk A, Memisoglu G, Mendes A F, Meng D, Meng F, Meng T, Menna-Barreto R, Menon M B, Mercer C, Mercier A E, Mergny J-L, Merighi A, Merkley S D, Merla G, Meske V, Mestre A C, Metur S P, Meyer C, Meyer H, Mi W, Mialet-Perez J, Miao J, Micale L, Miki Y, Milan E, Milczarek M, Miller D L, Miller S I, Miller S, Millward S W, Milosevic I, Minina E A, Mirzaei H, Mirzaei H R, Mirzaei M, Mishra A, Mishra N, Mishra P K, Misirkic Marjanovic M, Misasi R, Misra A, Misso G, Mitchell C, Mitou G, Miura T, Miyamoto S, Miyazaki M, Miyazaki M, Miyazaki T, Miyazawa K, Mizushima N, Mogensen T H, Mograbi B, Mohammadinejad R, Mohamud Y, Mohanty A, Mohapatra S, Möhlmann T, Mohmmed A, Moles A, Moley K H, Molinari M, Mollace V, Møller A B, Mollereau B, Mollinedo F, Montagna C, Monteiro M J, Montella A, Montes L R, Montico B, Mony V K, Monzio Compagnoni G, Moore M N, Moosavi M A, Mora A L, Mora M, Morales-Alamo D, Moratalla R, Moreira P I, Morelli E, Moreno S, Moreno-Blas D, Moresi V, Morga B, Morgan A H, Morin F, Morishita H, Moritz O L, Moriyama M, Moriyasu Y, Morleo M, Morselli E, Moruno-Manchon J F, Moscat J, Mostowy S, Motori E, Moura A F, Moustaid-Moussa N, Mrakovcic M, Muciño-Hernández G, Mukherjee A, Mukhopadhyay S, Mulcahy Levy J M, Mulero V, Muller S, Münch C, Munjal A, Munoz-Canoves P, Muñoz-Galdeano T, Münz C, Murakawa T, Muratori C, Murphy B M, Murphy J P, Murthy A, Myöhänen T T, Mysorekar I U, Mytych J, Nabavi S M, Nabissi M, Nagy P, Nah J, Nahimana A, Nakagawa I, Nakamura K, Nakatogawa H, Nandi S S, Nanjundan M, Nanni M, Napolitano G, Nardacci R, Narita M, Nassif M, Nathan I, Natsumeda M, Naude R J, Naumann C, Naveiras O, Navid F, Nawrocki S T, Nazarko T Y, Nazio F, Negoita F, Neill T, Neisch A L, Neri L M, Netea M G, Neubert P, Neufeld T P, Neumann D, Neutzner A, Newton P T, Ney P A, Nezis I P, Ng C C W, Ng T B, Nguyen H T T, Nguyen L T, Ni H-M, Ní Cheallaigh C, Ni Z, Nicolao M C, Nicoli F, Nieto-Diaz M, Nilsson P, Ning S, Niranjan R, Nishimune H, Niso-Santano M, Nixon R A, Nobili A, Nobrega C, Noda T, Nogueira-Recalde U, Nolan T M, Nombela I, Novak I, Novoa B, Nozawa T, Nukina N, Nussbaum-Krammer C, Nylandsted J, O'Donovan T R, O'Leary S M, O'Rourke E J, O'Sullivan M P, O'Sullivan T E, Oddo S, Oehme I, Ogawa M, Ogier-Denis E, Ogmundsdottir M H, Ogretmen B, Oh G T, Oh S-H, Oh Y J, Ohama T, Ohashi Y, Ohmuraya M, Oikonomou V, Ojha R, Okamoto K, Okazawa H, Oku M, Oliván S, Oliveira J M A, Ollmann M, Olzmann J A, Omari S, Omary M B, Önal G, Ondrej M, Ong S-B, Ong S-G, Onnis A, Orellana J A, Orellana-

Muñoz S, Ortega-Villaizan M D M, Ortiz-Gonzalez X R, Ortona E, Osiewacz H D, Osman A-H K, Osta R, Otegui M S, Otsu K, Ott C, Ottobrini L, Ou J J, Outeiro T F, Oynebraten I, Ozturk M, Pagès G, Pahari S, Pajares M, Pajvani U B, Pal R, Paladino S, Pallet N, Palmieri M, Palmisano G, Palumbo C, Pampaloni F, Pan L, Pan Q, Pan W, Pan X, Panasyuk G, Pandey R, Pandey U B, Pandya V, Paneni F, Pang S Y, Panzarini E, Papademetrio D L, Papaleo E, Papinski D, Papp D, Park E C, Park H T, Park J-M, Park J-I, Park J T, Park J, Park S C, Park S-Y, Parola A H, Parys J B, Pasquier A, Pasquier B, Passos J F, Pastore N, Patel H H, Patschan D, Pattingre S, Pedraza-Alva G, Pedraza-Chaverri J, Pedrozo Z, Pei G, Pei J, Peled-Zehavi H, Pellegrini J M, Pelletier J, Peñalva M A, Peng D, Peng Y, Penna F, Pennuto M, Pentimalli F, Pereira C M, Pereira G J S, Pereira L C, Pereira de Almeida L, Perera N D, Pérez-Lara Á, Perez-Oliva A B, Pérez-Pérez M E, Periyasamy P, Perl A, Perrotta C, Perrotta I, Pestell R G, Petersen M, Petrache I, Petrovski G, Pfirrmann T, Pfister A S, Philips J A, Pi H, Picca A, Pickrell A M, Picot S, Pierantoni G M, Pierdominici M, Pierre P, Pierrefite-Carle V, Pierzynowska K, Pietrocola F, Pietruczuk M, Pignata C, Pimentel-Muiños F X, Pinar M, Pinheiro R O, Pinkas-Kramarski R, Pinton P, Pircs K, Piya S, Pizzo P, Plantinga T S, Platta H W, Plaza-Zabala A, Plomann M, Plotnikov E Y, Plun-Favreau H, Pluta R, Pocock R, Pöggeler S, Pohl C, Poirot M, Poletti A, Ponpuak M, Popelka H, Popova B, Porta H, Porte Alcon S, Portilla-Fernandez E, Post M, Potts M B, Poulton J, Powers T, Prahlad V, Prajsnar T K, Praticò D, Prencipe R, Priault M, Proikas-Cezanne T, Promponas V J, Proud C G, Puertollano R, Puglielli L, Pulinilkunnil T, Puri D, Puri R, Puyal J, Qi X, Qi Y, Qian W, Qiang L, Qiu Y, Quadrilatero J, Quarleri J, Raben N, Rabinowich H, Ragona D, Ragusa M J, Rahimi N, Rahmati M, Raia V, Raimundo N, Rajasekaran N-S, Ramachandra Rao S, Rami A, Ramírez-Pardo I, Ramsden D B, Randow F, Rangarajan P N, Ranieri D, Rao H, Rao L, Rao R, Rathore S, Ratnayaka J A, Ratovitski E A, Ravanan P, Ravegnini G, Ray S K, Razani B, Rebecca V, Reggiori F, Régnier-Vigouroux A, Reichert A S, Reigada D, Reiling J H, Rein T, Reipert S, Rekha R S, Ren H, Ren J, Ren W, Renault T, Renga G, Reue K, Rewitz K, Ribeiro de Andrade Ramos B, Riazuddin S A, Ribeiro-Rodrigues T M, Ricci J-E, Ricci R, Riccio V, Richardson D R, Rikihisa Y, Risbud M V, Risueño R M, Ritis K, Rizza S, Rizzuto R, Roberts H C, Roberts L D, Robinson K J, Roccheri M C, Rocchi S, Rodney G G, Rodrigues T, Rodrigues Silva V R, Rodriguez A, Rodriguez-Barrueco R, Rodriguez-Henche N, Rodriguez-Rocha H, Roelofs J, Rogers R S, Rogov V V, Rojo A I, Rolka K, Romanello V, Romani L, Romano A, Romano P S, Romeo-Guitart D, Romero L C, Romero M, Roney J C, Rongo C, Roperto S, Rosenfeldt M T, Rosenstiel P, Rosenwald A G, Roth K A, Roth L, Roth S, Rouschop K M A, Roussel B D, Roux S, Rovere-Querini P, Roy A, Rozieres A, Ruano D, Rubinsztein D C, Rubtsova M P, Ruckdeschel K, Ruckenstuhl C, Rudolf E, Rudolf R, Ruggieri A, Ruparelia A A, Rusmini P, Russell R R, Russo G L, Russo M, Russo R, Ryabaya O O, Ryan K M, Ryu K-Y, Sabater-Arcis M, Sachdev U, Sacher M, Sachse C, Sadhu A, Sadoshima J, Safren N, Saftig P, Sagona A P, Sahay G, Sahebkar A, Sahin M, Sahin O, Sahni S, Saito N, Saito S, Saito T, Sakai R, Sakai Y, Sakamaki J-I, Saksela K, Salazar G, Salazar-Degracia A, Salekdeh G H, Saluja A K, Sampaio-Marques B, Sanchez M C, Sanchez-Alcazar J A, Sanchez-Vera V, Sancho-Shimizu V, Sanderson J T, Sandri M, Santaguida S, Santambrogio L, Santana M M, Santoni G, Sanz A, Sanz P, Saran S, Sardiello M, Sargeant T J, Sarin A, Sarkar C, Sarkar S, Sarrias M-R, Sarkar S, Sarmah D T, Sarparanta J, Sathyanarayan A, Sathyanarayanan R, Scaglione K M, Scatozza F, Schaefer L, Schafer Z T, Schaible U E, Schapira A H V, Scharl M, Schatzl H M, Schein C H, Scheper W, Scheuring D, Schiaffino M V,

Schiappacassi M, Schindl R, Schlattner U, Schmidt O, Schmitt R, Schmidt S D, Schmitz I, Schmukler E, Schneider A, Schneider B E, Schober R, Schoijet A C, Schott M B, Schramm M, Schröder B, Schuh K, Schüller C, Schulze R J, Schürmanns L, Schwamborn J C, Schwarten M, Scialo F, Sciarretta S, Scott M J, Scotto K W, Scovassi A I, Scrima A, Scrivo A, Sebastian D, Sebti S, Sedej S, Segatori L, Segev N, Seglen P O, Seiliez I, Seki E, Selleck S B, Sellke F W, Selsby J T, Sendtner M, Senturk S, Seranova E, Sergi C, Serra-Moreno R, Sesaki H, Settembre C, Setty S R G, Sgarbi G, Sha O, Shacka J J, Shah J A, Shang D, Shao C, Shao F, Sharbati S, Sharkey L M, Sharma D, Sharma G, Sharma K, Sharma P, Sharma S, Shen H-M, Shen H, Shen J, Shen M, Shen W, Shen Z, Sheng R, Sheng Z, Sheng Z-H, Shi J, Shi X, Shi Y-H, Shiba-Fukushima K, Shieh J-J, Shimada Y, Shimizu S, Shimozawa M, Shintani T, Shoemaker C J, Shojaei S, Shoji I, Shravage B V, Shridhar V, Shu C-W, Shu H-B, Shui K, Shukla A K, Shutt T E, Sica V, Siddiqui A, Sierra A, Sierra-Torre V, Signorelli S, Sil P, Silva B J de A, Silva J D, Silva-Pavez E, Silvente-Poirot S, Simmonds R E, Simon A K, Simon H-U, Simons M, Singh A, Singh L P, Singh R, Singh S V, Singh S K, Singh S B, Singh S, Singh S P, Sinha D, Sinha R A, Sinha S, Sirko A, Sirohi K, Sivridis E L, Skendros P, Skirycz A, Slaninová I, Smaili S S, Smertenko A, Smith M D, Soenen S J, Sohn E J, Sok S P M, Solaini G, Soldati T, Soleimanpour S A, Soler R M, Solovchenko A, Somarelli J A, Sonawane A, Song F, Song H K, Song J-X, Song K, Song Z, Soria L R, Sorice M, Soukas A A, Soukup S-F, Sousa D, Sousa N, Spagnuolo P A, Spector S A, Srinivas Bharath M M, St. Clair D, Stagni V, Staiano L, Stalnecker C A, Stankov M V, Stathopulos P B, Stefan K, Stefan S M, Stefanis L, Steffan J S, Steinkasserer A, Stenmark H, Sterneckert J, Stevens C, Stoka V, Storch S, Stork B, Strappazzon F, Strohecker A M, Stupack D G, Su H, Su L-Y, Su L, Suarez-Fontes A M, Subauste C S, Subbian S, Subirada P V, Sudhandiran G, Sue C M, Sui X, Summers C, Sun G, Sun J, Sun K, Sun M, Sun Q, Sun Y, Sun Z, Sunahara K K S, Sundberg E, Susztak K, Sutovsky P, Suzuki H, Sweeney G, Symons J D, Sze S C W, Szewczyk N J, Tabęcka-Łonczynska A, Tabolacci C, Tacke F, Taegtmeyer H, Tafani M, Tagaya M, Tai H, Tait S W G, Takahashi Y, Takats S, Talwar P, Tam C, Tam S Y, Tampellini D, Tamura A, Tan C T, Tan E-K, Tan Y-Q, Tanaka M, Tanaka M, Tang D, Tang J, Tang T-S, Tanida I, Tao Z, Taouis M, Tatenhorst L, Tavernarakis N, Taylor A, Taylor G A, Taylor J M, Tchetina E, Tee A R, Tegeder I, Teis D, Teixeira N, Teixeira-Clerc F, Tekirdag K A, Tencomnao T, Tenreiro S, Tepikin A V, Testillano P S, Tettamanti G, Tharaux P-L, Thedieck K, Thekkinghat A A, Thellung S, Thinwa J W, Thirumalaikumar V P, Thomas S M, Thomes P G, Thorburn A, Thukral L, Thum T, Thumm M, Tian L, Tichy A, Till A, Timmerman V, Titorenko V I, Todi S V, Todorova K, Toivonen J M, Tomaipitinca L, Tomar D, Tomas-Zapico C, Tomić S, Tong B C-K, Tong C, Tong X, Tooze S A, Torgersen M L, Torii S, Torres-López L, Torriglia A, Towers C G, Towns R, Toyokuni S, Trajkovic V, Tramontano D, Tran Q-G, Travassos L H, Trelford C B, Tremel S, Triola G, Trougakos I P, Tsao B P, Tschan M P, Tse H-F, Tse T F, Tsugawa H, Tsvetkov A S, Tumbarello D A, Tumtas Y, Tuñón M J, Turcotte S, Turk B, Turk V, Turner B J, Tuxworth R I, Tyler J K, Tyutereva E V, Uchiyama Y, Ugun-Klusek A, Uhlig H H, Ułamek-Kozioł M, Ulasov I V, Umekawa M, Ungermann C, Unno R, Urbe S, Uribe-Carretero E, Üstün S, Uversky V N, Vaccari T, Vaccaro M I, Vahsen B F, Vakifahmetoglu-Norberg H, Valdor R, Valente M J, Valko A, Vallee R B, Valverde A M, Van den Berghe G, van der Veen S, Van Kaer L, van Loosdregt J, van Wijk S J L, Vandenberghe W, Vanhorebeek I, Vannier-Santos M A, Vannini N, Vanrell M C, Vantaggiato C, Varano G, Varela-Nieto I, Varga M, Vasconcelos M

H, Vats S, Vavvas D G, Vega-Naredo I, Vega-Rubin-de-Celis S, Velasco G, Velázquez A P, Vellai T, Vellenga E, Velotti F, Verdier M, Verginis P, Vergne I, Verkade P, Verma M, Verstreken P, Vervliet T, Vervoorts J, Vessoni A T, Victor V M, Vidal M, Vidoni C, Vieira O V, Vierstra R D, Viganó S, Vihinen H, Vijayan V, Vila M, Vilar M, Villalba J M, Villalobo A, Villarejo-Zori B, Villarroya F, Villarroya J, Vincent O, Vindis C, Viret C, Viscomi M T, Visnjic D, Vitale I, Vocadlo D J, Voitsekhovskaja O V, Volonté C, Volta M, Vomero M, Von Haefen C, Vooijs M A, Voos W, Vucicevic L, Wade-Martins R, Waguri S, Waite K A, Wakatsuki S, Walker D W, Walker M J, Walker S A, Walter J, Wandosell F G, Wang B, Wang C-Y, Wang C, Wang C, Wang C, Wang C-Y, Wang D, Wang F, Wang F, Wang F, Wang G, Wang H, Wang H, Wang H, Wang H-G, Wang J, Wang J, Wang J, Wang J, Wang K, Wang L, Wang L, Wang M H, Wang M, Wang N, Wang P, Wang P, Wang P, Wang P, Wang Q J, Wang Q, Wang Q K, Wang Q A, Wang W-T, Wang W, Wang X, Wang X, Wang Y, Wang Y, Wang Y, Wang Y-Y, Wang Y, Wang Y, Wang Y, Wang Y, Wang Z, Wang Z, Wang Z, Warnes G, Warnsmann V, Watada H, Watanabe E, Watchon M, Wawrzyńska A, Weaver T E, Wegrzyn G, Wehman A M, Wei H, Wei L, Wei T, Wei Y, Weiergräber O H, Weihl C C, Weindl G, Weiskirchen R, Wells A, Wen R H, Wen X, Werner A, Weykopf B, Wheatley S P, Whitton J L, Whitworth A J, Wiktorska K, Wildenberg M E, Wileman T, Wilkinson S, Willbold D, Williams B, Williams R S B, Williams R L, Williamson P R, Wilson R A, Winner B, Winsor N J, Witkin S S, Wodrich H, Woehlbier U, Wollert T, Wong E, Wong J H, Wong R W, Wong V K W, Wong W W-L, Wu A-G, Wu C, Wu J, Wu J, Wu K K, Wu M, Wu S-Y, Wu S, Wu S-Y, Wu S, Wu W K K, Wu X, Wu X, Wu Y-W, Wu Y, Xavier R J, Xia H, Xia L, Xia Z, Xiang G, Xiang J, Xiang M, Xiang W, Xiao B, Xiao G, Xiao H, Xiao H, Xiao J, Xiao L, Xiao S, Xiao Y, Xie B, Xie C-M, Xie M, Xie Y, Xie Z, Xie Z, Xilouri M, Xu C, Xu E, Xu H, Xu J, Xu J, Xu L, Xu W W, Xu X, Xue Y, Yakhine-Diop S M S, Yamaguchi M, Yamaguchi O, Yamamoto A, Yamashina S, Yan S, Yan S-J, Yan Z, Yanagi Y, Yang C, Yang D-S, Yang H, Yang H-T, Yang H, Yang J-M, Yang J, Yang J, Yang L, Yang L, Yang M, Yang P-M, Yang Q, Yang S, Yang S, Yang S-F, Yang W, Yang W Y, Yang X, Yang X, Yang Y, Yang Y, Yao H, Yao S, Yao X, Yao Y-G, Yao Y-M, Yasui T, Yazdankhah M, Yen P M, Yi C, Yin X-M, Yin Y, Yin Z, Yin Z, Ying M, Ying Z, Yip C K, Yiu S P T, Yoo Y H, Yoshida K, Yoshii S R, Yoshimori T, Yousefi B, Yu B, Yu H, Yu J, Yu J, Yu L, Yu M-L, Yu S-W, Yu V C, Yu W H, Yu Z, Yu Z, Yuan J, Yuan L-Q, Yuan S, Yuan S-S F, Yuan Y, Yuan Z, Yue J, Yue Z, Yun J, Yung R L, Zacks D N, Zaffagnini G, Zambelli V O, Zanella I, Zang Q S, Zanivan S, Zappavigna S, Zaragoza P, Zarbalis K S, Zarebkohan A, Zarrouk A, Zeitlin S O, Zeng J, Zeng J, Žerovnik E, Zhan L, Zhang B, Zhang D D, Zhang H, Zhang H, Zhang H, Zhang H, Zhang H, Zhang H, Zhang H, Zhang H-L, Zhang J, Zhang J, Zhang J-P, Zhang K Y B, Zhang L W, Zhang L, Zhang L, Zhang L, Zhang L, Zhang M, Zhang P, Zhang S, Zhang W, Zhang X, Zhang X-W, Zhang X, Zhang X, Zhang X, Zhang X, Zhang X D, Zhang Y, Zhang Y, Zhang Y, Zhang Y-D, Zhang Y, Zhang Y-Y, Zhang Y, Zhang Z, Zhang Z, Zhang Z, Zhang Z, Zhang Z, Zhang Z, Zhao H, Zhao L, Zhao S, Zhao T, Zhao X-F, Zhao Y, Zhao Y, Zhao Y, Zhao Y, Zheng G, Zheng K, Zheng L, Zheng S, Zheng X-L, Zheng Y, Zheng Z-G, Zhivotovsky B, Zhong Q, Zhou A, Zhou B, Zhou C, Zhou G, Zhou H, Zhou H, Zhou H, Zhou J, Zhou J, Zhou J, Zhou J, Zhou K, Zhou R, Zhou X-J, Zhou Y, Zhou Y, Zhou Y, Zhou Z-Y, Zhou Z, Zhu B, Zhu C, Zhu G-Q, Zhu H, Zhu H, Zhu H, Zhu W-G, Zhu Y, Zhu Y, Zhuang H, Zhuang X, Zientara-Rytter K, Zimmermann C M, Ziviani E, Zoladek T, Zong W-X, Zorov D B, Zorzano A, Zou W, Zou Z, Zou Z,

Zuryn S, Zwerschke W, Brand-Saberi B, Dong X C, Kenchappa C S, Li Z, Lin Y, Oshima S, Rong Y, Sluimer J C, Stallings C L, Tong C-K: Guidelines for the Use and Interpretation of Assays for Monitoring Autophagy (4th Edition). Autophagy 17 1–382 (2021)

(88) Klionsky D J, Elazar Z, Seglen P O, Rubinsztein D C: Does Bafilomycin A1 Block the Fusion of Autophagosomes with Lysosomes? Autophagy 4 849–850 (2008)

(89) Koepke L, Gack M U, Sparrer K M: The Antiviral Activities of TRIM Proteins. Current Opinion in Microbiology 59 50–57 (2021)

(90) Koepke L, Hirschenberger M, Hayn M, Kirchhoff F, Sparrer K M J: Manipulation of Autophagy by SARS-CoV-2 Proteins. Autophagy 17 2659–2661 (2021)

(91) Koepke L, Winter B, Grenzner A, Regensburger K, Engelhart S, van der Merwe J A, Krebs S, Blum H, Kirchhoff F, Sparrer K M J: An Improved Method for High-Throughput Quantification of Autophagy in Mammalian Cells. Sci Rep 10 12241 (2020)

(92) Kravic B, Harbauer A B, Romanello V, Simeone L, Vögtle F-N, Kaiser T, Straubinger M, Huraskin D, Böttcher M, Cerqua C, Martin E D, Poveda-Huertes D, Buttgereit A, Rabalski A J, Heuss D, Rudolf R, Friedrich O, Litchfield D, Marber M, Salviati L, Mougiakakos D, Neuhuber W, Sandri M, Meisinger C, Hashemolhosseini S: In Mammalian Skeletal Muscle, Phosphorylation of TOMM22 by Protein Kinase CSNK2/CK2 Controls Mitophagy. Autophagy 14 311–335 (2018)

(93) Kumar A, Prasoon P, Kumari C, Pareek V, Faiq M A, Narayan R K, Kulandhasamy M, Kant K: SARS-CoV-2-Specific Virulence Factors in COVID-19. Journal of Medical Virology 93 1343–1350 (2021)

(94) Kumar M, Michael S, Alvarado-Valverde J, Mészáros B, Sámano-Sánchez H, Zeke A, Dobson L, Lazar T, Örd M, Nagpal A, Farahi N, Käser M, Kraleti R, Davey N E, Pancsa R, Chemes L B, Gibson T J: The Eukaryotic Linear Motif Resource: 2022 Release. Nucleic Acids Research 50 D497–D508 (2022)

(95) Kumari P, Aeschimann F, Gaidatzis D, Keusch J J, Ghosh P, Neagu A, Pachulska-Wieczorek K, Bujnicki J M, Gut H, Großhans H, Ciosk R: Evolutionary Plasticity of the NHL Domain Underlies Distinct Solutions to RNA Recognition. Nat Commun 9 1549 (2018)

(96) Kyei G B, Dinkins C, Davis A S, Roberts E, Singh S B, Dong C, Wu L, Kominami E, Ueno T, Yamamoto A, Federico M, Panganiban A, Vergne I, Deretic V: Autophagy Pathway Intersects with HIV-1 Biosynthesis and Regulates Viral Yields in Macrophages. Journal of Cell Biology 186 255–268 (2009)

(97) Larsen K B, Lamark T, Øvervatn A, Harneshaug I, Johansen T, Bjørkøy G: A Reporter Cell System to Monitor Autophagy Based on P62/SQSTM1. Autophagy 6 784–793 (2010)

(98) Lashuel H A, Overk C R, Oueslati A, Masliah E: The Many Faces of α-Synuclein: From Structure and Toxicity to Therapeutic Target. Nat Rev Neurosci 14 38–48 (2013)

(99) Lee J-H, Koepke L, Kirchhoff F, Sparrer K M J: Interferon Antagonists Encoded by SARS-CoV-2 at a Glance. Med Microbiol Immunol (2022)

(100) Lee Y-K, Lee J-A: Role of the Mammalian ATG8/LC3 Family in Autophagy: Differential and Compensatory Roles in the Spatiotemporal Regulation of Autophagy. BMB Rep 49 424–430 (2016)

(101) Lei X, Dong X, Ma R, Wang W, Xiao X, Tian Z, Wang C, Wang Y, Li L, Ren L, Guo F, Zhao Z, Zhou Z, Xiang Z, Wang J: Activation and Evasion of Type I Interferon Responses by SARS-CoV-2. Nat Commun 11 3810 (2020)

(102) Lenzken S C, Stanga S, Lanni C, De Leonardis F, Govoni S, Racchi M: Recruitment of Casein Kinase 2 Is Involved in AbetaPP Processing Following Cholinergic Stimulation. J Alzheimers Dis 20 1133–1141 (2010)
(103) Levine B, Kroemer G: Autophagy in the Pathogenesis of Disease. Cell 132 27–42 (2008)
(104) Li M-Y, Li L, Zhang Y, Wang X-S: Expression of the SARS-CoV-2 Cell Receptor Gene ACE2 in a Wide Variety of Human Tissues. Infectious Diseases of Poverty 9 45 (2020)
(105) Li Y, McGreal S, Zhao J, Huang R, Zhou Y, Zhong H, Xia M, Ding W-X: A Cell-Based Quantitative High-Throughput Image Screening Identified Novel Autophagy Modulators. Pharmacological Research 110 35–49 (2016)
(106) Liang C, Lee J, Inn K-S, Gack M U, Li Q, Roberts E A, Vergne I, Deretic V, Feng P, Akazawa C, Jung J U: Beclin1-Binding UVRAG Targets the Class C Vps Complex to Coordinate Autophagosome Maturation and Endocytic Trafficking. Nat Cell Biol 10 776–787 (2008)
(107) Liang Q, Luo Z, Zeng J, Chen W, Foo S-S, Lee S-A, Ge J, Wang S, Goldman S A, Zlokovic B V, Zhao Z, Jung J U: Zika Virus NS4A and NS4B Proteins Deregulate Akt-MTOR Signaling in Human Fetal Neural Stem Cells to Inhibit Neurogenesis and Induce Autophagy. Cell Stem Cell 19 663–671 (2016)
(108) Liu G, Lee J-H, Parker Z M, Acharya D, Chiang J J, van Gent M, Riedl W, Davis-Gardner M E, Wies E, Chiang C, Gack M U: ISG15-Dependent Activation of the Sensor MDA5 Is Antagonized by the SARS-CoV-2 Papain-like Protease to Evade Host Innate Immunity. Nat Microbiol 6 467–478 (2021)
(109) Liu J, Cao R, Xu M, Wang X, Zhang H, Hu H, Li Y, Hu Z, Zhong W, Wang M: Hydroxychloroquine, a Less Toxic Derivative of Chloroquine, Is Effective in Inhibiting SARS-CoV-2 Infection in Vitro. Cell Discov 6 1–4 (2020)
(110) Liu T, Tang Q, Liu K, Xie W, Liu X, Wang H, Wang R-F, Cui J: TRIM11 Suppresses AIM2 Inflammasome by Degrading AIM2 via P62-Dependent Selective Autophagy. Cell Reports 16 1988–2002 (2016)
(111) Liu Y, Qin C, Rao Y, Ngo C, Feng J J, Zhao J, Zhang S, Wang T-Y, Carriere J, Savas A C, Zarinfar M, Rice S, Yang H, Yuan W, Camarero J A, Yu J, Chen X S, Zhang C, Feng P: SARS-CoV-2 Nsp5 Demonstrates Two Distinct Mechanisms Targeting RIG-I and MAVS To Evade the Innate Immune Response. mBio 12 e02335-21 (2021)
(112) Liu Y, Raheja R, Yeh N, Ciznadija D, Pedraza A M, Ozawa T, Hukkelhoven E, Erdjument-Bromage H, Tempst P, Gauthier N P, Brennan C, Holland E C, Koff A: TRIM3, a Tumor Suppressor Linked to Regulation of P21Waf1/Cip1. Oncogene 33 308–315 (2014)
(113) Loedige I, Filipowicz W: TRIM-NHL Proteins Take on MiRNA Regulation. Cell 136 818–820 (2009)
(114) Ma J, Sun Q, Mi R, Zhang H: Avian Influenza A Virus H5N1 Causes Autophagy-Mediated Cell Death through Suppression of MTOR Signaling. Journal of Genetics and Genomics 38 533–537 (2011)
(115) Magri S, Danti F R, Balistreri F, Baratta S, Ciano C, Pagliano E, Taroni F, Moroni I: Expanding the Phenotypic Spectrum of TRIM2-Associated Charcot-Marie-Tooth Disease. Journal of the Peripheral Nervous System 25 429–432 (2020)
(116) Mandell M A, Jain A, Arko-Mensah J, Chauhan S, Kimura T, Dinkins C, Silvestri G, Münch J, Kirchhoff F, Simonsen A, Wei Y, Levine B, Johansen T, Deretic V: TRIM Proteins Regulate Autophagy and Can Target Autophagic Substrates by Direct Recognition. Developmental Cell 30 394–409 (2014)

(117) Mandell M A, Kimura T, Jain A, Johansen T, Deretic V: TRIM Proteins Regulate Autophagy: TRIM5 Is a Selective Autophagy Receptor Mediating HIV-1 Restriction. Autophagy 10 2387–2388 (2014)
(118) Marques-Pereira C, Pires M N, Gouveia R P, Pereira N N, Caniceiro A B, Rosário-Ferreira N, Moreira I S: SARS-CoV-2 Membrane Protein: From Genomic Data to Structural New Insights. International Journal of Molecular Sciences 23 2986 (2022)
(119) Marr R A, Guan H, Rockenstein E, Kindy M, Gage F H, Verma I, Masliah E, Hersh L B: Neprilysin Regulates Amyloid Beta Peptide Levels. J Mol Neurosci 22 5–11 (2004)
(120) Martens S, Fracchiolla D: Activation and Targeting of ATG8 Protein Lipidation. Cell Discov 6 1–11 (2020)
(121) Martins L R, Lúcio P, Melão A, Antunes I, Cardoso B A, Stansfield R, Bertilaccio M T S, Ghia P, Drygin D, Silva M G, Barata J T: Activity of the Clinical-Stage CK2-Specific Inhibitor CX-4945 against Chronic Lymphocytic Leukemia. Leukemia 28 179–182 (2014)
(122) Mathew R, Karantza-Wadsworth V, White E: Role of Autophagy in Cancer. Nat Rev Cancer 7 961–967 (2007)
(123) Meggio F, Marin O, Pinna L A: Substrate Specificity of Protein Kinase CK2. Cell Mol Biol Res 40 401–409 (1994)
(124) Meggio F, Pinna L A: One-Thousand-and-One Substrates of Protein Kinase CK2? FASEB J 17 349–368 (2003)
(125) Menzies F M, Fleming A, Rubinsztein D C: Compromised Autophagy and Neurodegenerative Diseases. Nat Rev Neurosci 16 345–357 (2015)
(126) Miao G, Zhao H, Li Y, Ji M, Chen Y, Shi Y, Bi Y, Wang P, Zhang H: ORF3a of the COVID-19 Virus SARS-CoV-2 Blocks HOPS Complex-Mediated Assembly of the SNARE Complex Required for Autolysosome Formation. Developmental Cell 56 427-442.e5 (2021)
(127) Mishra P, Dauphinee A N, Ward C, Sarkar S, Gunawardena A H L A N, Manjithaya R: Discovery of Pan Autophagy Inhibitors through a High-Throughput Screen Highlights Macroautophagy as an Evolutionarily Conserved Process across 3 Eukaryotic Kingdoms. Autophagy 13 1556–1572 (2017)
(128) Mizushima N, Yoshimori T: How to Interpret LC3 Immunoblotting. Autophagy 3 542–545 (2007)
(129) Mohamud Y, Xue Y C, Liu H, Ng C S, Bahreyni A, Jan E, Luo H: The Papain-like Protease of Coronaviruses Cleaves ULK1 to Disrupt Host Autophagy. Biochemical and Biophysical Research Communications 540 75–82 (2021)
(130) Mouna L, Hernandez E, Bonte D, Brost R, Amazit L, Delgui L R, Brune W, Geballe A P, Beau I, Esclatine A: Analysis of the Role of Autophagy Inhibition by Two Complementary Human Cytomegalovirus BECN1/Beclin 1-Binding Proteins. Autophagy 12 327–342 (2016)
(131) Nardacci R, Amendola A, Ciccosanti F, Corazzari M, Esposito V, Vlassi C, Taibi C, Fimia G M, Del Nonno F, Ippolito G, D'Offizi G, Piacentini M: Autophagy Plays an Important Role in the Containment of HIV-1 in Nonprogressor-Infected Patients. Autophagy 10 1167–1178 (2014)
(132) N'Diaye E-N, Kajihara K K, Hsieh I, Morisaki H, Debnath J, Brown E J: PLIC Proteins or Ubiquilins Regulate Autophagy-Dependent Cell Survival during Nutrient Starvation. EMBO Rep 10 173–179 (2009)
(133) Nilsson P, Loganathan K, Sekiguchi M, Matsuba Y, Hui K, Tsubuki S, Tanaka M, Iwata N, Saito T, Saido T C: Aβ Secretion and Plaque Formation Depend on Autophagy. Cell Reports 5 61–69 (2013)

(134) Oh S J, Shin O S: SARS-CoV-2 Nucleocapsid Protein Targets RIG-I-Like Receptor Pathways to Inhibit the Induction of Interferon Response. Cells 10 530 (2021)
(135) Ohsumi Y: Molecular Dissection of Autophagy: Two Ubiquitin-like Systems. Nat Rev Mol Cell Biol 2 211–216 (2001)
(136) Orvedahl A, Alexander D, Tallóczy Z, Sun Q, Wei Y, Zhang W, Burns D, Leib D A, Levine B: HSV-1 ICP34.5 Confers Neurovirulence by Targeting the Beclin 1 Autophagy Protein. Cell Host & Microbe 1 23–35 (2007)
(137) Orvedahl A, Levine B: Eating the Enemy within: Autophagy in Infectious Diseases. Cell Death Differ 16 57–69 (2009)
(138) Pankiv S, Clausen T H, Lamark T, Brech A, Bruun J-A, Outzen H, Øvervatn A, Bjørkøy G, Johansen T: P62/SQSTM1 Binds Directly to Atg8/LC3 to Facilitate Degradation of Ubiquitinated Protein Aggregates by Autophagy*. Journal of Biological Chemistry 282 24131–24145 (2007)
(139) Park H, Kang J-H, Lee S: Autophagy in Neurodegenerative Diseases: A Hunter for Aggregates. Int J Mol Sci 21 3369 (2020)
(140) Park J-W, Jeong J, Bae Y-S: Protein Kinase CK2 Is Upregulated by Calorie Restriction and Induces Autophagy. Mol Cells 45 112–121 (2022)
(141) Parzych K R, Klionsky D J: An Overview of Autophagy: Morphology, Mechanism, and Regulation. Antioxidants & Redox Signaling 20 460–473 (2014)
(142) Patocka J, Kuca K, Oleksak P, Nepovimova E, Valis M, Novotny M, Klimova B: Rapamycin: Drug Repurposing in SARS-CoV-2 Infection. Pharmaceuticals 14 217 (2021)
(143) Paul D, Bartenschlager R: Flaviviridae Replication Organelles: Oh, What a Tangled Web We Weave. Annu. Rev. Virol. 2 289–310 (2015)
(144) Pfefferle S, Oppong S, Drexler J F, Gloza-Rausch F, Ipsen A, Seebens A, Müller M A, Annan A, Vallo P, Adu-Sarkodie Y, Kruppa T F, Drosten C: Distant Relatives of Severe Acute Respiratory Syndrome Coronavirus and Close Relatives of Human Coronavirus 229E in Bats, Ghana. Emerg Infect Dis 15 1377–1384 (2009)
(145) Piao M-Y, Cao H-L, He N-N, Xu M-Q, Dong W-X, Wang W-Q, Wang B-M, Zhou B: Potential Role of TRIM3 as a Novel Tumour Suppressor in Colorectal Cancer (CRC) Development. Scandinavian Journal of Gastroenterology 51 572–582 (2016)
(146) Prentice E, Jerome W G, Yoshimori T, Mizushima N, Denison M R: Coronavirus Replication Complex Formation Utilizes Components of Cellular Autophagy. J Biol Chem 279 10136–10141 (2004)
(147) Ramón A C, Pérez G V, Caballero E, Rosales M, Aguilar D, Vázquez-Blomquist D, Ramos Y, Rodríguez-Ulloa A, Falcón V, Rodríguez-Moltó M P, Yang K, Perera Y, Perea S E: Targeting of Protein Kinase CK2 Elicits Antiviral Activity on Bovine Coronavirus Infection. Viruses 14 552 (2022)
(148) Raught B, Gingras A C, Sonenberg N: The Target of Rapamycin (TOR) Proteins. Proc Natl Acad Sci U S A 98 7037–7044 (2001)
(149) Research C for D E and: FDA Approves Sirolimus Protein-Bound Particles for Malignant Perivascular Epithelioid Cell Tumor. FDA (2021)
(150) Romao S, Münz C: LC3-Associated Phagocytosis. Autophagy 10 526–528 (2014)
(151) Rubio R M, Mohr I: Inhibition of ULK1 and Beclin1 by an α-Herpesvirus Akt-like Ser/Thr Kinase Limits Autophagy to Stimulate Virus Replication. Proceedings of the National Academy of Sciences 116 26941–26950 (2019)
(152) Salvi M, Borgo C, Pinna L A, Ruzzene M: Targeting CK2 in Cancer: A Valuable Strategy or a Waste of Time? Cell Death Discov. 7 1–5 (2021)

(153) Sanchez J G, Chiang J J, Sparrer K M J, Alam S L, Chi M, Roganowicz M D, Sankaran B, Gack M U, Pornillos O: Mechanism of TRIM25 Catalytic Activation in the Antiviral RIG-I Pathway. Cell Reports 16 1315–1325 (2016)
(154) Sardiello M, Cairo S, Fontanella B, Ballabio A, Meroni G: Genomic Analysis of the TRIM Family Reveals Two Groups of Genes with Distinct Evolutionary Properties. BMC Evol Biol 8 225 (2008)
(155) Sarkar M, Saha S: Structural Insight into the Role of Novel SARS-CoV-2 E Protein: A Potential Target for Vaccine Development and Other Therapeutic Strategies. PLOS ONE 15 e0237300 (2020)
(156) Sarute N, Ibrahim N, Medegan Fagla B, Lavanya M, Cuevas C, Stavrou S, Otkiran-Clare G, Tyynismaa H, Henao-Mejia J, Ross S R: TRIM2, a Novel Member of the Antiviral Family, Limits New World Arenavirus Entry. PLoS Biol 17 e3000137 (2019)
(157) SenthilKumar G, Skiba J H, Kimple R J: High-Throughput Quantitative Detection of Basal Autophagy and Autophagic Flux Using Image Cytometry. BioTechniques 67 70–73 (2019)
(158) Shi C-S, Qi H-Y, Boularan C, Huang N-N, Abu-Asab M, Shelhamer J H, Kehrl J H: SARS-Coronavirus Open Reading Frame-9b Suppresses Innate Immunity by Targeting Mitochondria and the MAVS/TRAF3/TRAF6 Signalosome. The Journal of Immunology 193 3080–3089 (2014)
(159) Shirakabe A, Fritzky L, Saito T, Zhai P, Miyamoto S, Gustafsson Å B, Kitsis R N, Sadoshima J: Evaluating Mitochondrial Autophagy in the Mouse Heart. Journal of Molecular and Cellular Cardiology 92 134–139 (2016)
(160) Shojaei S, Suresh M, Klionsky D J, Labouta H I, Ghavami S: Autophagy and SARS-CoV-2 Infection: A Possible Smart Targeting of the Autophagy Pathway. Virulence 11 805–810 (2020)
(161) Shvets E, Fass E, Elazar Z: Utilizing Flow Cytometry to Monitor Autophagy in Living Mammalian Cells. Autophagy 4 621–628 (2008)
(162) Slack F J, Ruvkun G: A Novel Repeat Domain That Is Often Associated with RING Finger and B-Box Motifs. Trends in Biochemical Sciences 23 474–475 (1998)
(163) Sparrer K M J, Gableske S, Zurenski M A, Parker Z M, Full F, Baumgart G J, Kato J, Pacheco-Rodriguez G, Liang C, Pornillos O, Moss J, Vaughan M, Gack M U: TRIM23 Mediates Virus-Induced Autophagy via Activation of TBK1. Nat Microbiol 2 1543–1557 (2017)
(164) Sparrer K M J, Gack M U: TRIM Proteins: New Players in Virus-Induced Autophagy. PLOS Pathogens 14 e1006787 (2018)
(165) Sridharan S, Jain K, Basu A: Regulation of Autophagy by Kinases. Cancers 3 2630–2654 (2011)
(166) Stange Overå K, Garcia Garcia J, Bhujabal Z, Jain A, Øvervatn A, Larsen K B, Deretic V, Johansen T, Lamark T, Sjøttem E: TRIM32 Acts Both as a Substrate and a Positive Regulator of P62/SQSTM1 Impaired in a Muscular Dystrophy Disease. Journal of Cell Science jcs.236596 (2019)
(167) Stepanenko A A, Heng H H: Transient and Stable Vector Transfection: Pitfalls, off-Target Effects, Artifacts. Mutation Research/Reviews in Mutation Research 773 91–103 (2017)
(168) Steward A, Adhya S, Clarke J: Sequence Conservation in Ig-like Domains: The Role of Highly Conserved Proline Residues in the Fibronectin Type III Superfamily. Journal of Molecular Biology 318 935–940 (2002)

(169) Sui L, Zhao Y, Wang W, Wu P, Wang Z, Yu Y, Hou Z, Tan G, Liu Q: SARS-CoV-2 Membrane Protein Inhibits Type I Interferon Production Through Ubiquitin-Mediated Degradation of TBK1. Frontiers in Immunology 12 (2021)
(170) Tanida I, Minematsu-Ikeguchi N, Ueno T, Kominami E: Lysosomal Turnover, but Not a Cellular Level, of Endogenous LC3 Is a Marker for Autophagy. Autophagy 1 84–91 (2005)
(171) Teyssou E, Takeda T, Lebon V, Boillée S, Doukouré B, Bataillon G, Sazdovitch V, Cazeneuve C, Meininger V, LeGuern E, Salachas F, Seilhean D, Millecamps S: Mutations in SQSTM1 Encoding P62 in Amyotrophic Lateral Sclerosis: Genetics and Neuropathology. Acta Neuropathol 125 511–522 (2013)
(172) Thoms M, Buschauer R, Ameismeier M, Koepke L, Denk T, Hirschenberger M, Kratzat H, Hayn M, Mackens-Kiani T, Cheng J, Straub J H, Stürzel C M, Fröhlich T, Berninghausen O, Becker T, Kirchhoff F, Sparrer K M J, Beckmann R: Structural Basis for Translational Shutdown and Immune Evasion by the Nsp1 Protein of SARS-CoV-2. Science 369 1249–1255 (2020)
(173) Tian S, Jin S, Wu Y, Liu T, Luo M, Ou J, Xie W, Cui J: High-Throughput Screening of Functional Deubiquitinating Enzymes in Autophagy. Autophagy 17 1367–1378 (2021)
(174) Tiessen I, Abildgaard M H, Lubas M, Gylling H M, Steinhauer C, Pietras E J, Diederichs S, Frankel L B, Lund A H: A High-Throughput Screen Identifies the Long Non-Coding RNA DRAIC as a Regulator of Autophagy. Oncogene 38 5127–5141 (2019)
(175) Tsuchida T, Zou J, Saitoh T, Kumar H, Abe T, Matsuura Y, Kawai T, Akira S: The Ubiquitin Ligase TRIM56 Regulates Innate Immune Responses to Intracellular Double-Stranded DNA. Immunity 33 765–776 (2010)
(176) Tsuchiya Y, Taniguchi H, Ito Y, Morita T, Karim M R, Ohtake N, Fukagai K, Ito T, Okamuro S, Iemura S, Natsume T, Nishida E, Kobayashi A: The Casein Kinase 2-Nrf1 Axis Controls the Clearance of Ubiquitinated Proteins by Regulating Proteasome Gene Expression. Molecular and Cellular Biology 33 3461–3472 (2013)
(177) Turowec J P, Duncan J S, French A C, Gyenis L, St. Denis N A, Vilk G, Litchfield D W: Protein Kinase CK2 Is a Constitutively Active Enzyme That Promotes Cell Survival: Strategies to Identify CK2 Substrates and Manipulate Its Activity in Mammalian Cells. In *Methods in Enzymology*; Elsevier, 2010; Vol. 484, pp 471–493
(178) University of Arizona: *Phase II, Randomized, Investigator Initiated Trial to Evaluate Safety and to Explore Clinical Benefit of Silmitasertib (CX-4945) in Patients With Severe Coronavirus Disease 2019 (COVID-19)*; Clinical trial registration NCT04668209; clinicaltrials.gov, 2022
(179) Vijgen L, Keyaerts E, Moës E, Thoelen I, Wollants E, Lemey P, Vandamme A-M, Van Ranst M: Complete Genomic Sequence of Human Coronavirus OC43: Molecular Clock Analysis Suggests a Relatively Recent Zoonotic Coronavirus Transmission Event. Journal of Virology 79 1595–1604 (2005)
(180) Wang J, Cao B, Han D, Sun M, Feng J: Long Non-Coding RNA H19 Induces Cerebral Ischemia Reperfusion Injury via Activation of Autophagy. Aging Dis 8 71–84 (2017)
(181) Wang R, Yang X, Chang M, Xue Z, Wang W, Bai L, Zhao S, Liu E: ORF3a Protein of Severe Acute Respiratory Syndrome Coronavirus 2 Inhibits Interferon-Activated Janus Kinase/Signal Transducer and Activator of Transcription Signaling via Elevating Suppressor of Cytokine Signaling 1. Front. Microbiol. 12 752597 (2021)
(182) Watabe M, Nakaki T: CK2 as Anti-Stress Factor. Communicative & Integrative Biology 5 278–280 (2012)

(183) Woo P C Y, Lau S K P, Chu C, Chan K, Tsoi H, Huang Y, Wong B H L, Poon R W S, Cai J J, Luk W, Poon L L M, Wong S S Y, Guan Y, Peiris J S M, Yuen K: Characterization and Complete Genome Sequence of a Novel Coronavirus, Coronavirus HKU1, from Patients with Pneumonia. Journal of Virology 79 884–895 (2005)

(184) Worringer K A, Rand T A, Hayashi Y, Sami S, Takahashi K, Tanabe K, Narita M, Srivastava D, Yamanaka S: The Let-7/LIN-41 Pathway Regulates Reprogramming to Human Induced Pluripotent Stem Cells by Controlling Expression of Prodifferentiation Genes. Cell Stem Cell 14 40–52 (2014)

(185) Wu Y, Ma L, Zhuang Z, Cai S, Zhao Z, Zhou L, Zhang J, Wang P-H, Zhao J, Cui J: Main Protease of SARS-CoV-2 Serves as a Bifunctional Molecule in Restricting Type I Interferon Antiviral Signaling. Sig Transduct Target Ther 5 1–3 (2020)

(186) Xia H, Cao Z, Xie X, Zhang X, Chen J Y-C, Wang H, Menachery V D, Rajsbaum R, Shi P-Y: Evasion of Type I Interferon by SARS-CoV-2. Cell Reports 33 108234 (2020)

(187) Xiao C-Y, Hübner S, Elliot R M, Caon A, Jans D A: A Consensus CAMP-Dependent Protein Kinase (PK-A) Site in Place of the CcN Motif Casein Kinase II Site of Simian Virus 40 Large T-Antigen Confers PK-A-Mediated Regulation of Nuclear Import (∗). Journal of Biological Chemistry 271 6451–6457 (1996)

(188) Yalcinkaya M, Liu W, Islam M N, Kotini A G, Gusarova G A, Fidler T P, Papapetrou E P, Bhattacharya J, Wang N, Tall A R: Modulation of the NLRP3 Inflammasome by Sars-CoV-2 Envelope Protein. Sci Rep 11 24432 (2021)

(189) Yang J, Zheng Z, Yan X, Li X, Liu Z, Ma Z: Integration of Autophagy and Anoikis Resistance in Solid Tumors. The Anatomical Record 296 1501–1508 (2013)

(190) Yang L, Liu S, Liu J, Zhang Z, Wan X, Huang B, Chen Y, Zhang Y: COVID-19: Immunopathogenesis and Immunotherapeutics. Sig Transduct Target Ther 5 1–8 (2020)

(191) Yang Y, Fiskus W, Yong B, Atadja P, Takahashi Y, Pandita T K, Wang H-G, Bhalla K N: Acetylated Hsp70 and KAP1-Mediated Vps34 SUMOylation Is Required for Autophagosome Creation in Autophagy. Proc. Natl. Acad. Sci. U.S.A. 110 6841–6846 (2013)

(192) Yang Y, Wu Y, Meng X, Wang Z, Younis M, Liu Y, Wang P, Huang X: SARS-CoV-2 Membrane Protein Causes the Mitochondrial Apoptosis and Pulmonary Edema via Targeting BOK. Cell Death Differ 29 1395–1408 (2022)

(193) Yang Z, Klionsky D J: Mammalian Autophagy: Core Molecular Machinery and Signaling Regulation. Current Opinion in Cell Biology 22 124–131 (2010)

(194) Ylikallio E, Poyhonen R, Zimon M, De Vriendt E, Hilander T, Paetau A, Jordanova A, Lonnqvist T, Tyynismaa H: Deficiency of the E3 Ubiquitin Ligase TRIM2 in Early-Onset Axonal Neuropathy. Human Molecular Genetics 22 2975–2983 (2013)

(195) Zachari M, Ganley I G: The Mammalian ULK1 Complex and Autophagy Initiation. Essays Biochem 61 585–596 (2017)

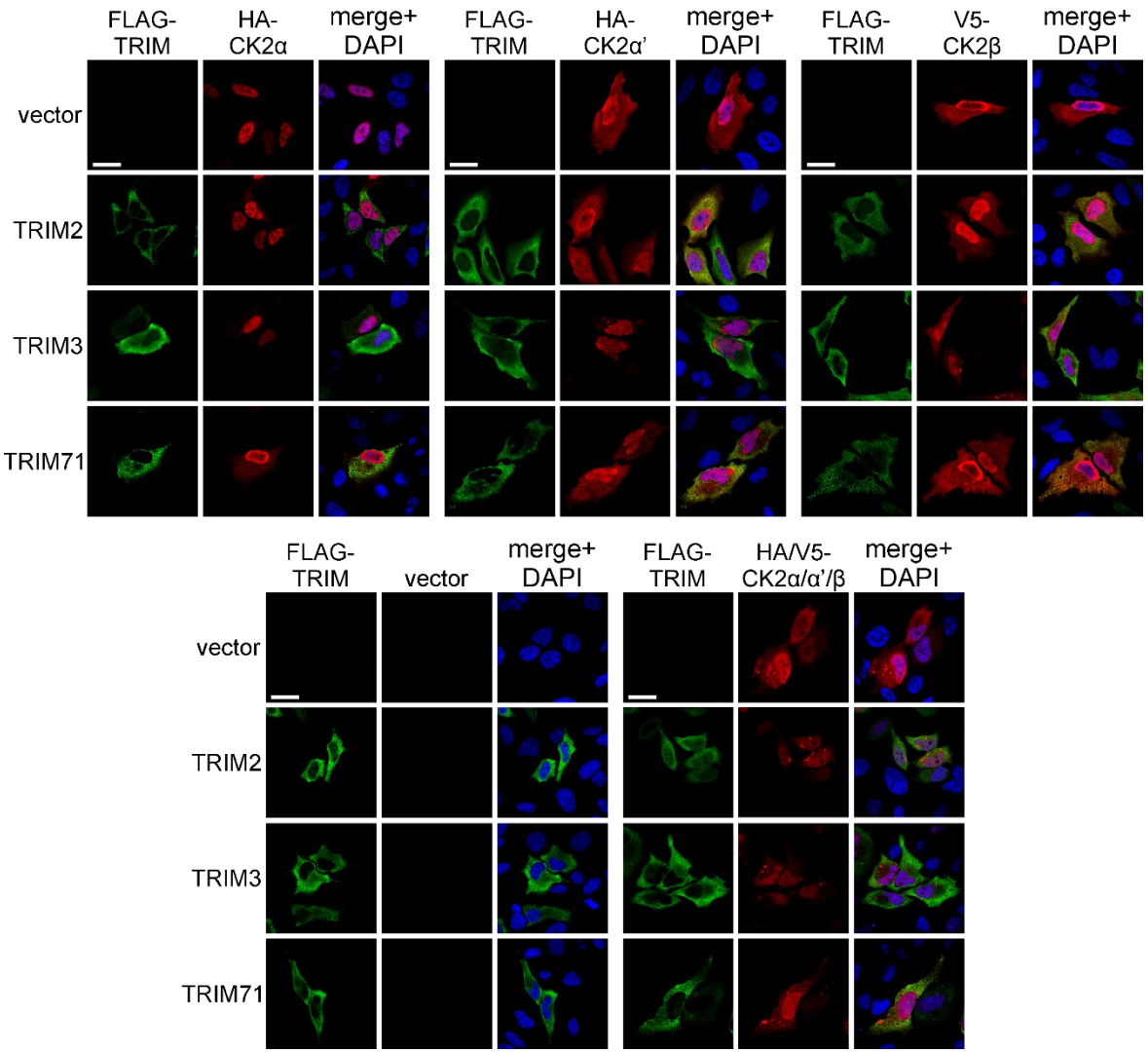
(196) Zaim S, Chong J H, Sankaranarayanan V, Harky A: COVID-19 and Multiorgan Response. Current Problems in Cardiology 45 100618 (2020)

(197) Zakharia K, Miyabe K, Wang Y, Wu D, Moser C D, Borad M J, Roberts L R: Preclinical In Vitro and In Vivo Evidence of an Antitumor Effect of CX-4945, a Casein Kinase II Inhibitor, in Cholangiocarcinoma. Translational Oncology 12 143–153 (2019)

(198) Zhang L, Yu J, Pan H, Hu P, Hao Y, Cai W, Zhu H, Yu A D, Xie X, Ma D, Yuan J: Small Molecule Regulators of Autophagy Identified by an Image-Based High-Throughput Screen. Proc. Natl. Acad. Sci. U.S.A. 104 19023–19028 (2007)

(199) Zhou Y, Hou Y, Shen J, Huang Y, Martin W, Cheng F: Network-Based Drug Repurposing for Novel Coronavirus 2019-NCoV/SARS-CoV-2. Cell Discov 6 1–18 (2020)
(200) Zhou Z, Jiang X, Liu D, Fan Z, Hu X, Yan J, Wang M, Gao G F: Autophagy Is Involved in Influenza A Virus Replication. Autophagy 5 321–328 (2009)
(201) Mowiol Mounting Medium. Cold Spring Harb Protoc 2006 pdb.rec10255 (2006)
(202) *Search Orphan Drug Designations and Approvals*. https://www.accessdata.fda.gov/scripts/opdlisting/oopd/detailedIndex.cfm?cfgridkey=548516 (accessed 2022-09-12)
(203) *Drugs@FDA: FDA-Approved Drugs*. https://www.accessdata.fda.gov/scripts/cder/daf/index.cfm?event=overview.process&varApplNo=006002 (accessed 2022-06-30)

9. Appendix



Supplementary Figure 1: Cellular distribution of filamin-NHL TRIMs and CK2. Extension of Fig. 12D. Representative confocal microscopy images of HeLa cells transfected with the indicated constructs. FLAG (TRIMs, green), HA and V5 (CK2 subunits, red) and DAPI (blue). Scale bar=10 µm. The experiments generating the data shown in the figure were performed and analyzed myself.

10. Acknowledgements

First and foremost, I want to express my deepest gratitude to Konstantin Sparrer. He continues to exceed all expectations as my mentor and has guided me through the entirety of my PhD. On top of that, he supports me at any given chance and ensures that I can further myself at any opportunity. Konstantin is always available for discussion and has taught me a great deal about scientific work and maneuvering the scientific landscape. He has become a good friend who is a pleasure to spend time with and is always up for a laugh and conversation. I cannot say how thankful I am for everything you have done for me.

I want to thank Frank Kirchhoff, who provided guidance whenever needed and gave me the freedom to work and explore science on my terms. Frank is a great scientific role model that I happily look up to. Frank and Jan Münch, as the heads of the Institute of Molecular Virology, provide both the means to freely explore scientific questions and an enjoyable and supportive working environment. I am grateful to you for my time at the institute.

I want to thank Jana-Romana Fischer and Birgit Ott for their excellent assistance, which was critical to many undertakings that would have been impossible otherwise. They play a huge part in running our laboratory and are invaluable partners through their kindness and reliability. I hope you enjoy working with me as much as I enjoy working with you.

Throughout my time at the institute, I relied on the assistance Martha Mayer, Kerstin Regensburger, Regina Burger, Daniela Krnavek, and Nicola Schrott provided to achieve my goals. I am thankful for the practical instructions they offered and their critical contribution to running the institute. You truly make this all work.

I want to thank Rüdiger Groß and Carina Conzelmann, who accompanied me during my PhD and were always available to for any conversation. Both of them helped me navigate the sometimes-complicated route through the PhD. Rüdiger is a great friend who never ceases to motivate me, whether at work or in the gym. Things would have been much more tedious without you.

I thank my fellow group members Maximilian Hirschenberger, Susanne Klute, Victoria Hunszinger, Helene Hönigsperger and Dennis Freisem. It is a pleasure working with you, and you seem to never run out of ideas to make day-to-day work exciting.

I am thankful to Alexander Grenzner and Benjamin Winter, who were great students I had the pleasure of teaching. Both enriched the working environment with fun, fruitful discussions and excellent work. Alexander continues to be a reliable friend whose company is always enjoyable. Working with both of you was a blast.

I am thankful to Elisabeth Braun and Daniel Sauter, who guided me through my beginnings in science. They happily answered any question and played a significant role in sparking my passion for research.

I want to thank Dré van der Merwe for ensuring that I can work without interruption and simultaneously being a super nice colleague who is always ready for a joke or a light conversation. His great attitude and broad knowledge add a lot to the institute. Having you around and working with you is always enjoyable.

I am grateful to have colleagues like Rayhane Nchioua, Caterina Prelli-Bozzo, Fabian Zech, and Alexandre Laliberté, that always make sure to inject plenty of fun into the office work and, at the same time, are great partners for discussion. With such lovely people around, work never gets dull.

I want to thank all members of the institute for being part of such an excellent and friendly working environment. Every day working with you is a pleasure.

I want to thank Julia Nemeth and Dimitri Nikolaenko. They have accompanied me from the start at Ulm University and are great friends who always support me and offer an outstanding work-life balance. Both of them played a significant role in me making it this far and getting through university. I am looking forward to many more years with you two.

I want to express my gratitude to my girlfriend Annika Schundner, who, on top of taking care of me and providing support, never stopped pushing me to achieve my goals and do the best I could. She is always there when I need her and is happy to advise and assist on any topic. Spending my time with you is the best, and I could not be happier than with you.

Finally, I want to thank my family, that supported me from the start and made all of this possible. My parents, Marlise and Harald, and my sisters Carolin and Isabel are always there to help with any problem and have given me so much. Without them, I could not have pursued my passion for science and would not be where I am today. I am grateful for all of you and could not imagine a better family to grow up in.

11. Statutory declaration

Declaration:

I hereby declare that I wrote the present dissertation with the topic:

“Regulation of Autophagy by SARS-CoV-2 and Host Proteins”

independently and used no other aids than those cited. In each individual case, I have clearly identified the source of the passages that are taken word for word or paraphrased from other works.

I also hereby declare that I have carried out my scientific work according to the principles of good scientific practice in accordance with the current „Satzung der Universität Ulm zur Sicherung guter wissenschaftlicher Praxis“ [Rules of the University of Ulm for Assuring Good Scientific Practice].

Ulm, 29.09.2022

Lennart Koepke